DEBRE BERHAN UNIVERSITY

COLLEGE OF ENGINEERING

Synthesis, Characterization and Optimization of Bionanocomposites for the Application of Methylene Blue Dye Degradation under Light Irradiation

A Research Submitted to the Department of Chemical Engineering, College of Engineering, Debre Berhan University

In partial Fulfillment of the Requirements for the Degree of Master of Science in Chemical Engineering (Process Engineering)

By: Salem Yohannes Mena

Principal Advisor: Asfaw Negash (PhD)

Co-Advisors: Kitaw Abrham (MSc. degree)

Minbale Gashu (PhD)

December, 2022

Debre Berhan, Ethiopia

Approval Page

We, the undersigned members of the boarded of the examiners of the final open defense by Ms. Salem Yohannes Mena have read and evaluated her thesis entitled: "**Synthesis, Characterization and Optimization of Bionanocomposites for the Application of Methylene Blue Dye Degradation under Light Irradiation**" and examined the candidate. This is to certify that the research has been accepted in a partial fulfillment of the requirements for the award of the Degree of Master of Science in Chemical Engineering (Chemical process) complies with the regulations of the university and meets the accepted standards with respect to originality, content and quality.

Name of the Chairperson	Signature	Date
Name of Principal Advisor	Signature	Date
Name of Internal Examiner	Signature	Date
Name of External Examiner	Signature	Date

DECLARATION

I declare that this research entitled: **Synthesis, Characterization and Optimization of Bionanocomposite for the Application of Methylene Blue Dye Degradation under Light Irradiation**: has not been submitted in any form for another degree, diploma or an award at any University or other institution of the tertiary education. The contributions of all individuals were acknowledged in the thesis. The supported information taken from published and unpublished work of others has been recognized in the text and a list of reference is given. The work was under the guidance of my supervisors those are instructor in Debre Berhan University, department of Chemical Engineering and Chemistry.

_____	_____	_____
Author name	Signature	Date

Witnessed by:

_____	_____	_____
Name of Advisor	Signature	Date
_____	_____	_____
Name of Co-advisor-1	Signature	Date
_____	_____	_____
Name of Co-advisor-2	Signature	Date

ACKNOWLEDGEMENTS

First, I would like to thank the Almighty GOD for giving me all his amazing provisions, strength and patience for the successful accomplishment of this research work.

I would like to express my heartfelt appreciation and thank to my Advisor Dr. Asfaw Negash for his sustainable and appreciable guidance, tireless advising, for sharing his knowledge, skill, experience and fine-tuning up to the successful completion of this research work.

Nextly, I would like to make my deepest appreciation and gratitude to chemical engineering department staffs specially my co-advisor Mr. Kitaw Abrham for his patience, kindness, right encouragement from the beginning of this research work. In addition, my sincere thanks goes to chemistry sttafs particularly my co-advisor Dr. Minbale Gashu for his unlimitted guiding and special support during laboratory work.

I also thank all chemical engineering and chemistry department laboratory technicians for helping me by emotional, physically and materially to over-come all the obstacles I faced during my work. Thanks to them I arrive to this level and I will remain always grateful toward them for what they have been doing.

I would like to express my deep appreciation to Mr. Abera, who works in UNISA, South Africa for his great contribution to characterize the samples with SEM-EDX and TGA analyzer.

Furthermore, I would like to thank Ms. Semira Kedir for her great contribution to getting real textile wastewater from one way textile manufacturing P.L.C. At the end of my thesis, I want to thank and give credit to all individuals who have provided me with invaluable assistance. My deepest thanks go to my family for their true inspiration, I would not have been able to do any of this without their pray and that give me the strength and support.

Lists of Abbreviations and Acronyms

WH	Water Hyacinth
CNCs	Cellulose nano crystals
BNCs	Bionanocomposites
Ag @ ZnO NPs	Plant extract assisted Silver doped Zinc Oxide Nano particles
UV-Vis	Ultraviolet-visible spectrophotometer
FTIR	Fourier transform infrared
XRD	Xray diffraction
SEM-EDX	Scanning Electron Microscopy with Energy Dispersive X-Ray
BET	Brunauer-Emmett-Teller
DLS	Dynamic light scattering
TGA	Thermogravimetric analysis
DoE	Design of experiment
a.s.l.	Above sea level
Ha	Hectar
CNCs/Ag@ZnO (1:1)	1g of cellulose nano crystals combined with 1g of silver doped zinc oxide
CNCs/Ag@ZnO (1:0.5)	1g of cellulose nano crystals combined with 0.5g of silver doped zinc oxide
CNCs/Ag@ZnO (0.5:1)	0.5g of cellulose nano crystals combined with 1g of silver doped zinc oxide
RSM-BBD	Response surface methodology with Box Behnken design

Abstract

Water hyacinth (Eichornia crassipes) is a free floating aquatic weed that potentially damages the aquatic ecosystem by colonizing rapidly and it causes drying of water bodies. In addition, releasing of colored textile wastewater into nearby water bodies potentially damage the aquatic creatures and surrounding lives. But behind the negative assumptions of Water hyacinth (WH) weed, it is rich in natural fiber content, namely cellulose and its leaves used as a reducing and capping agent during nanoparticles (NPs) synthesis. Therefore; this research mainly focus on utilization of the weed's stem and leaves to develop cellulose nano crystals (CNCs) and as capping and reducing agent during silver doped zinc oxide nanoparticles (Ag@ZnO NPs) synthesis, respectively. Furthermore; the developed CNCs to behave as a photocatalyst, it was combined with a green synthesized Ag@ZnO NPs to develop a bionanocomposite (BNC). The characterization techniques i.e. UV-Vis spectrophotometer, FTIR, XRD, TGA, BET, DLS and SEM-EDX were confirm the obtained CNCs and Ag@ZnO NPs were effectively synthesized. Also each characterization results exhibit the formation of pure BNCs (i.e. CNC/Ag@ZnO (1:1), CNC/Ag@ZnO (1:0.5) and CNC/Ag@ZnO (0.5:1)). The synthetic Methylene Blue (MB) dye solution and real textile wastewater were used in photodegradation study. Moreover, the effect of operating parameters i.e. pH, BNCs dosage, initial MB concentration, and irradiation time was investigated under sunlight irradiation. According to the results, CNC/Ag@ZnO (1:0.5) BNC has higher photodegradation efficiency (98.8%) than CNC/Ag@ZnO (1:1) and CNC/Ag@ZnO (0.5:1) BNCs at the optimum condition. In addition, the RSM-BBD analysis results showed that pH = 10, CNCs/Ag@ZnO (1:0.5) BNC dosage =18.075 mg/L, MB dye concentration = 17.468 mg/L and Irradiation time = 111.855 min were the optimal level of the studied process parameters using CNC/Ag@ZnO (1:0.5) BNC. Also, the desirability of the process was 1.00; it confirms the acceptance and applicability of the model. Moreover, the recyclability test confirms CNC/Ag@ZnO (1:0.5) BNC has high recyclability efficiency even after 7^{th} round than the left synthesized BNCs. Therefore; the facile synthesis and high degradation efficiency of CNC/Ag@ZnO (1:0.5) BNC photocatalyst make it a promising candidate for real-world dye containing textile wastewater treatment under light irradiation with low operating cost.

Keywords: *Water Hyacinth, Textile Wastewater, Methylene Blue, Bionanocomposite*

Table of Contents

List of Tables

List of Figures

CHAPTER ONE

1. Introduction

1.1 Background

Water is an essential element for sustaining all forms of life existence on the earth. Its utility is not limited to survival of lives, but also it is a valuable natural resource for many productive actions such as; agricultural activities, industrial processes, hydropower generation, etc. (A. Gupta, 2017). However, deterioration of the limited water resources has an adverse effect on human beings as well as aquatic ecosystem directly or indirectly (Fahad et al., 2019). Water Hyacinth (Eichhornia crassipes) is a free floating invasive aquatic weed (see Figure 1.1). It damages the water resources and aquatic ecological stability through rapid colonization of water bodies. Due to that it becomes a current challenges of developing countries including, Ethiopia (Abera and Hailu, 2018). Water hyacinth (WH) has a rapid propagation and morphological characteristics that makes the weed well adapted to rapid distance dispersal and successful colonization of varying habitats in a short time by eliminating native aquatic plants (Punitha et al., 2015).

Figure 1.1 Water Hyacinth weed

In the absence of effective controlling system, this weed potentially reduce sunlight penetration, changes the temperature and pH levels of the water and causes de-oxygenation of water by forming thick and extensive mats (Omondi et al., 2019). In consequences, it damage the aquatic ecosystems, reduce the production of fish and causes drying of water bodies (Serrano et al.,

2016). The recent studies showed that controlling of this weed through physical, mechanical, chemical, and biological methods causes additional environmental and financial complications.

But rather than eradication, changing this weed for potential use and value-added products is a positive aspect for tackling both ecological problems and economic setbacks caused by WH weed (Harun et al., 2021). Behind it's impacts, this aquatic weed is basically a source of natural fiber particularly, it contains approximately 40% of cellulose. This bio-polymer mainly used as a raw material in the process of cellulose nano crystals synthesis (Istirokhatun et al., 2015). Cellulose nano crystals (CNCs) are a unique, non-toxic, and biodegradable nanomaterial which primarily obtained from naturally occurring cellulose fibers by means of acid hydrolysis, enzymatic hydrolysis or mechanical treatment (Pandi et al., 2021). It has large specific surface area to volume ratio, high strength and low density that serve to develop a sustainable and environmentally friend materials (Setyaningsih et al., 2019).

Likewise WH, 80% of earth's water bodies mainly polluted by industrial disposals, mainly releasing of colored effluents from textile industry (Bailey et al., 2022). The textile industry commonly characterized by discharging of massive quantity of colored effluent in to nearby water bodies (Fito et al., 2020). This industry uses more than 10,000 dyes and pigments for painting and dyeing fabrics. Among the different organic dyes, Methylene Blue ($C_{16}H_{18}ClN_3S$) is the most common dye which utilized for dyeing of cotton, fabric and silk in the textile factory (Khan et al., 2022).

Figure 1.2 MB dye containing textile wastewater

It has complicate chemical structure and forms a stable solution with water due to that it resist the conventional wastewater treatment processes (Azzaz et al., 2021). The presence of high

concentration of Methylene Blue (MB) dye in the textile wastewater can damages the aquatic ecosystem and water quality and it causes allergy and skin irritation on human and animal bodies (Dey and Islam, 2015).

Various traditional methods such as physical, biological and chemical treatments have been tried for the removal of MB dyes from aquatic media but those methods result additional water polution and financial problems (Periyasamy et al., 2018). Advanced oxidation processes (AOPs) are the most attractive and favorable option for the effective removal of organic pollutants (i.e. dyes) from wastewater. It involves the use of powerful oxidizing intermediates (e.g. hydroxyl radical (•OH)) that can oxidize and degrade primary toxic organic pollutants into non-hazardous compounds (CO_2 and H_2O) (Parvin et al., 2018). Among AOPs, semiconductor-mediated heterogeneous photocatalysis is a promising technique, which is valuable for environmental and energy applications. Owing to its advantages such as low cost, non-toxic, complete mineralization and reusability; it has become a fast growing research area in the past decades (Maynez and Sánchez, 2018). Some notable semiconductors applied as photocatalysts are included Titanium dioxide (TiO_2), Zinc oxide (ZnO), Cadmium sulfide (CdS), Tungsten trioxide (WO_3), Tin(IV) oxide (SnO_2), Zinc sulfide (ZnS), Cadmium telluride (CdTe), Iron oxide (α-$Fe2O_3$), Niobium silver trioxide ($AgNbO_3$) and Strontium titanate ($SrTiO_3$) (Shatnawi et al., 2016).

Among the above semiconductors, Zinc Oxide (ZnO) in the wurtzite phase is the most used metal oxides as photocatalysts due to its environmental sustainability, high photocatalytic efficiency, nontoxicity and low cost for massive synthesis (Samadi et al., 2016). In addition, it is efficient to remove organic compounds present in industrial wastewater (Sharma and Nain, 2017). But, the photocatalytic performance of ZnO nanoparticles is limited to irradiation wavelengths in the UV region due to its wide band-gap energy (3.37 eV) (Song et al., 2018). This problem can be overcome through reducing electron-hole recombination by doping of transition metals such as Silver, Manganese, Copper, Cobalt, Platinum, and Gold into ZnO structure. Silver (Ag) is the most effective dopant element that has the ability to generate region of electric field and improved electrical properties by optical vibration of surface Plasmon resonance (Kamarulzaman et al., 2015).

The main objective of this research is developing of high performance BNC by combing of WH CNCs with Ag@ZnO NPs. During preparation of CNCs acid hydrolysis method was used. In case of Ag@ZnO NPs synthesis; the WH leaf extracts was used for capping and reducing agent, which is a good stabilizer that inhibit the over-growth of NPs and prevent their coagulation (Zelekew et al., 2021). In addition, in this research the combination ratio of CNC to Ag@ZnO NPs was optimized using three combination ratios (wt/wt) (i.e.CNCs/Ag@ZnO (1:1), CNCs/Ag@ZnO (1:0.5) and CNCs/Ag@ZnO (0.5:1) BNC). The synthesized samples were characterized through UV-Vis spectrophotometer, FTIR, XRD, TGA, BET, DLS and SEM-EDX techniques. In addition, the effects of process parameters i.e. pH of dye solution, BNCs dosage, MB dye concentration, and irradiation time on the dye degradation efficiency were examined under light irradiation. Moreover, the optimization of process conditions studies were carried out RSM-BBD software analyzer using highest performance BNC ratio. The dye degradation performance of each BNCs also examined using real textile wastewater sample. Furthermore, the recyclability performance of each composites were investigated to determine the feasibility of the study. The outcomes of this study can fill the research gaps and promote the sustainability of fresh water by reducing the two major water related problems.

1.2 Statement of the Problem

The freshwater ecosystems of the world comprise only 0.5% of the earth's surface and the left is too salty and not easily available (Paul et al., 2012). Nowadays, promoting of the water sustainability either by eliminating the sources of water pollution or removing the pollutants using cost effective and eco-friendly material is the major challenges of the world (Mironga et al., 2014). WH is the most worst aquatic weed in the world that potentially damages the water bodies by quickly colonizing of stagnant and slow moving water resources (Mahamadi, 2012). It forms thick floating mats on the water surface that tends to reduce sunlight penetration and the exchange of gasses between the water surface and the atmosphere (Worku and Sahile, 2017). In addition, it has rapid regeneration property that can double its mass every 5 days and yield 4700 seeds under favorable conditions which helps to invade the water bodies in a short period of time (Hailu and Degaga, 2019). Its seeds can remain viable for up to 20 years and may germinate in moist soil or warm, shallow waters (Worku and Sahile, 2017).

In the present day this aquatic weed becomes the major problem of developing countries including, Ethiopia. Its impact is not only loss of biodiversity in aquatic ecosystems but also it affects human wellbeing by results of vector diseases. It also reduce the financial income of local community especially those who depend on water bodies for their livelihoods i.e. fishing and tourism (Gopal, 2017). To eradicate the propagation of this aquatic weed, different conventional techniques i.e. mechanical, physical and chemical methods were used but those leads to additional cost and water pollution.

In addition to WH weed, releasing colored textile effluent in to surrounding water resources is another major source of water pollution (Dey and Islam, 2015). Textile industry is the second world water polluting sector which mostly builds near to water bodies for its requirement of huge amounts of water. This manufacturing sector commonly known by continuously disposing of its dye containing wastewater into rivers as effluents (Bailey et al., 2022). In dying process 10% of MB dyes are remaining on the fabrics and the left 90% discharged in to nearby water bodies that potentially damage the aquatic ecosystem (Šmelcerović, 2019). The presence of a small amount of MB dye (even 1 mg/L) in textile wastewater seriously affects the aesthetic and transparency of water bodies and indirectly alters the functioning of aquatic life (Tarekegn and Balakrishnan,

2021). Additionally, it damages the human and animal health by causing diarrhea, skin allergy, swallowing of stomach, etc. (Sahoo et al., 2012).

Therefore; this study aimed to possibly finding cost effective and efficient solution for water related problems by developing high performance nano-materials from water damaging aquatic weed (i.e. WH weed). In addition, to have a photocatalytic property the produced CNCs combined with green synthesized NPs for the application of dye degradation under light irradiation. The photocatalytic performance of the developed BNCs photocatalyst was investigated using synthetic MB dye solution and real textile wastewater as an organic pollutant. At the end of this research, it will add value in textile wastewater treatment process and provide a clean, eco-friend, flexible, cost effective, recyclable and sustainable BNC photocatalyst. In addition, it promote the sustainability of limited water resources by developing valuable material from water damaging weed as a solution for removing of water polluting organic pollutants (i.e. dyes).

1.3 Objective of the Study

1.3.1 General Objective

The general objective of this study is to synthesize CNCs/Ag@ZnO BNC photocatalyst for the application of MB dye degradation under light irradiation.

1.3.2 Specific Objectives

- To synthesize CNCs and Ag@ZnO NPs for developing of CNCs/Ag@ZnO BNC photocatalyst.
- To characterize the synthesized each sample using UV-Vis spectrophotometer, FTIR, XRD, TGA, BET, DLS and SEM-EDX techniques.
- To study the effects of process parameters (i.e. pH of dye solution, BNCs dosage, MB dye concentration, and irradiation time) on dye degradation efficiency of BNCs and to compare their photocatalytic performance.
- To study the MB dye degradation kinetics using the three developed CNCs/Ag@ZnO BNCs.
- To study and optimize the interactions of process conditions (i.e. pH of dye solution, BNC, dosage, MB dye concentration, and irradiation time) through DoE software analyzer.

1.4 Significant of the Study

This research introduces a novel BNC by utilizing of WH weed bio-mass to develop CNCs from its stem and combined with high performance NPs to behave as a photocatalyst. Currently, attaining of eco-friendly photocatalyst with low cost is the major challenges of scientific community thus; this study can fill such kind of gaps. The developed BNC photocatalyst designed to degrade MB dye from synthetic and textile wastewater with low cost of activation energy (i.e. light irradiation). Furthermore, the following benefits will be obtained from the study:

- It aids technological progress in the field and helps to fill the research gap.
- It will reduce using of UV light in dye degradation process.
- The operation was designed to be more simple, recyclable, flexible, and easily adaptable.
- The developed BNC photocatalyst is environmentally friend, low cost and it can be easily recovered after photocatalysis.
- It will reduce the impacts of WH weed and colored textile wastewater on water qualities and aquatic creatures.
- It will create a linkage between university and textile industries to solve such kind of environmental problems.

CHAPTER TWO

2. Literature Review

2.1 Overview of Water Hyacinth

Water Hyacinth (Eichhornia crassipes) is one of the world's worst free-floating invasive aquatic weed that has the ability to cover the whole waterways rapidly (Agengo, 2013). The weed is native to Brazil, Amazon basin and Ecuador region (Bolorunduro, 2019). The weed was introduced as an ornamental species to decorate the water bodies (Figure 2.1) in many countries for their attractive blue or purple flowers, oval glossy leaves with bulbous petioles (see Figure 2.1(b)) (Gopal, 1987). Starting from the Amazon basin it reached many tropical and sub-tropical countries of Latin America, the Caribbean, Southeast Asia and Africa including Ethiopia (Hailu and Degaga, 2019). The growth of WH weed within 6 months reaches 125 tones wet weight in the area of 1 ha (Istirokhatun et al., 2015). It forms dense, impenetrable mats over the water surface, and results different problems such as: blocking irrigation channels and rivers, restricting livestock access to water, destroying natural wetlands, eliminating native aquatic plants, reducing penetration of sunlight, etc. (Enyew et al., 2020).

Figure 2.1 (a) Invasions of WH weed and (b) W H weed morphology

2.1.1 Ecology of Water Hyacinth

WH has broad, wide canopy-like waxy leaves and purple clustered flowers that grow in spikes (Carneiro et al., 2022). The petioles of the weed appear round with air-sacs that help make it to float on water bodies (Harun et al., 2021). WH can sometimes become rooted when it lodges in muddy, shallow waters and the flowers may be blue or white (Gopal, 1987). It has the ability to

reproduce both sexually through seed propagation and asexually through stolon vegetative reproduction thus, it can invade the water bodies rapidly (Hailu and Degaga, 2019). The chemical composition of the WH stem shown below in Table 2.1.

Table 2.1Chemical composition of water hyacinth stem (Omondi et al., 2019)

Parameters	WH weed stem composition
Moisture content (%)	85.15 - 96.13
Ash content (%)	16.79 - 39.80
Lipid (%)	10.17
Fiber content	12.15% from 21.97% of whole plant
Protein (%)	1.45-3.85
Nitrogen (%)	0.62
Carbohydrate (%)	69.15
Phosphorous (mg/Kg)	97.50
Sodium (mg/Kg)	1.11
Potassium (mg/Kg)	2.85
Calcium (mg/Kg)	47.65
Magnesium (mg/Kg)	6.84
Extractive content (%)	14.6-25
Hemicellulose content (%)	22.6-48.7
Lignin content (%)	3-28
Cellulose content (%)	35-58.62

2.2 Water Hyacinth in Ethiopia

In Ethiopia, WH weed also known as “Emboch” was first reported in 1956 in Koka Lake and Awash River as a decorative plant (Taye et al., 2011). Currently, the weed become worsen and most noxious aquatic pest that rapidly damages the water bodies of Ethiopia, particularly Lake Tana (Abera Hailu Degaga, 2018). As shown in Figure 2.2, the hotspot areas of Lake Tana invaded by the invasive species is located on the northeastern shore of the Lake (6-10 October 2018). In the rainy season (August), the western part is also susceptible to be invaded by the weed (Aragaw et al., 2020). According to the Ethiopian Ministry of Water, Irrigation, and Electricity (EMoWIE), about 5759 ha flood plain is invaded by WH weed due to this area has a

great potential to sink nutrients and the substantial amount of sediment deposition from the major rivers (Agengo, 2013).

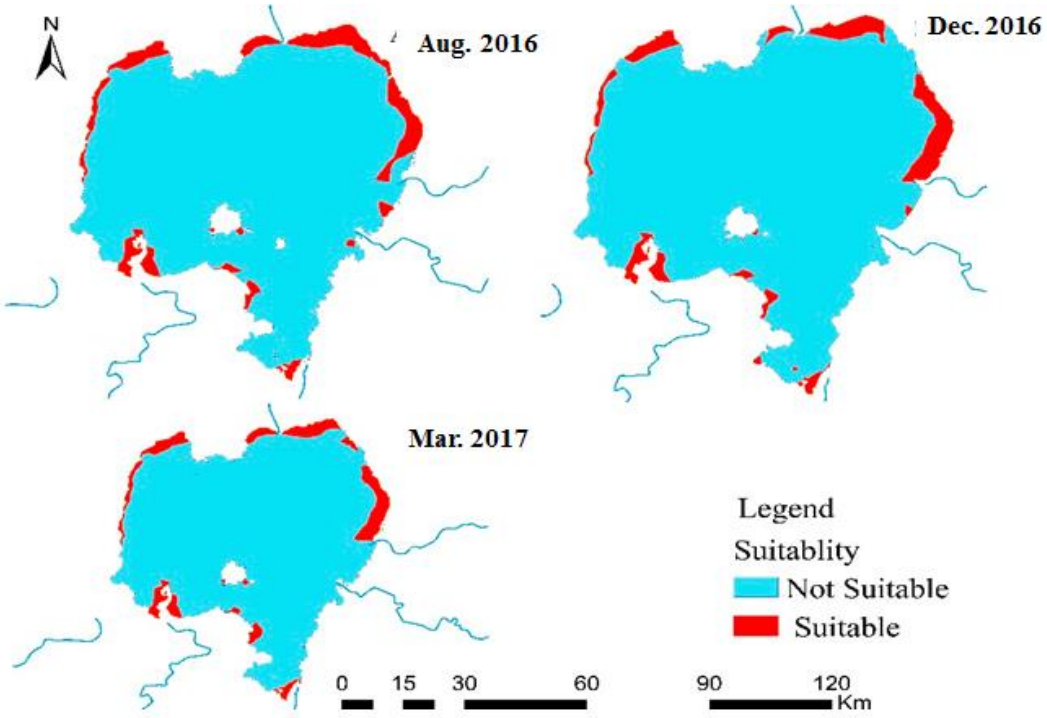

Figure 2.2 Map of Lake Tana and its invaded area by WH weed (Aragaw et al., 2020).

2.2.1 Impacts of Water Hyacinth Weed in Ethiopia

WH is the greatest destructive weed of biosphere in the world due to its reproduction nature and the ability to resist different conventional controlling mechanisms (Akendo et al., 2008). Due to its fast colonization, it prevents the growth of vital phytoplankton, which is the main source of food for fishes (Harun et al., 2021). In the present day, fish production of Lake Tana reduced from 13,000 to 1,000 tons a year (Abera Hailu Degaga, 2018). In addition, this weed highly destroyed variety of grass species and as a result the grazing land has been substantially reduced. Feeding of WH weed caused gut bloating and continuous diarrhea, which results loss of body weight and death of livestock (Enyew et al., 2020).

Moreover, the thick mat of WH trapped water way shipment transporting tourists, traders and goods in Ethiopia which causes adverse effect on trade, transport and tourism sectors. Additionally, the death and decay of water hyacinth vegetation in large masses create anaerobic conditions and production of lethal gases (Tewabe, 2018). Disrupting of hydro-electric power

generation, blockage of irrigation canals and rivers, and interference with irrigation activities are also the major problem of WH infestation (Taye et al., 2011). Currently it is a great fear of many Ethiopian naturalists and scientists for the Ethiopia Great Renaissance Dam (EGRD) project due to it may be block the water inlet streams (Akendo et al., 2008).

2.2.2 Applications of Water Hyacinth

WH weed potentially used as biological agent for treating sewage wastewaters. Several researchers states the root of water hyacinth capable to adsorb heavy metals (Chromium, Cadmium, Lead, Nickel, etc.) from aqueous solution (Kay et al., 1984). Additionally, the WH weed is characterized by a high content of lignocellulosic biomass, with a 10% average content of lignin, useful in both thermochemical and biochemical processes (Carneiro et al., 2022). The WH cellulose fiber mostly used for various applications such as; production of fiber, paper, fiber board, yam and rope. It also used to make charcoal briquetting, biogas, activated carbon and fertilizer (Azam et al., 2022). In addition, its stem contains high cellulose content approximately, 40% that mainly used for various application as a raw material.

2.3 Lignocellulose Materials

Lignocellulose biomass is an abundant and renewable resource from plants which is the largest amount of maintainable carbon material group. It is the most promising feedstock for the supportable production of high value-added materials (Muniz et al., 2016). These lignocellulosic resources may include; agricultural residues, forest residues, energy crops switch grass, food wastes, and municipal and industrial wastes (Chonsakorn et al., 2019). Changing of these low cost and abundantly available lignocellulose materials into valuable products is a feasible option for improvement of energy security and greenhouse emission reduction. It can be considered as main source for the fabrication of biofuel, biochemical, biopolymer materials and other value added products for economical and sustainable development (Lara-Serrano et al., 2016). Most of the lignocellulose biomasses are comprised of about 20-50% hemicellulose, 7-25% lignin, and 30-65% cellulose.

2.3.1 Hemicellulose

Hemicellulose is an amorphous heterogeneous polysaccharide that composed polymer of pentose's (xylose and arabinose), hexoses (mannose, glucose, and galactose) and acetylated sugars as shown in Figure 2.3 (Chonsakorn et al., 2019). Hemicellulose forming an interface

between hydrophobic lignin and hydrophilic cellulose, and it links with cellulose and lignin in plant fiber cells. Hemicellulose adheres to the cellulose fibrils through hydrogen bonds and Van der Waal's interactions and also cross-links with lignin (Phanthong, 2015). Hemicellulose can be hydrolyzed by acid, alkali, or enzymes from lignocellulose material. It can be applicable for packaging materials and used as biopolymers in cosmetics and mining industries (Bronzato et al., 2017).

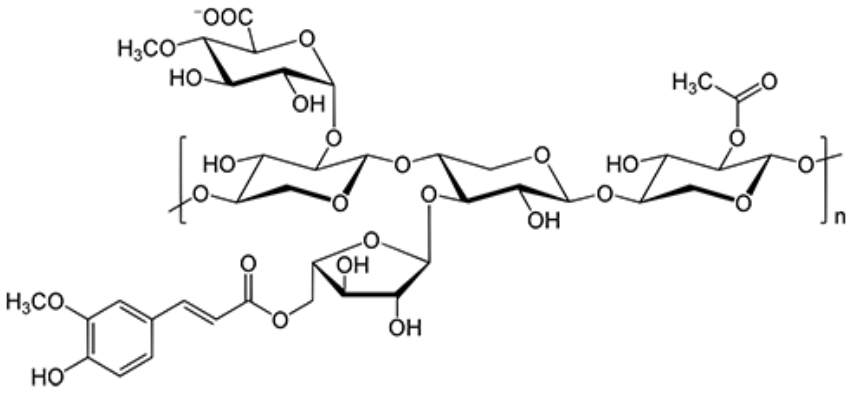

Figure 2.3 Chemical structure of Hemicellulose

2.3.2 Lignin

Lignin is defined as an amorphous three-dimension complex hetero polymer that composed of propyl–phenol groups linked by C–C bonds and an ether group as shown in Figure 2.4. It consists of the cross-linked amorphous copolymer and serves as the binder which holds between cellulose and hemicellulose complexion (Omondi et al., 2019).

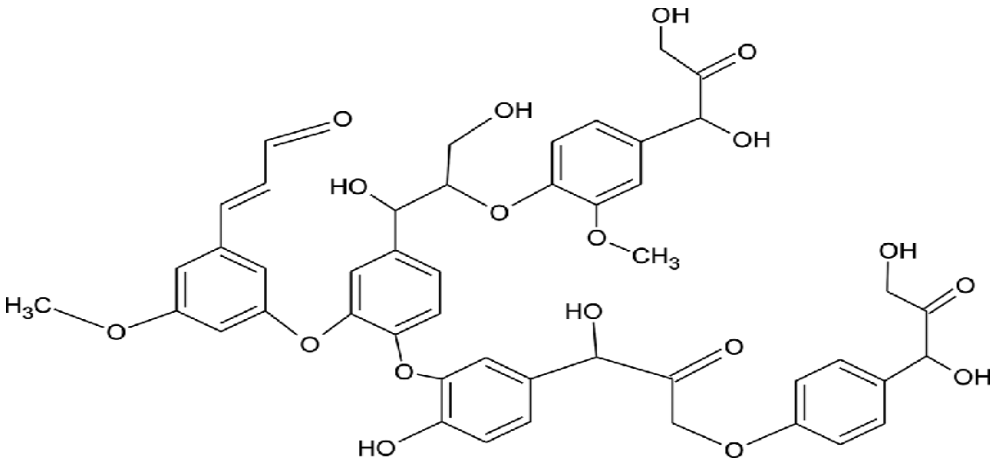

Figure 2.4 Chemical structure of Lignin

Due to its strong binding function, lignin provides the stiffness, compressive strength, resistant to decay, resistance to microbial attack, oxidative stress and water impermeability to plant cell wall to act as physical protective barrier for plant cell wall (Parvin et al., 2018). Removal of lignin is an important process to cause biomass swelling, disruption of lignin structure, increase in internal surface area, and increase accessibility of hydrolysis reaction. It can serve as a future aromatic source for the green chemicals used as building block for polymer such as polyester and polyurethanes due to its large quantities of poly-aromatic structure (Idrees et al., 2013).

2.3.3 Cellulose

Cellulose ($C_6H_{10}O_5$) is one of the most abundant renewable biopolymer resources on earth. It has 162.14 g/mole molar mass, non-soluble in water, and exists in white powder form (Bronzato et al., 2017). Cellulose basically consists of α-glucose pyranose residues linked through β-1, 4 bonds and its chains tend to be very close to each other as shown in Figure 2.5 (Kargarzadeh et al., 2017). This leads the polymer to be stable and having crystalline structure. Due to its attractive characteristic it used in various applications (Asrofi et al., 2018).

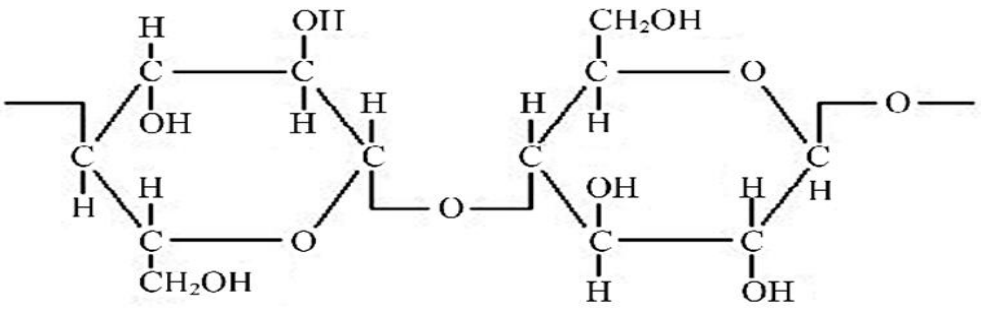

Figure 2.5 Chemical structure of Cellulose

2.3.4 Cellulose Nano Crystal

A cellulose nano crystals (CNCs) is a recyclable natural nanomaterial (Nicholas et al., 2015). It can be extracted from cellulose of plants such as wood, non-wood fibers, algae, tunicates, and agro-industrial residue or biomass and microorganisms. The dimensionof the CNCs is in the nanometer scale range approximately 1 to 100 nm (Mustikaningrum et al., 2021). In recent decades it becomes one of the most attractive nano materials in various fields due to its unique reinforcement properties i.e. unique nanostructure, purity, higher-dimensional stability, greater mechanical strength, and greater capacity to hold water (Song et al., 2019). Additionally, it has

attractive properties such as high modulus of elasticity, high strength, large surface area, large aspect ratio, and lower breaking expansion (Fang et al., 2020).

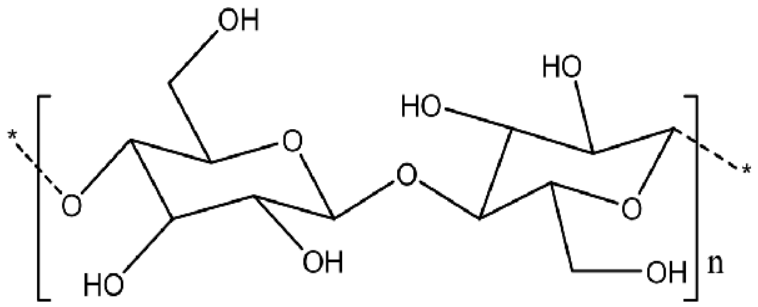

Figure 2.6 Chemical structure of CNCs

2.3.5 Cellulose Nano Crystals Synthesis Methods

The plant fibers are usually employed in preparing the CNCs due to its low price and abundance, whose common size is 0.5~3.0 mm in length and 20~40 μm in diameter. Meanwhile, the size of any one dimensionality of cellulose locating around 100 nm is called the CNCs (Sundari and Ramesh, 2012). Therefore, the methods for obtaining the CNCs are the processes of decreasing the size of natural cellulose, which includes acid hydrolysis, enzymatic hydrolysis and mechanical process (Doner et al., 1997).

2.3.5.1 Mechanical process

In this method a plant cell wall subjected to strong mechanical disintegration, the original structure of cellulose fiber is degraded and the fibers turn to cellulose nano crystals (CNCs) in the diameters range of 10–100 nm (Chonsakorn et al., 2019). Several mechanical techniques can be used to extract CNCs from various feed stocks, i.e. homogenization, microfludization, grinding, crushing, and ultrasonication. Among these techniques grinding method is mostly applied to isolate CNCs from cellulose sources. But, the principal drawback of this methods is the consumption of high energy, insufficient disintegration of the fibers and clogging of the homogenizer when the pulp is pumped through a very small orifice and excessive mechanical damage of the crystalline structure of the CNCs (Chonsakorn et al., 2019).

2.3.5.2. Enzymatic Hydrolysis

Enzymatic hydrolysis is a kind of biological treatment that includes enzymes for digestion or modification of cellulose fiber to obtain the washed CNCs. In this process the cellulose chains

are broken into glucose molecules by cellulose enzymes. Ligninases and xylanases enzymes are some common enzymes, which can convert many cellulosic agricultural residues into fermentable sugars (Dussán et al., 2014). The major drawbacks of this method are consuming of operating time (5–12 h), high cost, difficult to operate and low analytic recoveries.

2.3.5.3 Acid Hydrolysis

Acid hydrolysis is the most common approach for isolation of CNCs from cellulose materials (Song et al., 2019). In this method, the amorphous region of the cellulose fibrils may be easily hydrolyzed by strong acids (i.e. sulfuric acid) through esterification of hydroxyl groups with sulfate ions (Degaga, 2019). During acid hydrolysis, concentrated acids i.e. HCl, H_2PO_4 and H_2SO_4 have been used to pretreat lignocellulosic biomass. Diluted H_2SO_4 (30-60%) is mostly used in hydrolysis of CNCs (Kusmono et al., 2020). In this process, cellulose can be converted into several oligosaccharides containing glucose units, mainly cellotetraose (four-glucose polymers). With further dilution by water and heating for a certain time, cellotetraose is hydrolyzed to glucose monosaccharide (Idrees et al., 2013). The acid hydrolysis reaction relies upon on response time, temperature, and acid attention which have an effect on the properties and yields of final cellulose nano crystals. The washing system is usually carried out through cold water pursued, centrifugation or utilizing sodium hydroxide until neutral pH obtained (Lusiana et al., 2019).

2.4 Textile Industries Wastewater

Textile industry is the second most water polluting sector in the world (Bidu et al., 2021). It is responsible approximately 20% of global clean water pollution from dyeing and finishing products (Kausar et al., 2019). It consumes numerous volume of water approximately 425,000,000 gallons of water per day and use more than 20,000 different chemicals for their manufacturing processes such as bleaching, dyeing, printing and stiffening fabric products (Mehari et al., 2015). Each of these unit operations are highly water intensive and continuously discharges a huge volume of toxic wastewater in to water bodies. It potentially damages the aquatic ecosystem and brings some carcinogenic diseases on human and animal health. Some toxic compounds generated from each textile processing and their natures are given below in Figure 2.7 (Periyasamy et al., 2018).

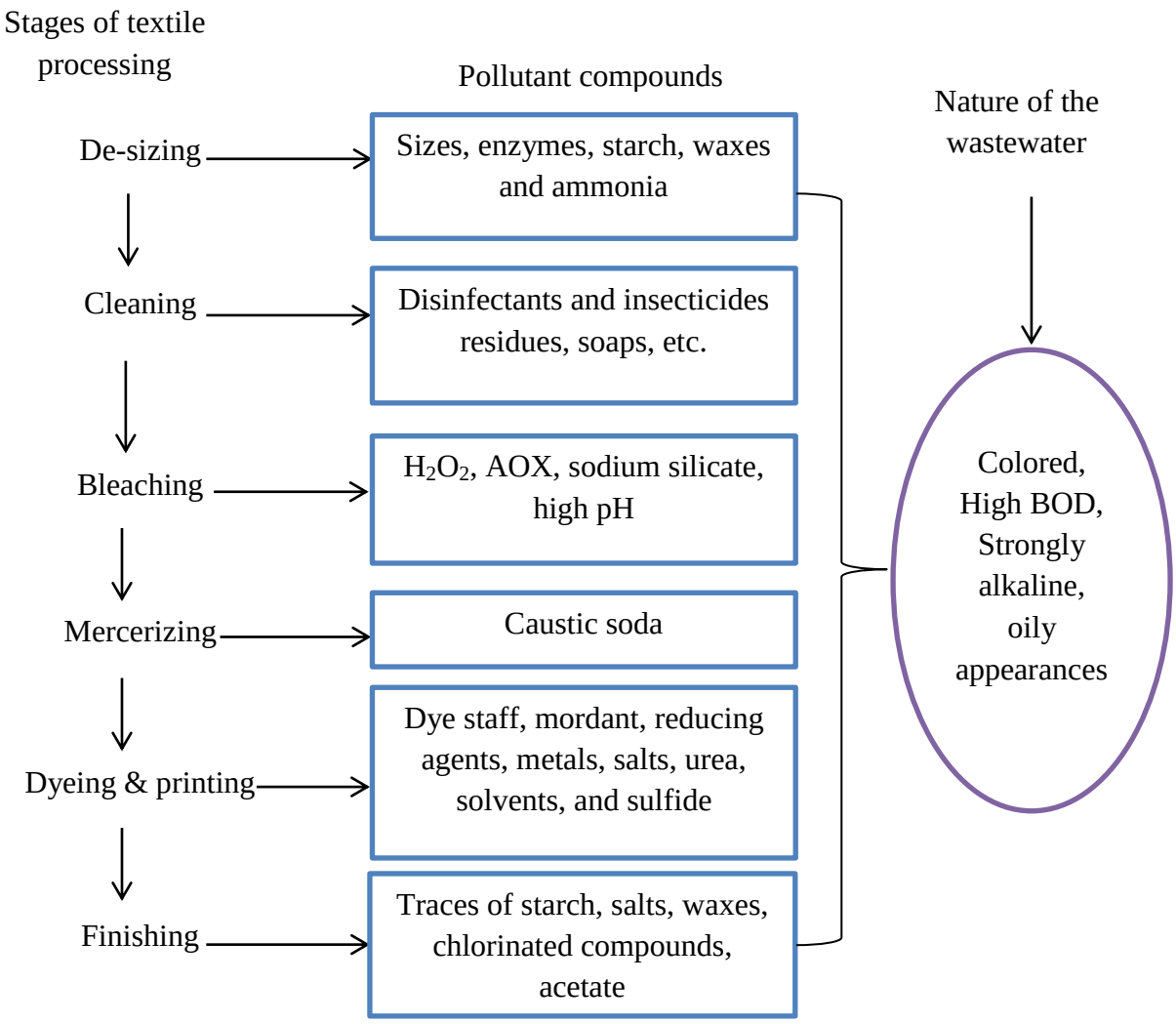

Figure 2.7 Possible pollutants from each stage of textile processes

In the textile dyeing process an extensive amount of synthetic dyes are consumed and continuously discharges colored wastewater into the adjacent waterway, farming fields, irrigation channels, etc. These organic dyes have high chemical and photolytic stability due to that the different conventional treatment methods do not degrade the dyes found in textile wastewater effectively (Said et al., 2020). The color associated with textile dyes not only causes aesthetic damage to the water bodies but also prevents the penetration of light through water which leads to a reduction in the rate of photosynthesis and dissolved oxygen levels affecting the entire aquatic ecosystems (Bailey et al., 2022).

2.4.1 Methylene Blue

Methylene Blue (MB) is a well-known cationic dye commonly used for dying fabrics in textile industry. It is a positively charged basic dye and highly water soluble, thus it forms a stable solution with water at room temperature (Kareem et al., 2022). It is a solid, odorless, dark green powder at room temperature which has a characteristic deep blue color in the oxidized state when it dissolved in water (Singh et al., 2017). During dying process, about 90% of inputs (i.e. dyes, water and other organic chemicals) get discharged as effluents into natural water bodies as shown in Figure 2.8 (Periyasamy et al., 2018). This saturated effluent particularly, MB containing wastewater disturbs the ecological balance of aquatic systems by blocking sunlight and altering photosynthetic activities etc. (Mohamed et al., 2022). In addition, MB dyes typically constitute carcinogenic aromatic amines and toxic heavy metals that affect the central nervous system, reproductive system, and kidneys of human beings and animals (Hameed et al., 2010).

Figure 2.8 Water pollution by colored textile wastewater

Treatment of MB dye containing wastewater before discharging into the environment is crucial solution to protect the limited water resource quality (Mulugeta and Lelisa, 2014). The three methods commonly used in wastewater treatment i.e. physical, chemical and biological methods (Mondal et al., 2017). Most of the treatment systems are simple to use and their disadvantage is high cost and disposal problems. The conventional methods for treating dyes from textile wastewater are explained as follows: (Khodaie et al., 2013)

2.4.1.1 Physical Method

Removing of MB dye molecules through physical methods are usually straightforward methods commonly accomplished by the mass transfer mechanism (Yadav et al., 2022). Some physical methods are adsorption, coagulation or flocculation, ion exchange, irradiation, membrane filtration, nano filtration or ultra-filtration and reverse osmosis. These methods are often chosen for its simplicity, efficiency and least amount of chemical requirement (Fito et al., 2020). However, its disadvantages are high pressure-demanding, the generated sludge has to be separately handled making the processes relatively expensive, low decolorization efficiency and less feasible for large-scale treatments (Chonsakorn et al., 2019).

2.4.1.2 Chemical Method

Chemical methods are the most common and efficient approaches in decolorization of dye containing textile wastewater. In this process the dye molecules are removed or degrade from a given wastewater by the addition of chemicals i.e. lime aided with aluminum sulfate. Some chemical dye removal methods include advanced oxidation process, electrochemical destruction, Fenton reaction dye removal, oxidation, ozonation, photochemical process and ultraviolet irradiation (Sakamoto et al., 2019). The undesirable characteristic of this method is the generation of secondary water pollution problem and high operating cost (Fobiri, 2022).

2.4.1.3 Biological Method

Biological wastewater treatment is designed to degrade pollutants dissolved in effluents by the action of microorganisms. During removal of dye molecules from a given wastewater the microorganisms uses the pollutant compounds as a nutrients. The efficiency this method mainly depends on the amount of dissolved mater (waste), microorganisms load, temperature and the amount of organic loading rate etc. (Katheresan et al., 2018). This treatment is carried out in activated sludge and rotating biological contactor in the presence of microorganisms i.e. yeasts, bacteria, fungi and algae (Lellis et al., 2019). There are some drawbacks in this approaches such as requiring of a large land area for operation, sensitivity of process variation as well as toxicity of some chemicals, sludge formation and less flexibility in design (Contreras et al., 2019).

2.5 Photocatalytic Process

Advanced oxidation processes (AOPs) are the most attractive and favorable option for the effective removal of organic pollutants from a given wastewater (Mondal et al., 2017). It involves the use of powerful oxidizing intermediates (e.g., the hydroxyl radical, •OH) that can oxidize and degrade primary toxic organic pollutants into non-hazardous compounds (CO_2 and H_2O). Most of the commercially viable AOPs used photochemical processes (i.e., ultraviolet (UV) or visible light) to generate •OH radicals (Samadi et al., 2016). Hydroxyl radicals are effective in the destruction of organic chemicals due to they are rapidly reactive electrophiles (Wang et al., 2022). Their oxidation potential is quantified as 2.80V and this makes them to exhibit faster rates of oxidation reactions compared to conventional oxidations. Once the hydroxyl radicals are generated, they are able to attack organic chemicals through electron transfer, hydrogen abstraction and radical combination (Mayyahi and Al-asadi, 2018).

Among AOPs, semiconductor mediated heterogeneous photocatalysis is a promising technique, which is valuable for environmental and energy applications (Akram et al., 2016). Owing to its advantages such as low cost, non-toxic, complete mineralization and reusability; it has become a fast growing research area in the past decades (Sievers, 2011). In this process, the photo-excitation of semiconductor surfaces using ultraviolet or visible radiation can be generating photo-activated electron-hole pairs. Then the electrons (e^-) are migrating to the conduction band and holes (h^+) are produced in the valance band (Figure 2.9). The photogenerated electrons and holes are responsible to react with the electrophilic (electron deficient species) and nucleophilic (electron-rich species) organic pollutant absorbed on the photocatalyst surface, respectively (Nova et al., 2009).

$$\text{Semiconductor} \xrightarrow{h\nu} \text{electron (-) +hole (+)} \xrightarrow{\text{Recombination}} \text{semiconductor + heat}$$

$$\text{Electron (-) + electrophilic molecules} \longrightarrow \text{product A} \quad (1)$$

$$\text{Hole (+) + nuceophilic molecules} \longrightarrow \text{product B} \quad (2)$$

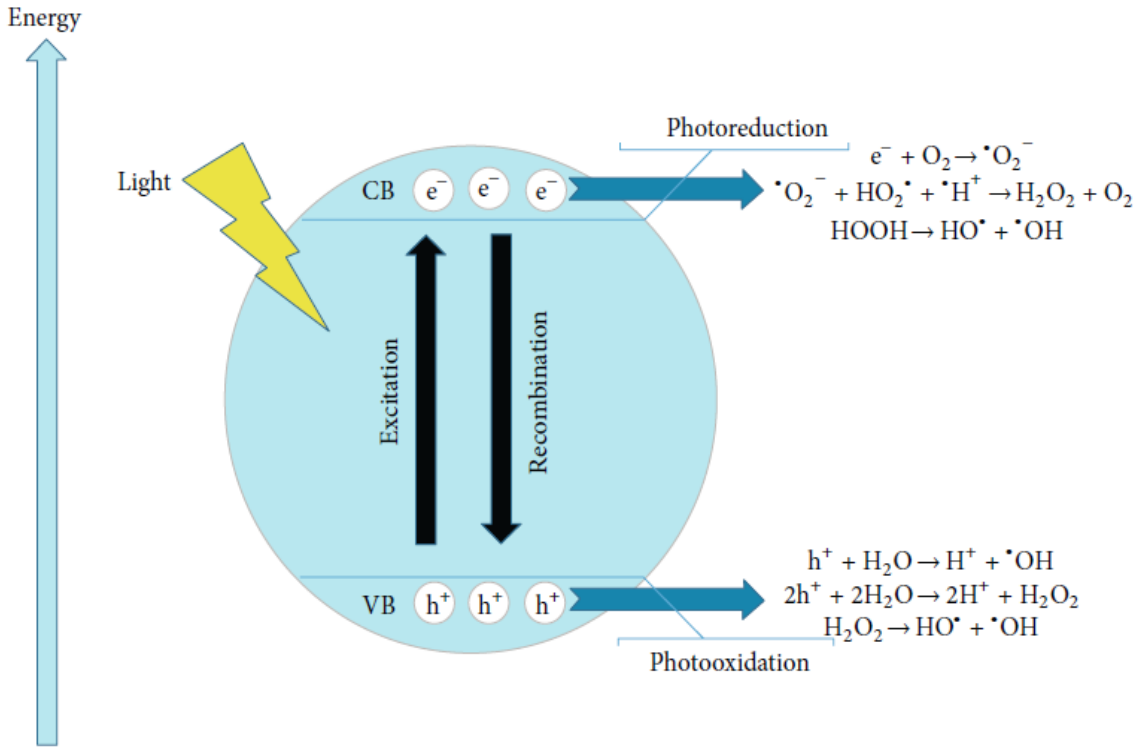

Figure 2.9 Schematics of principle of photocatalysis.

Some notable semiconductors applied as photocatalysts are included Titanium dioxide (TiO_2), Zinc oxide (ZnO), Cadmium sulfide (CdS), Tungsten trioxide (WO_3), Tin oxide (SnO_2), Zinc sulfide (ZnS), Cadmium telluride (CdTe), Ferric oxide (α-Fe_2O_3), Niobium silver trioxide ($AgNbO_3$) and Strontium titanate ($SrTiO_3$) (Azzaz et al., 2021).

2.5.1 Zinc Oxide

Zinc Oxide (ZnO) is a semiconductor compound whose ionicity resides at the borderline between the covalent and ionic semiconductors (Sharma and Nain, 2017). It exists in wurtzite, rock-salt, and zinc-blende crystal structures. Under ambient conditions, wurtzite phase is thermodynamically stable and mostly used as photocatalysts due to its excellent optoelectronic (emitting, modulating, transmitting, and sensing light) properties (Morkoç and Özgür, 2009). Additionally it has high biocompatibility behaviors and environmentally friendly nature. The ZnO crystal structure can be exists in the form of cubic rock salt, cubic zinc blende and hexagonal wurtzite as shown in Figure 2.10 and the shaded gray and black spheres denote Zn and O atoms, respectively (Song et al., 2018).

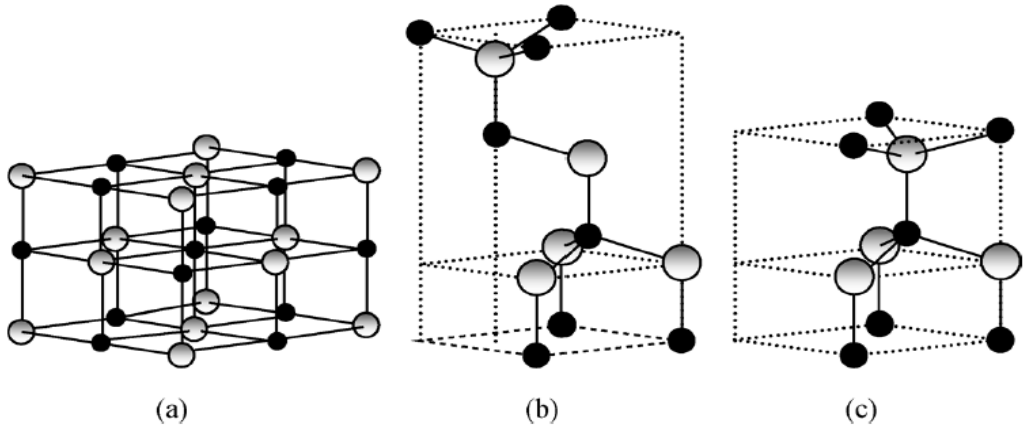

Figure 2.10 Types ZnO crystal structures: (a) cubic rock salt, (b) cubic zinc blende, and (c) hexagonal wurtzite (Jemal et al., 2017).

However, the photocatalytic performance of ZnO is limited under UV light radiation due to having a wide band gap (E_g = 3.37 eV), which is greater than photon energy (hv). Therefore, considerable effort has been applied to extend the photo-response of ZnO into visible-light region (~43% of solar spectrum). To harvest the visible solar radiation, reduction of the band gap of ZnO nano structure is one of the main strategies for removing organic pollutants (Mohamed et al., 2022).

2.5.2 Modification Strategies

The efficiency of photocatalysis depends upon harvested region of the solar spectrum by ZnO nanostructures and the lifetime of the generated electron-hole pair. As ZnO is a wide band gap semiconductor and its band gap is in UV region. To improve the photocatalytic efficiency of ZnO under visible light, two major approaches have been employed.

i) Surface modification by coupling with a narrow band gap semiconductor and
ii) Band gap engineering by doping metals or nonmetals.

Doping with metals and nonmetals is being widely considered to extend the absorption wavelength range of ZnO through modifying the electronic band structure in the visible-light spectrum to increase the photocatalytic activity (Ashebir et al., 2018). Generally, narrowing of ZnO band gap through doping of metal or nonmetals (see Figure 2.11) can be achieved by three main approaches, these are: -

a) The elevation of the valence band maximum,
b) Lowering of the conduction band minimum, and
c) Introduction of localized energy levels within the band gap.

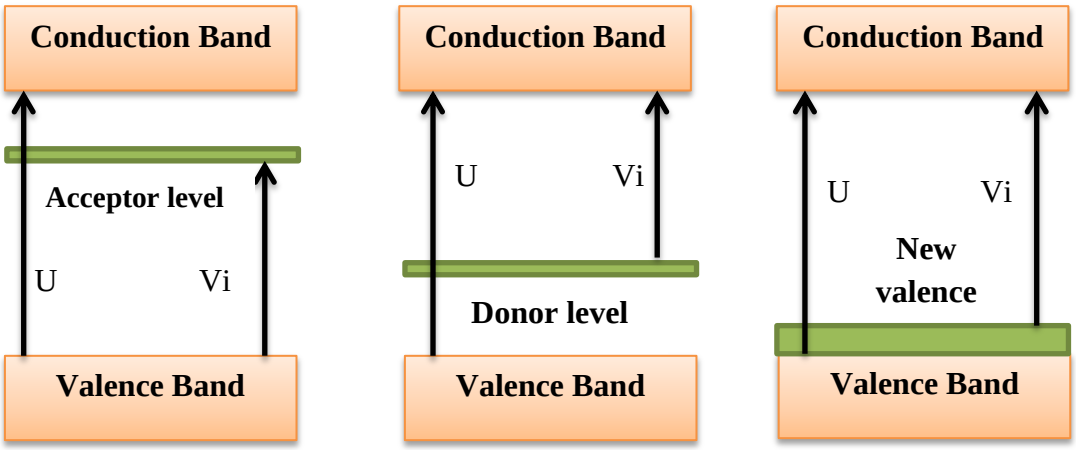

Figure 2.11 The three situations for achieving visible-light driven photo catalyst (Kamarulzaman et al., 2015)**.**

2.5.3 Zinc Oxide Band Gap Reduction with Silver

Some transition metals such as Iron, Cobalt, Nickel, Manganese, Silver and Copper can be useful to increase the activity of ZnO photocatalysts under visible light for degrading organic compounds (Silva et al., 2013). Silver (Ag) is an interesting material to modify the optical properties and enhance the photocatalytic activity of ZnO nanostructures (see Figure 2.15) by creating an acceptor levels inside the ZnO energy band gap (Sang-aroon et al., 2015). It can generate an effective Schottky barrier at the junction interface, supporting electron capture, thereby increasing the separation efficiency of electron-hole pairs and boost visible light harvesting capability (Srithar et al., 2017). In the Ag-Zn doped on ZnO nanostructure, a new acceptor state is created above the VB. Therefore, electrons can be excited from the VB to this gap state, which leads to a visible-light absorption edge (Thakur et al., 2020). These can be explained by the following reactions:

$$ZnO + hv \longrightarrow ZnO\ (e^{+}) + h^{+} \quad (1)$$

$$ZnO\ (e^{+}) + Ag \longrightarrow ZnO + Ag\ (e^{-}) \quad (2)$$

$$Ag\ (e^{-}) + O_2 \longrightarrow O_2^{-} + Ag \quad (3)$$

$$ZnO\ (h^{+}) + H_2O \longrightarrow ZnO + H^{+} + \bullet OH \quad (4)$$

$$(O_2^{-} + \bullet OH) + MB \longrightarrow \text{Intermediate products} \quad (5)$$

$$(O_2^{-} + \bullet OH) + \text{Intermediate products} \longrightarrow CO_2 + H_2O \quad (6)$$

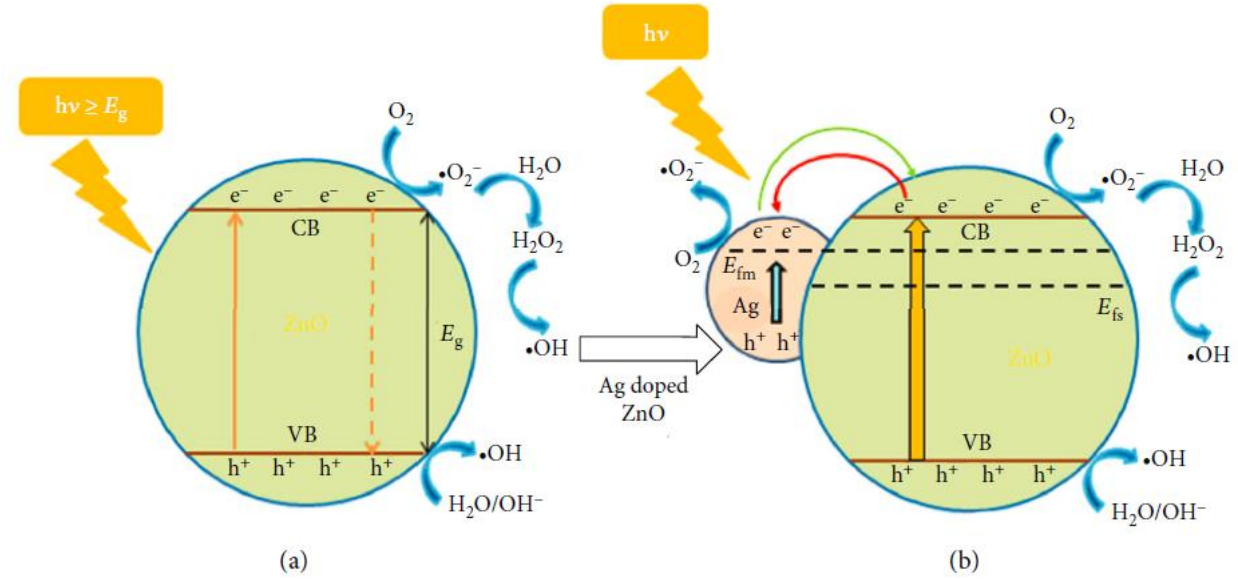

Figure 2.12 (a) Photocatalytic mechanism using pure ZnO NPs, (b) Photocatalytic mechanism using Ag@ZnO NPs (Pham et al., 2020).

2.5.4 Green Synthesis of Nano Particles

Green synthesis of nanomaterials as a valuable alternatives route to the chemical methods for the preparation of NPs using natural sources including plant materials, microorganisms, and various bio-wastes (Lau et al., 2020). Among the different synthesis methods, plant mediated NPs developing methods are considerably preferred for biosynthesis of noble metal NPs (Chauhan et al., 2020). Plant extracts offers a simple and cost effective approach to synthesis NPs at large scale. The plant extract play an important role as a reducing and capping agent. Plants possess rich genetic variability with respect to number of biomolecules and metabolites like protein, coenzymes, based intermediates, phenols, flavonoids, and carbohydrates. These plant metabolites contain hydroxyl, carbonyl, and amine functional groups that react with metal ions and reduce their size in to Nano range (Iravani, 2011).

2.6 Bionanocomposite

Bio-Nano composite (BNC) is also called "green composites," or, "bio-hybrids" that naturally occurring polymer (biopolymer) in mix with an inorganic nanomaterials, and appearing no less than one measurement on the nanometer scale (Shchipunov, 2012). It is a composite substances composed of organic or natural, biodegradable polymer, and nanomaterials (nano fillers). BNCs are significant due to their Nano scale dispersion with size less than 1,000nm (Youssef et al., 2019). Dimensionality assumes a basic part in deciding the properties of issue. The nanostructure

of a material is the key factor in the advancement of novel properties and in controlling the structure at the nano level. Nanotechnology is in this way an exceedingly encouraging field of the twenty-first century. It is required to thoroughly rebuild the innovative applications in the fields of semiconductors, inorganic, and additionally natural materials, vitality stockpiling, and biotechnology (Mousa et al., 2016). Some components of BNC are biomaterials, cellulose, nanoparticles, poly lactic acid (PLA), nanotubes, etc. (Zayed et al., 2021):

2.6.1 Method of Preparation of Bionanocomposite

Among the different BNC preparation method, the followings are some of the major:

- **Solution intercalation:** In this method, the bio-polymer such as starch and protein is added into the solvent i.e. water, chloroform or toluene and the inorganic nano fillers are swollen in a solvent. Then, the biopolymer and solution of swollen NPs are mixed, then after polymer chains intercalate and displace the solvent within the interlayer of the NPs. Upon solvent removal, the intercalated structure remains, resulting in a formation of biopolymer/ layered NPs BNC (Fernando et al., 2019).
- **Magnetically stir:** This method is simple and cost effective in the presence of capping reagents i.e. ethanol, acetic acid, citric acid etc. In this method the NPs combined with biopolymer under vigorous magnetic stir for 8-12hr to forms bionanocomposite.
- **Melt intercalation:** it is a standard method for the preparation of polymer/layered NPs BNC. There are many advantages compared with solution intercalation and in situ intercalative polymerization. In this method, the polymer is heated at specific temperature to get a molten mass and mixed with NPs (Justin et al., 2018).

2.6.2 Application of Bionanocomposites

BNCs have various applications due to its simplicity, better reinforcement and cost effectiveness (John, et al, 2017). Some applications of bionanocomposites are:

- Good candidates for catalysts, gas-separation membranes, contact lenses and bioactive implant materials.
- It used in fabrication of scaffolds, implants, diagnostics and biomedical devices and drug-delivery systems.
- It used in the cosmetics industries.
- In tissue engineering, drug and gene delivery, wound healing and bio imaging.
- For wastewater treatment.

2.7 Gaps in Literature Reviewed

In the review of related literature, it was found that a lot of studies had been done on the environmental impacts of the WH weed and colored MB containing textile wastewater mainly damaging of the water quality and its creatures (Kharat, 2015). But no studies had been done on converting of this aquatic weed into nanomaterials and used it for the application of colored textile wastewater treatment. Both water related problems were still a major challenges of the world that potentially damages the limitted water resources.

Review of literature related to WH (Agengo, 2013; Akendo et al., 2008; Chonsakorn et al., 2019; Enyew et al., 2020; Worku & Sahile, 2017) indicated that it is the most dangerous and worst invasive aquatic weed in the world and negatively affecting millions of water resources, fisheries, transportation and social structure (Hailu & Degaga, 2019). It caused wastage of water through excessive evapotranspiration, recreational use of aquatic ecosystem, and poses of mechanical damage to hydroelectric systems. This weed also responsible for drastic changes in the fishery communities of water environments and acts as an agent for the spread of serious diseases in water bodies (Gopal, 1987). To overcome this problem, some researchers the integrated management program which involving mechanical, manual and chemical measures was implemented but the spread of the weed in different part of water bodies of Ethiopia was continued. For effective management of WH weed, there is need for cost wise, sustainable, environmental friend, and flexible approaches (Tanpichai et al., 2019).

On the other hand, other studies (Bailey et al., 2022; Kumaran et al., 2020; Šmelcerović, 2019) related to textile wastewater were reported that the effluent contains high amounts of agents causing damage to the environment and human health including suspended and dissolved solids, biological oxygen demand (BOD), chemical oxygen demand (COD), chemicals, odour and colour. In addition, it is responsible in degrading the water quality by releasing their effluents directly in canals, river, lakes and oceans that is harming our planet to the point, where organisms are dying at a very frightening rate. It is reported that the presence of dye compounds in water, that inhibit the activity phothosynthesis and aqua-lives (Gupta et al., 2015). This study mainly focused changing of this water damaging and invasive aquatic weed into valuable product and used as a solution in textile industries to save limited fresh water from pollution. In addition, it can open the opportunities to reduce WH invasions with minimum cost.

CHAPTER THREE

3. Materials and Methods

3.1. Raw Materials, Chemicals and Equipment

3.1.1 Raw Materials

In this study the main raw material used for experimental work was WH (Eichhornia crassipes) plant. Initially, the sample was collected from Lake Tana, North-Western Amhara region, Ethiopia. It is located about 350 miles from Addis Ababa. This aquatic weed potentially one of natural sources that contain high cellulose content approximately 40% in its stem which used as a major raw material to develop CNCs. Additionally, its leaves were used as a natural reducing and capping agent during Ag@ZnO NPs synthesis.

3.1.2 Chemicals and Reagents

Major Chemicals and reagents used in this thesis work were listed in Table 3.1 and all chemicals used in this experimental work have high analytical grade.

Table 3.1 Major chemicals and reagents that were used in the experiment

Chemicals	Sources	Uses
Absolute ethanol (99%)	Cherkose chemical suppliers	Removing extractive materials
Hexane	Cherkose chemical suppliers	To remove non-polar components
Sodium hydroxide (NaOH)	Wise team chemical supplier	To remove hemicellulose and some amount of lignin content
Acetic acid	Wise team chemical supplier	pH adjustment and as capping agent during BNCs synthesis
Hydrogen per oxide (H_2O_2)	Wise team chemical supplier	To remove colored lignin from the cellulose.
Sulfuric acid (H_2SO_4)	Cherkose chemical suppliers	For the removal of amorphous regions from cellulose fibers
Zinc acetate	Cherkose chemical suppliers	Used as Zinc precursor
Silver nitrate	Cherkose chemical suppliers	Used as silver precursor

3.1.3 Equipment and Instruments

In this thesis the equipment and instruments i.e. electronic beam balance, grinder, muffle furnace, magnetic stirrer, deep freezer, shaker, centrifuge, sieve, soxlet apparatus, pH meter, oven, tray dryer, desiccator, beaker, measuring cylinder, crucibles, spatula, conical and round bottom flasks and heating mantel were used to synthesis a bio-nano composite. Furthermore, some advanced analytical instruments i.e. UV-Vis spectrophotometer, FTIR, XRD, TGA, BET, DLS, and SEM-EDX were used for characterization of the samples.

3.2 Methods

3.2.1 Isolation of Cellulose

To extract and purify cellulose material from WH stem, the raw sample was passed through different pretreatment stages. The major pretreatments i.e. size reduction, extraction of non-cellulosic components, alkaline treatment, and bleaching were performed for the removal of impurities that was found in the WH stem.

3.2.1.1 Size reduction and De-Waxing Process

The stem and leaves were separated from other parts of the weed by using laboratory knife. Then, the isolated stem and leaves were washed repeatedly with distilled water to remove dusts and unwanted impurities and then allowed the sample to dry at room temperature. The air dried stem and leaves of WH was chopped, grinded and sieved using 60-mesh (250 μm) sieve separately. The obtained powder was sealed in the plastic (polyethylene) bag and stored in desiccator until using it for further characterization and de-waxing process. Then after, the powdered WH stem was de-waxed in a soxhlet apparatus using mixture of hexane and ethanol solvents with the ratio of 2:1 (v/v) at 80 ^{0}C for 6hr to remove extractive components i.e. wax, pectin and oils. During de-waxing process the solid to liquid ratio were 1:20 (w/v). Then the de-waxed powder was washed with distilled water and ethanol repeatedly. Then after, the washed sample was filtered and finally dried in oven at 80 ^{0}C for 6hrs (Nicolas et al., 2015).

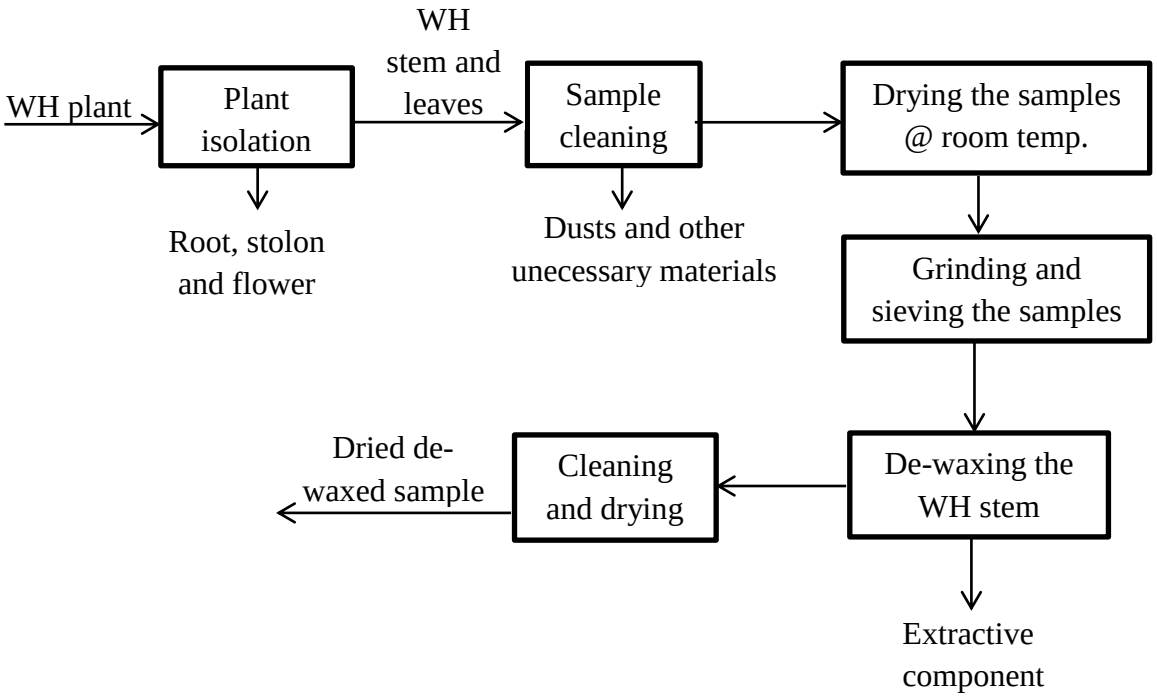

Figure 3.1 Process flow diagram of sample preparation and solvent extraction

3.2.1.2 Alkaline Treatment

In this step sodium hydroxide (NaOH) was commonly used to remove hemicellulose components from de-waxed sample. In addition, this process increase the surface roughness of the sample for better mechanical interlocking (Germiel et al., 2020). The de-waxed sample was treated with 4% NaOH (wt/v) solution at 80 ^{0}C for 3hr using magnetic stirrer under constant agitation at 500rpm. The ratio between solid to liquid was 1:20 (g/ml) (Mustikaningrum et al., 2021). Then the alkaline treated sample was repeatedly washed with distilled water until neutral pH obtained. Successive centrifugation at 8000rpm was also performed during washing process. Then after, the clean alkaline treated sample was dried in the oven at 80 ^{o}C for 6hr and then the dried sample sealed in plastic bag and kept in desiccator until use for further characterization and application (Barbash et al., 2019).

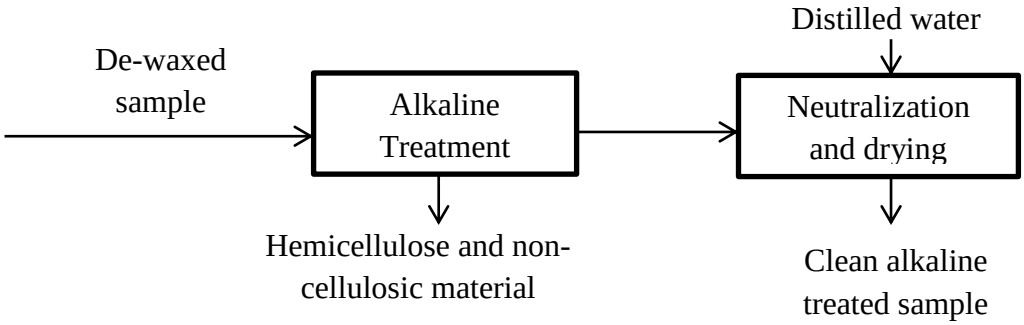

Figure 3.2 Process flow diagram of alkaline treatment

3.2.1.3 Bleaching of Cellulose

The dried alkaline treated sample bleached by using a mixture of 8% (v/v) H_2O_2 and 0.07 M NaOH solution under vigorous stir. During bleaching process the solid to liquid ratio was 1:30 (g/v). This process performed twice with magnetic stir at 80 ^{0}C for 50min to remove the colored lignin and remaining hemicellulose content from the sample (Pratama et al., 2020). Then after, the bleached sample repeatedly washed and centrifuged with distilled water until it achieved neutral pH. Finally, the obtained white cellulose was dried in oven at 80^{0}C for 6hr and the dried sample sealed in plastic bag and stored in desiccator until use for further characterization and application (Mustikaningrum et al., 2021).

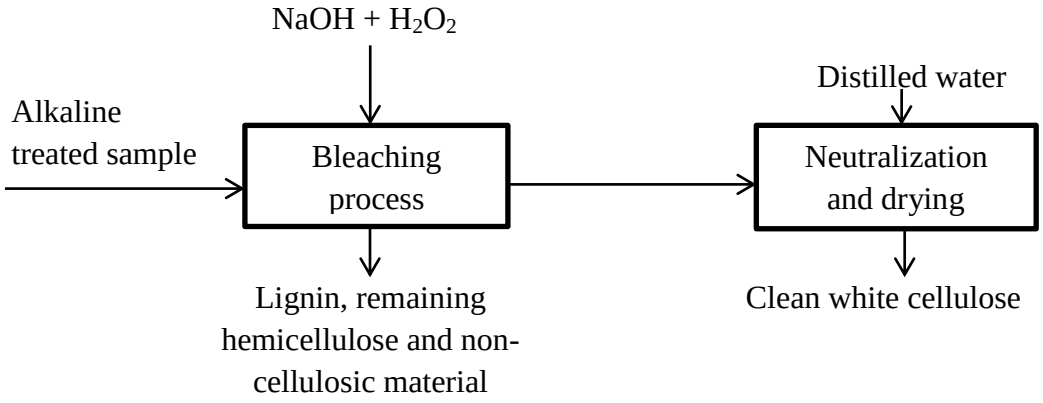

Figure 3.3 Process flow diagram of bleaching process

3.2.2 Synthesis of Cellulose Nano Crystals

The CNCs were synthesized by controlled acid hydrolysis method using 30 % of H_2SO_4. The sample and acid mixture was vigorously stirred at 45 °C for 30 min. The solid to liquid ratio was 1:8.75 (g/v). Then after, add excessive amount of cold distilled water immediately into the suspension to quench the reaction (Modi & Fulekar, 2020). The cold suspension was continuously diluted and centrifuged using cold distilled water until it became neutral pH. Then the neutral suspension was kept in a deep refrigerator for 72hr to form crystals. Finally the obtained CNCs were dried using oven at 80 ^{0}C for 6hr and stored in plastic bag until use for further characterization and application (Barbash et al., 2019).

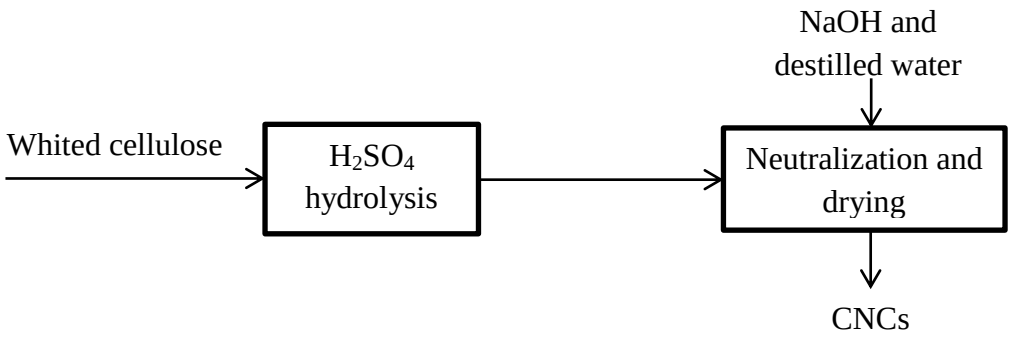

Figure 3.4 Process flow diagram of H_2SO_4 hydrolysis

3.2.3 Synthesis of Water Hyacinth Leaf Extract

In case of aqueous filtrate preparation, 15g of powdered water hyacinth leave was weighed and added into 500ml distilled water then stirred at 50 ^{0}C for 1hr (Aragaw et al., 2020). And then, the resulting solution was filtered and the plant extract was kept for NPs synthesis. The WH leaf extract play an important role during NPs synthesis as a reducing and capping agents. That used to reduce the particle size by increasing the surface area of the material and act as stabilizers that inhibit the over-growth of NPs which prevent their aggregation/coagulation in colloidal synthesis (Javed et al., 2020).

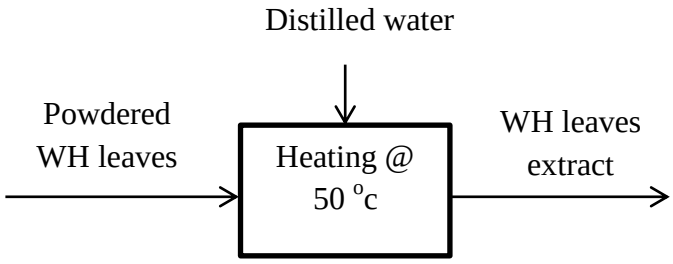

Figure 3.5 Process flow diagram of WH leaves extraction

3.2.4 Synthesis of Silver Doped Zinc Oxide Nanoparticles

For the preparation of silver doped Zinc Oxide (Ag doped ZnO) nanoparticles, 0.5M of zinc acetate and 0.02M of silver nitrate solution was prepared in 100ml and 50ml distilled water, respectively. Then the two solutions were poured in 500ml round bottom flask and magnetically stirred at 40^{0}C for 15min. Then after, 5ml solution of 0.2M NaOH was added into the previous solution and stirred for 50 min. Then, 20 ml of WH leaf extract was added into the solution and stirred for 2hr (Thakur et al., 2020). After the addition of leaf extracts, the brown colored precipitates were observed in the solution. The obtained precipitates were collected using a

centrifuge and washed 5 times with distilled water for the removal of impurities. The purified NPs were dried at 80^0C for 6hr and then calcinate using a muffle furnace at 500 ^{0}C for 3hr. Finally the whitish Ag@ZnO NPs was collected and stored in glass sample holder until use for further characterization and application (Alterz & Mohammed, 2022).

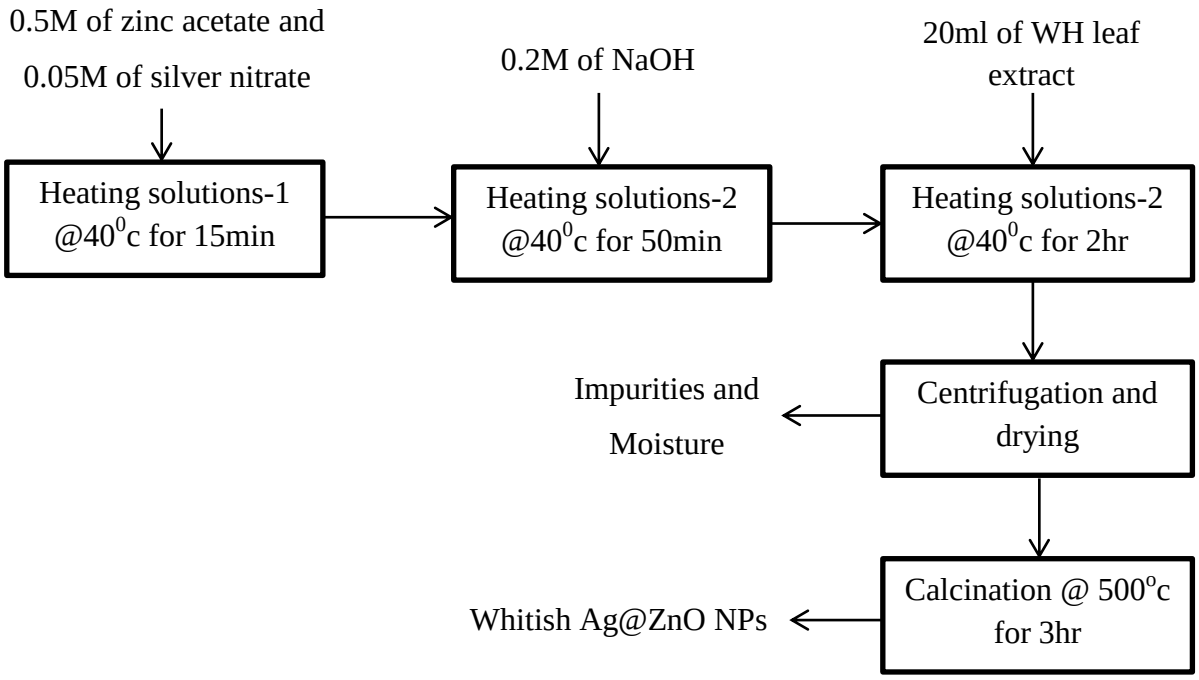

Figure 3.6 Process flow diagram of Ag@ZnO NPs synthesis

3.2.5 Preparation of CNCs/Ag@ZnO Bionanocomposites

To develop CNCs/Ag@ZnO BNCs, three different CNCs to Ag@ZnO composite ratios (g/g) i.e. CNCs/Ag@ZnO (1:1), CNCs/Ag@ZnO (1:0.5) and CNCs/Ag@ZnO (0.5:1) BNCs were synthesized to investigate the optimum BNC ratio. First, 1g of CNCs and 1g of Ag@ZnO NPs were taken and then each measured sample was stirred with 1% acetic acid solution separately for 30min (Mousa et al., 2016). Then mixes the two solutions and vigorously stirred for 12hr to develop a BNC. After that, the solution was centrifuged at 8000rpm for 15min and washed with distilled water several times (Youssef et al., 2019). The clean BNC was dried at 80 °C for 6hr. The obtained BNCs were kept in plastic sample holder for further characterization and application. The same procedure was repeated for the left BNC ratios.

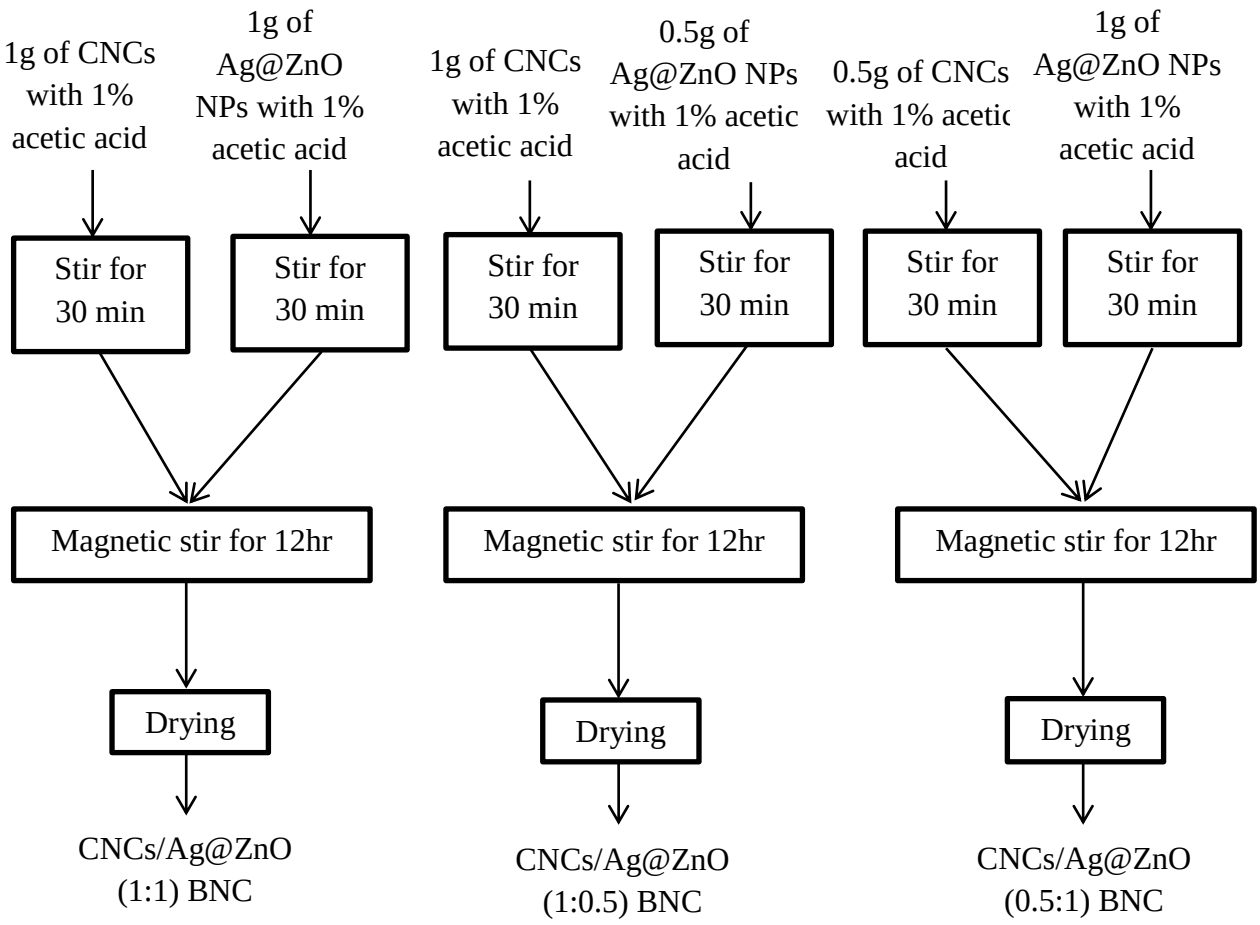

Figure 3.7 Process flow diagram of BNCs synthesis

3.3 General Processs Flow Diagram of Bionanocomposites Photocatalyst Synthesis

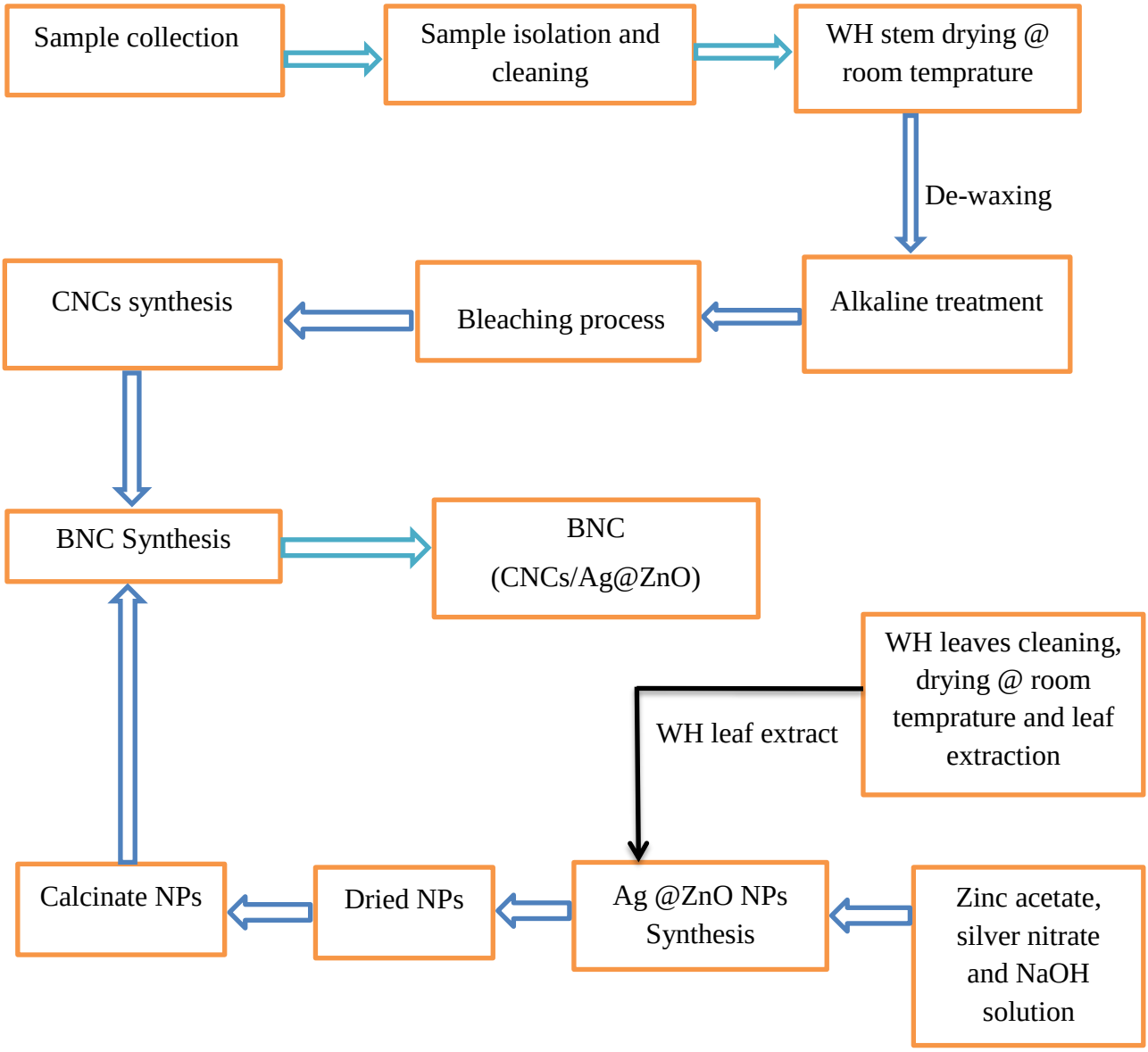

Figure 3.8 General process flow diagram of CNCs/Ag@ZnO BNC synthesis

3.3 Characterization of Materials

3.3.1 Proximate Analysis of WH

Proximate analysis is the process of identifying the amount of elements contained in a plant or compound. It covers the determination of moisture, and ash content on an as-received basis (Bronzato et al., 2017).

3.3.1.1 Moisture Content

Measurement of moisture content of WH stem was carried out by weighing about 5g of air-dried sample into a crucible and drying it in an oven preheated to temperatures of 100 $\pm$ 5^0C for 1hr. Then the dried sample was placed in a desiccator until cooled and weighted again. The dry basis moisture content of the sample was then calculated using Eq. (1).

$$\text{Moisture (\%)} = \frac{S_1 - S_2}{S_1} * 100 \quad \text{(1)}$$

Where: S_1 = mass of air-dried sample (g)

S_2 = mass of the oven dried (g)

3.3.1.2 Ash Content

The ceramic crucible was placed in the muffle at a temperature of 575^0C for 1hr. The crucible was removed and, after cooling in desiccator, put the oven dried sample in the crucible and calcinate using muffle furnace at 575°C for 3hr. The ash content was determined by Eq. (2).

$$\text{Ash content (\%)} = \frac{M_o}{M_i} * 100 \quad \text{(2)}$$

Where: Mo = mass of the obtained ash (g)

M_i = mass of the initial sample (g)

3.3.2 Compositional Analysis of Water Hyacinth Stem

3.3.2.1 Extractive Content

The total extractive content in water hyacinth stem was determined by taken 5g of air dried sample and extracted with a mixture of ethanol-hexane (1:2) using Soxhlet apparatus for 6hr. Then the samples were removed from soxhlet apparatus and then washed the sample with distilled water several times until the solvent removed. Then the sample dried using blast oven at 80 ^{0}C for 6hr. The determination of extractive content in WH stem was performed according to Eq. (3) (Sukarni et al., 2019).

$$\text{Extractive content (\%)} = \frac{W_1 - W_2}{W_1} * 100 \quad \text{(3)}$$

Where: W_1 = mass of air-dried sample (g)

W_2 = mass of oven dried extracted sample (g)

3.3.2.2 Determination of Hemicellulose

The hemicellulose content of the sample was analyzed using dried de-waxed WH stem. First, the sample was transferred into a 500mL Erlenmeyer flask and 150 mL of 4% NaOH (w/v) was added into the flask. The mixture was heat up at 80 ^{0}C for 3hr under a constant agitation by using magnetic stirrer. The ratio between de-waxed sample to NaOH solution is 1:20 (g/ml). After that the alkaline treated sample was washed and centrifuged repeatedly with distilled water until neutral pH achieved and non-cellulose materials removed. Then, the sample was transferred into the oven at a temperature of 80ºC for 6hr. The hemicellulose content present in WH stem was calculated by using Eq. (4) (Idrees et al., 2013).

$$\text{Hemicellulose content (\%)} = \frac{M_d - M_a}{M_d} * 100 \qquad (4)$$

Where: M_d = mass of initial de-waxed sample (g)

M_a = mass of oven dried alkaline treated sample (g)

3.3.2.3 Determination of Lignin

The lignin content in WH stem was determined based on ASTM D 1106-96 (2013) standard (Sukarni et al., 2019). First, the 8% (v/v) H_2O_2 and 0.07M NaOH solution was prepared and poured into round bottom flask to remove colored lignin content. Then the obtained oven dried alkaline treated sample was mixed with 60ml of alkaline-peroxide solution and stirred the mixture at 70^{0}C for 40min using magnetic stirrer. Then after, the de-lignified sample was repeatedly washed and centrifuged using distilled water. This process was repeated twice for better de-lignification. Finally, the sample was oven dried at 105℃ until a constant mass is achieved. The amount of lignin content was determined in Eq. (5) (Idrees et al., 2013).

$$\text{Lignin content (\%)} = \frac{M_1 - M_2}{M_1} * 100 \qquad (5)$$

Where: M_1= mass of dried alkaline treated sample (g)

M_2= mass of oven dried sample after bleaching process (g)

3.3.2.4 Determination of Cellulose

Cellulose content in the WH stem was determined using Eq. (6) by calculating the difference of extractives, hemicellulose, and lignin components of sample from 100% (Idrees et al., 2013).

$$\text{Cellulose content (\%)} = 100 - (EC + HC + LC) \qquad (6)$$

Where: HC = hemicellulose content (%)

LC = lignin content (%)

EC = extractives content (%)

3.3.3 Yield

The analysis for the determination of the CNCs content followed the methodology of TAPPI 203 om-99 (Liu et al., 2015). To estimate the CNCs yield first, filter the suspension and then dried using oven for 12hr at 85℃. Subsequently, the oven dried CNCs sample was weighed using analytical balance. The yield of CNCs was determined using Eq. (7).

$$\text{Yield (\%)} = \frac{M_1}{M_2} * 100 \quad \text{(7)}$$

Where: M_1 = mass of oven dried CNCs (g)

M_2 = mass of bleached cellulose (g)

3.3.4 UV-Vis Spectrophotometer

UV-Vis Spectroscopy is a quantitative technique used to measure how much a sample absorbs light (Tamgadge et al., 2018). This is done by measuring the intensity of light passes through the samples with respect to the intensity of light through a reference sample or blank (Kamarulzaman et al., 2015). The band gap of Ag@ZnO NPs was determined by Eq. (8).

$$E_g = \frac{1240}{\lambda} \quad \text{(8)}$$

Where: E_g = Energy band gap (eV)

λ = Wavelength of light (nm)

In addition, the absorption of WH stem, bleached cellulose, CNCs, CNCs/Ag@ZnO (1:1), CNCs/Ag@ZnO (1:0.5) and CNCs/Ag@ZnO (0.5:1) BNCs were studied using OPTIZEN POP UV-Vis spectrophotometer model by dispersing each sample in distilled water. Moreover, the absorbance of the sample after each irradiation time (i.e. 0, 30, 60, 90, 120, 150, and 180min) was recorded by placed the solution in the cuvette and scanned with UV-Vis spectrophotometer in the specific range of wavelength from 400 - 800nm. It used to determine the remaining MB dye molecules after Photodegradation process using CNCs/Ag@ZnO (1:1), CNCs/Ag@ZnO (1:0.5) and CNCs/Ag@ZnO (0.5:1) BNCs.

3.3.5 Fourier Transform Infrared Spectroscopy

Fourier transform infrared spectrometer (FTIR) is an analytical technique used to identify polymeric, organic and inorganic materials that present in a given sample. In addition to that it's studying the change of the functional groups of a given sample before and after chemical treatment and production process. FTIR spectra of WH stem and leave, bleached cellulose, CNCs, Ag@ZnO NPs, and the three synthesized BNCs were scanned at wavenumbers in the range of 399-4000 cm^{-1} with 0.964233cm^{-1} data interval and measured at 4cm^{-1} resolution with 64 repeated scans. The background was recorded at the beginning of the measurement. The samples FTIR spectra were obtained using Perkin Elmer FTIR spectrometer (Perkin Elmer, 65, USA) at Bahirdar Institute of Technology (Bahirdar, Ethiopia).

3.3.6 X-ray Diffraction

X-ray diffraction (XRD) was used for the determination of samples crystallinity and it shows cellulose amorphous region is hydrolyzed or not (Isai and Shrivastava, 2019). The XRD analysis of WH stem, bleached cellulose, CNCs, Ag@ZnO NPs, and the three synthesized BNCs were done at Adama science and Technology, School of Materials Science and Engineering using DW-XRD-Y7000 model. In addition, to compare the XRD patterns of pure ZnO NPs and Ag@ZnO NPs, plant extract mediated ZnO NPs were synthesized. First, 170 ml of 2 mM zinc nitrate solution was prepared and kept in stirrer for 50min. Then 50 ml of 0.1 M NaOH solution was added in the solution and stir for 3hr. Then, the 30 ml of WH leaves extract solution was added drop wise to the above solution under constant stirring condition. The color of the reaction mixture was changed after 30min. The solution was left in stirred for 4hr, and then after the resulted precipitate was separated from the reaction solution by centrifugation at 8000 rpm for 15 min by washing several times with distilled water followed by ethanol to remove organic impurities and the pellet was collected. Finally, the pellet was dried and preserved plastic sample holder for further characterization studies.

To examine the crystallinity of a given samples using XRD device initially, the samples were dried using oven for 24h at 100°C to remove the moisture content completely. Then after, the dried samples were prepared in powder form and scanned by varying the 2θ range from 5 to 85º and operated at an acceleration voltage of 40 kV, scanning rate 2 (deg/min), current 30 mA and using Cu Kα radiation (λ = 0.1540 nm). The crystallinity index was determined using Eq. (9)

$$\text{Crystallinity (CI \%)} = \frac{\text{Area of Crystalline peaks}}{\textit{Total area of peaks}} * 100 \qquad (9)$$

Where: Total area of peaks = the sum of the area of amorphous & crystalline peaks

Also the crystalline size of the sample can be calculated using Scherrer Equation as follows (Muniz et al., 2016): -

$$D = \frac{k\lambda}{\beta\cos\theta} \qquad (10)$$

Where: D = size of the particle

K = Scherer's constant (K=0.94)

λ = X-ray wavelength (1.54178Å)

β = full width at half maximum of the diffraction peak

θ = angle of diffraction (radian)

The d-spacing can be determined using Bragg's law in Eq. (11) (Asheville et al., 2018)

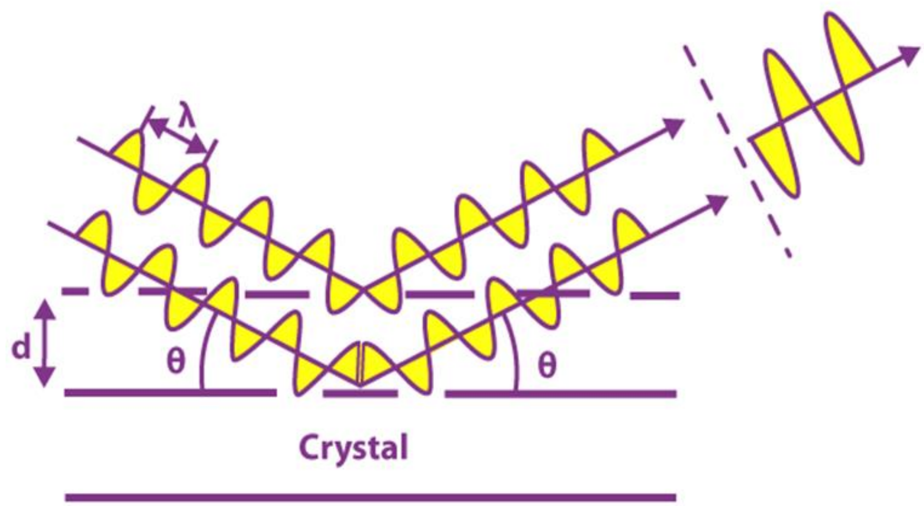

Figure 3.9 X-Ray Diffraction

$$d = \frac{n\lambda}{2\sin\theta} \qquad (11)$$

Where: d = path difference

n = order of diffraction (whole number)

λ = wave length of incident X-ray with value of 0.154060nm

θ = angle of scattering (in radian)

3.3.7 Thermo Gravimetric Analysis

The thermo gravimetric analysis (TGA) is a technique allows thermal analysis of a substance when subjected to a controlled temperature programmer. Its physical property is measured as a function of temperature or time (Kausar et al., 2019). This measurement provides information about physical phenomena, such as thermal decomposition, phase transition, absorption, adsorption, and desorption (Azizi et al., 2014). The principle of thermo gravimetric is based on measuring the changes in the mass of a substance when it is continuously being heated to elevated temperatures. In this study, thermal characterization of WH stem, bleached cellulose, CNCs, Ag@ZnO NPs, and CNCs/Ag@ZnO (1:0.5) BNC were tested by TGA-5500 model. Prior to this test, the samples were dry at 85°C for 24hr and kept in a desiccator. The thermal stability test was carried out from 10 - 900^0C at a heating rate of 10^0C/min under the inert atmosphere of nitrogen with a flow rate of 100ml/min.

3.3.8 Brunauer-Emmett-Teller

Brunauer-emmett-teller (BET) used to determine the physical adsorption of gas molecules on a solid surface and serves as the basis for an important analysis technique for the measurement of the specific surface area (m^2/g), pore size and volume of materials (Kausar et al., 2019). In this study, the adsorption–desorption experiments were studied using Quantachrome NovaWin BET model at Bahirdar Institute of Technology (Bahirdar, Ethiopia) using nitrogen gas. The used sample weight was 0.03g with 89.62 kPa gas pressure to determine the specific surface area, pore volume, and the particle size of the three synthesized BNCs.

3.3.9 Dynamic Light Scattering

Dynamic light scattering (DLS) was used to determine the range of the particle size distribution of the sample, which indicates the extent of the hydrolysis reaction. The particle size of the WH stem, bleached cellulose, CNCs, Ag@ZnO NPs, and the three synthesized BNCs were determined using zeta sizer nano series (ZE3600) at Addis Ababa science and technology university (AASTU). Each sample was dissolved with distilled water and the measurement was carryout at room temperature (25 ^{o}C) with the calibration time of 60 seconds. The obtained data was then processed by using Malvern Zeta sizer software.

3.3.10 Scanning Electron Microscopy with Energy Dispersive X-Ray

The scanning electron microscope (SEM) is a microscope that produces an image by scanning the surface the sample with a focused beam of electrons. SEM-EDX used to observe the morphological surface that closely spaced with high magnification and provide elemental identification and quantitative compositional information. The morphology of WH stem, bleached cellulose, CNCs, Ag@ZnO NPs, and CNCs/Ag@ZnO (1:0.5) BNC was carried out using FEI INSPECT F50 model with 10 kV operation voltage. The samples were placed on black carbon tape and the image was captured with various magnification level and working distance. The electrons interact with atoms in the samples, producing various signals that contain information about the surface morphology of the sample.

3.3.11 Point of Zero Charge

The point of zero charge (P_{ZC}) is generally described as the pH at which the net charge of total particle surface is equal to zero (Kausar et al., 2019). In another word it defines the pH of the solution for which the surface density of positive charge (contribution of cations) equals that of negative charges (ions) (Ahmad et al., 2019). It used to determine how easily a substrate (photocatalyst) was able to degrade harmful ions. To examine the P_{ZC} of CNCs, Ag@ZnO NPs, and the three synthesized BNCs, first 0.01 M of NaCl solution was prepared and 30ml of NaCl solution was added into each six labeled 250 ml of round bottom flasks. Then, the solution was adjusted to different pH values (2, 4, 6, 8, 10 and 12) using 0.1M NaOH and 0.1M HCl. After that fixed amount of CNCs (30 mg) was added in each adjusted solutions and then, shake for 24hr by using rotary shaker. After 24hr shaking the final pH was measured to calculate ΔpH. Finally, the surface charge of the prepared material was determined by plotted the graph P_{ZC} against the initial pH. The pH at which the curve crosses the line of initial pH was taken as pH of point of zero charge (P_{ZC}). The same experiment was conducted for Ag@ZnO NPs and CNCs/Ag@ZnO (1:1), CNCs/Ag@ZnO (1:0.5) and CNCs/Ag@ZnO (0.5:1) BNCs.

3.4 Photocatalytic Degradation Study

In this study the photocatalysis experiment was conducted using MB dye in aqueous solution as an organic pollutant to study the photocatalytic performance of the synthesized materials. Initially the photocatalytic performance of CNCs, Ag@ZnO NPs and CNCs/Ag@ZnO (1:1) BNC was investigated under light irradiation by varying pH of the dye solution at constant

sample dosage (30mg/L), MB dye concentration (10mg/L) and irradiation time (150min). It helps to select the higher photocatalytic performance material for further photocatalytic studies. Furthermore, the photocatalytic experiment was conducted using the selected sample by varying of process parameters (i.e. pH of the dye solution, BNCs dosage, MB dye concentration, and irradiation time) under light irradiation using single effect method. It used to investigate the effect of the single process parameter by considering the other parameters are constant. The suspension then exposed to solar light with constant stirring for the proper activation of the photocatalyst. The stirring rate of 600 rpm was kept fixed for all photocatalytic experiments. Then after, each sample was centrifuged at 8000 rpm for 15 min to separate the photocatalyst from the suspension. The residual MB concentration in the solution was analyzed by a UV-Vis spectrophotometer at 664 nm. All experiments were carried out in triplicate for reproducibility of results. The percentage of MB dye degradation for each experimental analysis was carried out using Eq. (12) (Sahoo et al., 2012).

$$\text{Degradation of MB (\%)} = \frac{A_o - A_t}{A_o} * 100 \text{ or } \frac{C_o - C_t}{C_o} * 100 \quad \ldots\ldots\ldots\ldots\ldots\ldots\ldots\ldots\ldots\ldots (12)$$

Where: A_0 = initial absorbance

A_t = absorbance at time t

C_0 = initial concentration MB

C_t = concentration of MB at time t

Photocatalytic degradation of MB dye is influenced by several process conditions, i.e. the pH of the aqueous dye solution, photocatalyst dosage, MB dye concentration, and irradiation time.

3.4.1 Effect of pH

To study the effect of pH, first 10mg/L of MB dye solution was prepared and 50ml of the prepared dye solution was taken and then, added into each six labeled round bottom flasks. Then, the pH of a solution was adjusted at 2, 4, 6, 8, 10 and12 using 0.1M of HCl or 0.1M of NaOH. After that, 30mg of CNCs/Ag@ZnO (1:1) was added into the solutions and shakes the suspension for 180min at room temperature using rotary shaker at 400 rpm. Finally, the fixed shaking time was completed each samples were centrifuged and measured their absorbance using UV-vis spectrophotometer. The pH with the highest degradation efficiency was taken as an

optimum pH. The same procedure was repeated for both CNCs/Ag@ZnO (1:0.5) and CNCs/Ag@ZnO (0.5:1) BNCs.

3.4.2 Effect of BNCs Dosage

To examine the effect of BNCs dosage on dye degradation efficiency, first 10mg/L of MB dye solution was prepared and then 50ml of the dye solution was taken and added into labeled beakers. After that the pH of the dye solutions were adjusted at optimum value using 0.1M of NaOH and 0.1M of HCl. Then, add 5 - 40mg/L of CNCs/Ag@ZnO (1:1) BNC in each labeled dye solution and vigorously stirred under light irradiation for 150min. After photocatalysis, the suspensions were centrifuged and measured the absorption of the sample to determine the remaining dye molecules. The same procedure was used for the left BNC ratios.

3.4.3 Effect of Methylene Blue Concentration

In this study the effect of initial MB dye concentration on dye degradation efficiency of BNC was studied at 1, 5, 10, 15 and 20 mg/L of synthetic MB dye solutions, while the pH, dosage of BNCs and irradiation time were kept as constant process parameters. The photocatalytic performance of each BNC was investigated under light irradiation. After 150min, each solution was centrifuged and measured its absorbance using UV-Vis spectrophotometer to determine the remaining dye molecules after photocatalysis.

3.4.4 Effect of Irradiation Time

The effect of irradiation time on the dye degradation efficiency of the three synthesized BNCs was examined at 30, 60, 90, 120, 150, 180, 210 and 240 min. The other process conditions i.e. the pH of the dye solution, dosage of the three BNC ratios, and concentration of MB dye was kept as constant parameters. After each irradiation time, the solution was centrifuged and measured the absorbance of the sample to determine the remaining dye molecules.

3.4.5 Kinetics Study of MB Dye Degradation

In this study, 20 mg/L dose of the BNCs were used to study the kinetics by varying the MB dye concentration from 5, 10, 15 and 20 mg/L at optimum pH= 8, 10, 10 for CNCs/Ag@ZnO (1:1), CNCs/Ag@ZnO (1:0.5) and CNCs/Ag@ZnO (0.5:1), respectively. Pseudo-first-order reaction has been widely and successfully used for photocatalytic degradation of different organic pollutants (Eldeeb et al., 2021). This is expressed in Eq. (13):

$$\ln\left(\frac{C_0}{C_t}\right) = Kt \quad \text{..... (13)}$$

Where: K = the reaction rate constant,

C_0 = the initial concentration of aqueous MB dye

C_t = the concentration of aqueous MB at the reaction time t.

t = time

3.4.6 Photocatalytic Performance Study under Dark Region

The dye degradation performance of CNCs, Ag@ZnO NPs, and CNCs/Ag@ZnO (1:1), CNCs/Ag@ZnO (1:0.5), and CNCs/Ag@ZnO (0.5:1) BNCs were examined under dark region at optimum process conditions. Initially, each sample was added in MB dye solution and stirred using magnetic stirrer under light irradiation for 40min. Then after, the suspension was stirred under dark region for 180min. Finally, the absorbance of each solution was measured within 30 min interval using UV-Vis spectrophotometer to determine the remaining dye molecules.

3.5 Response Surface Methodology Analysis

In this study, response surface methodology with Box Behnken design (RSM-BBD) method was used to assess an optimal points, process prediction by generating 2^{nd} order equation and to find a suitable approximation for the functional relationship between independent variables. Therefore, the experiments were planned and conducted according to a Box-Behnken response surface design using three levels for each process parameters (Ranganath and Vipin, 2015). The dye degradation efficiency of the selected BNC was investigated at a given process parameters (i.e. pH of the dye solution, dosage of BNC, MB dye concentration, and irradiation time). Furthermore, the photocatalytic efficiency of the left two BNCs was analyzed at optimal process parameters of RSM-BBD results. The Box-Behnken DoE runs for this study are given in Table 3.2.

Table 3.2 Experimental levels of factors for Box-Behnken Design

Factor	Name	Unit	level	
			Low (-1)	High (+1)
A	pH	-	2	10
B	BNC dosage	mg/L	5	30
C	MB concentration	mg/L	5	20
D	Time	min	30	180

The empirical relationship between experimental parameters and % MB degradation efficiency was expressed as it is shown in Eq. (14) below reference:

$$Y = b_o + \sum_{i=1}^{n} b_i X_i + \sum_{i=1}^{n} b_{ii} X^2{}_i \sum_{i=1}^{n-1} \sum_{j=i+1}^{n} b_{ii} X_i X_j \quad \text{..... (14)}$$

Where: Y = predicted response (degradation, %) of MB dye

b_o = constant

b_o, b_i, b_{ii}, and b_{ij} = regression coefficients for the intercept, linear, quadratic, and interaction coefficients, respectively.

Xi and Xj = independent variables from the lists of the coded values of factors and n=3, i.e. the number of independent variables.

3.6 Photodegradation Study on Real Textile Wastewater

3.6.1 Analysis of textile wastewater

In this study, the wastewater sample was collected from One Way Textile Manufacturing PLC, Debre Berhan Ethiopia. And it was confirmed by the sample provider that the company used MB dye for dyeing of fabric and jeans. The collected textile wastewater was first centrifuged and filtered to remove solid particles and then analyze the color, pH, and initial absorbance of the filtrate waste.

3.6.2 Spectrophotometric Determination of MB in Textile Wastewater Sample

To determine concentration of MB dye in the textile wastewater, five series of standard MB solutions of (5, 10, 15, 20, 25, and 30 mg/L) were prepared. Then, blank solution and working standards were run in UV-Vis Spectrophotometer at a maximum wavelength of 664 nm and five point's calibration curves were established. Then after, the filtered textile wastewater was taken

to the UV-Vis spectrophotometer without further wastewater degradation process and direct readings of the sample absorbance were recorded. Finally, the unknown dye concentration of the sample was determined using Beer's law equation (Eq. (15)).

$$A = \varepsilon bc \quad \text{(15)}$$

Where: A= absorbance of the sample

ε = molar absorptivity or extinction coefficient (L mol^{-1} cm^{-1})

b = path length of the sample (cm)

c = concentration of the sample (mole L^{-1})

3.6.3 Photodegradation of MB from Textile Wastewater

After determination of the unknown dye concentration of the sample, the photodegradation process was carried out by using the three synthesized BNCs at optimum process parameters (i.e. pH of the dye solution, BNCs dosage, and irradiation time). All optimum process parameters were obtained from DoE analyzer. For degradation of MB dye from real textile wastewater, sunlight irradiation was used as activation energy source. Finally the treated sample absorption spectrum was measured at λ_{max} of 664 nm and the degradation efficiency of each BNC was calculated using Eq. (12).

3.7 Recyclability Study

The recycling of the BNC is a very important method to reduce the cost and to investigate the stability of the BNC. To test and compare the reusability of the three synthesized BNCs, a recycling study was carried out at optimum process parameters, which is obtained from RSM-BBD results. Then, each sample was magnetically stirred under light irradiation in order to make a uniform suspension throughout the reaction. After that, the solution was centrifuged and measured its absorbance using UV-Vis spectrophotometer. The recovered BNCs were washed with distilled water, dried and reused in the next run. The same procedure was repeated for seven runs.

CHAPTER FOUR

4. Results and Discussion

4.1 Proximate Analysis of Water Hyacinth Stem

In this study, the proximate analysis of the WH stem mainly focused on the determination of moisture content, extractives, hemicellulose, lignin, cellulose, ash content, and yield of CNCs using standard procedure. The obtained results were given below in Table 4.1 and the detailed calculation was presented at Appendix C.

Table 4.1 Summary of proximate analysis results of WH stem

Parameter	Obtained Result
Moisture content (%)	15.21
Ash content (%)	21.6

4.1.1 Moisture Content

This analysis is performed to calculate the amount of dry matter present in the natural WH without any chemical treatment. The obtained moisture content of the air-dried sample using Eq. (1) was 15.21% which is similar to 13.4-19.65% reported by Hailu and Degaga (2019).

4.1.2 Ash Content

The experimental result exhibits 21.6% of ash content was presented in the WH stem. The high ash content indicates the inorganic elements (which are nonflammable part of biomass) are presented in the weed stem. Due to having high concentration of inorganic substances makes this plant attractive to use as compost because minerals are important for plant growth and wastewater treatment.

4.2 Compositional Analysis of Water Hyacinth Stem

The water hyacinth stem mainly comprised extractives, hemicellulose, lignin, and cellulose content in its structure. According to Table 4.2, the non-cellulosic (i.e. hemicellulose) content of WH stem was higher than Extractives and lignin content. From the analysis the following compositional values were obtained.

Table 4.2 Chemical composition values of WH stem

Chemical Compositions	Obtained Values
Extractives (%)	19.33
Hemicellulose (%)	27.24
Lignin(%)	5.27
Cellulose (%)	48.16

4.2.1 Extractive Content

In the literature, the stated percentage of total extractives content in the WH stem ranged from (16.8-47.5%) (Omondi et al., 2019). The obtained experimental analysis exhibits the total extractive content in WH stem was 19.33%, which is small and almost in range of the above reported of the extractive content. Generally, the high content of extractives in the sample can have a negative impact because the extractive content increases the chemical reagents (i.e. hexane, ethanol, toluene, etc.) consumption also increase which resulted high process cost.

4.2.2 Determination of Hemicellulose

The result of this study was shown that the hemicellulose content in the WH stem was 27.24% using Eq. (4), which is close to the reported result of 22.6-48.8% (Farhat et al., 2017). It confirmed that WH had greater proportion of hemicellulose content than other non-cellulosic compound. Due to the high content of hemicellulose in WH aquatic weed that could be led to uptake a huge volume of water which results the scarcity of water resources (Uddin et al., 2014).

4.2.3 Determination of Lignin

According to the reported data in the literature, the lignin content in WH stem was ranged from 3-12% which is lower than the other common wood biomasses (Bronzato et al., 2017). In this study, the obtained lignin content in WH stem was 5.27%. The low lignin content in WH makes this material attractive for the production various materials and expected that easily damaged by the action of microorganisms or chemical reagents, because this plant has high alkali solubility.

4.2.4 Determination of Cellulose

From proximate characteristics tests the obtained cellulose content was 48.16% using Eq. (6). It is the large percentage as compared as other non-cellulosic components (hemicellulose and

lignin). The high cellulose content of WH weed has the potential advantage to be used as a raw material for CNCs production (George and Sabapathi, 2015).

4.3 Yield of CNCs

The yield of CNCs was estimated using Eq. (7) and the obtained amount was 36.5%. It indicates this aquatic weed potentially used as a source of CNCs. In addition, uniformly dispersion of CNCs in the water was due to the negatively charged of CNCs that resulted from the applied 30% (v/v) sulfuric acid during acid hydrolysis process.

4.4 UV-Vis Spectrophotometer

The optical spectrum of Ag@ZnO NPs was shown in Figure 4.1 (a) and recorded in the wavelength range from 200 to 800 nm. The band gap energy of Ag@ZnO NPs have been calculated Eq. (8). In Figure 4.1 (a) the spectrum exhibits the absorbance peak at 402 nm it is called the edge wavelength, which is shifted towards the lower wavelength (i.e. below the band gap wavelength or known as blue shift). The band gap energy is obtained to be 3.08 eV using Eq.(8). It confirms the zinc sites get occupied by the Ag atoms in the ZnO lattice and Ag provides impurity band (sub energy levels) in the ZnO energy gap (Sagadevan et al., 2017). According to Figure 4.1 (a) no extra peak related with impurities is found in the spectrum and it confirms the synthesized NPs are pure. The band gap calculation was given in Appendix-D.

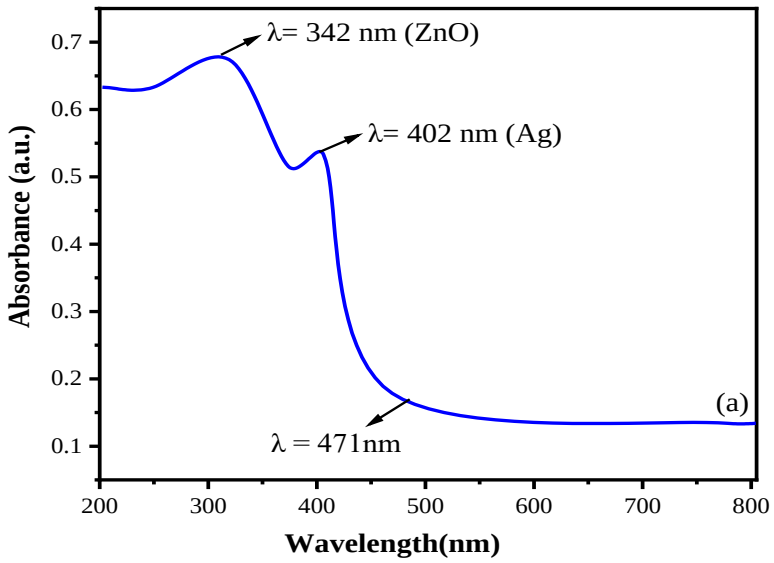

In addition, Figure 4.1 (b), (c) and (d) shows the UV-Vis absorption spectrum of WH stem, bleached cellulose and CNCs, respectively. The vibrational spectrum was observed from 200-

287nm in Figure 4.1 (b) due to the presence of non-cellulosic (i.e. hemicellulose, lignin, etc.) bonds in the WH stem. In Figure 4.1 (c) weak vibration appeared at the same wavelength region, which indicates the presence of the remaining non-cellulosic materials. However, this vibration completely disappeared in Figure 4.1 (d) it confirms remaining non-cellulosic materials dispersed and removed after acid hydrolysis process.

Additionally, UV-Vis absorption spectra of the CNCs/Ag@ZnO (1:1), CNCs/Ag@ZnO (1:0.5) and CNCs/Ag@ZnO (0.5:1) BNCs were shown in Figure 4.1 (e), (f) and (g), respectively. In each absorption spectra a new characteristic peak at 309nm (ZnO) and 398nm (Ag) were exhibited, which could be ascribed to the presence of Ag@ZnO NPs. It confirms sucessfully incorporation of Ag@ZnO NPs with CNCs

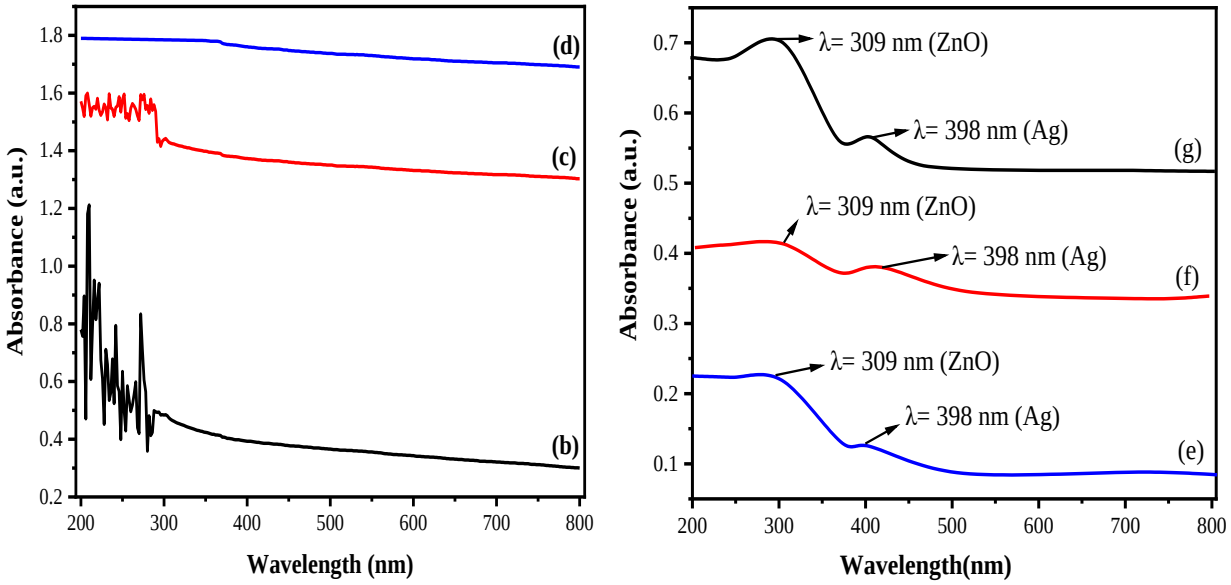

Figure 4.1 UV-Vis absorption spectrum. (a) Ag@ZnO NPs, (b) WH stem, (c) Bleached cellulose, (d) CNCs, (e) CNCs/Ag@ZnO (1:1) BNC, (f) CNCs/Ag@ZnO (1:0.5) BNC and (g) CNCs/Ag@ZnO (0.5:1) BNC.

Furthermore, Figure 4.2 (a), (b) and (c) shows the absorption intensity of MB dye at 664 nm gradually decreased with increasing the light irradiation time in the precence of CNCs/Ag@ZnO (1:1), CNCs/Ag@ZnO (1:0.5) and CNCs/Ag@ZnO (0.5:1) BNCs, respectively. According to UV-Vis spectra, the photodegradation efficiency of each BNC was increased when the irradiation time was increased. In this study, CNCs/Ag@ZnO (1:0.5) and CNCs/Ag@ZnO (0.5:1) BNCs have higher photodegradation efficiency (see Figure 4.2) as compared to CNCs/Ag@ZnO (1:1) BNC .

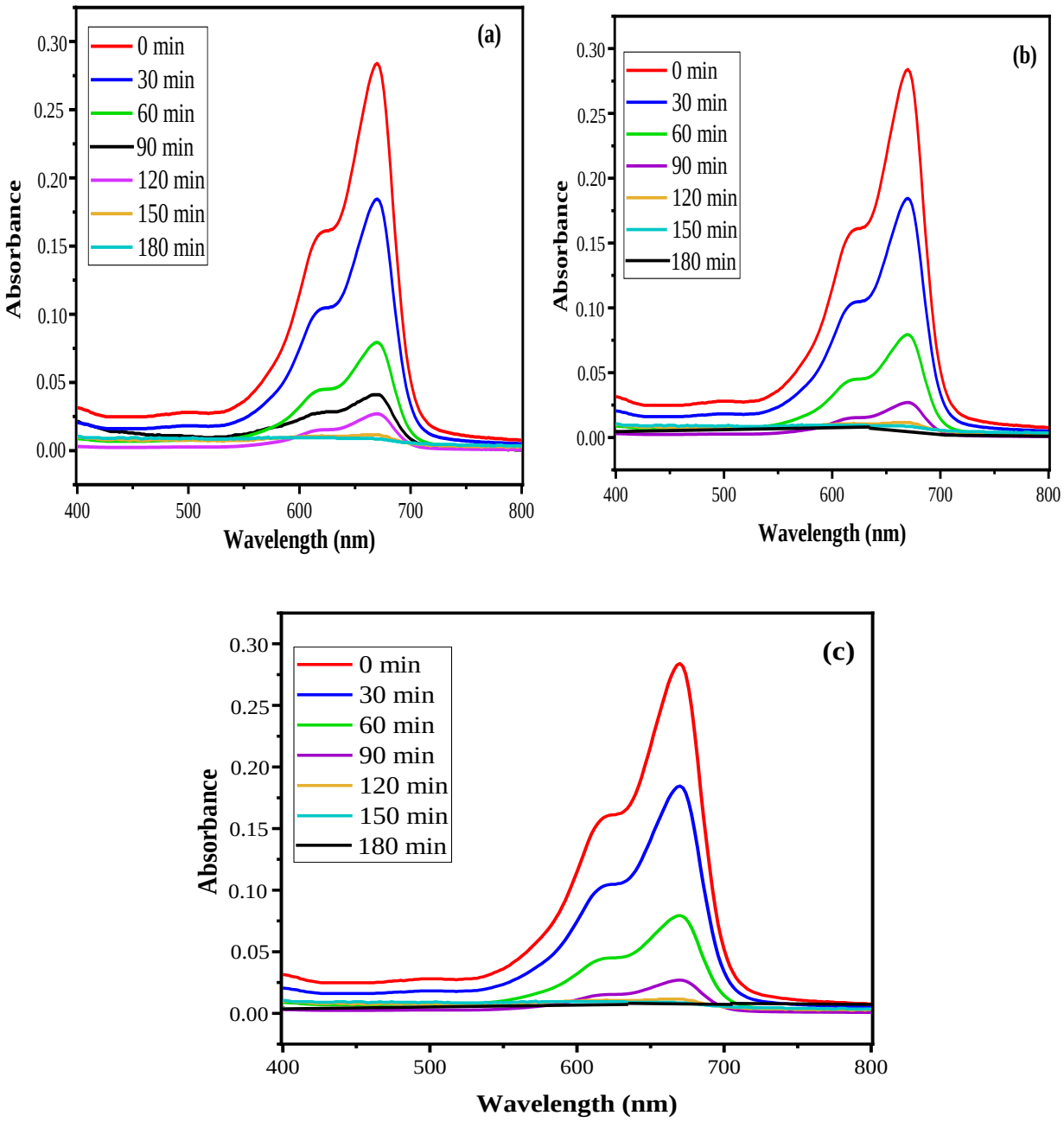

Figure 4.2 Time dependent UV-Vis absorption spectra of MB dye (15mg/L) degradation under light irradiation. (a) CNCs/Ag@ZnO (1:1), (b) CNCs/Ag@ZnO (1:0.5) and (c) CNCs/Ag@ZnO (0.5:1) BNC.

4.3 Fourier Transform Infrared Spectroscopy Analysis

To determine the functional groups present in the sample, the FTIR spectra of WH stem, bleached cellulose, and CNCs were recorded between the wavenumber spanning over a range of 4000 - 400cm^{-1} (Figure 4.3). The broad band at 3434, 3447, 3433cm^{-1} for WH stem, bleached

cellulose, and CNCs, respectively spectra was corresponds to -OH stretch (Bronzato et al., 2017). The formation of -OH group in each sample was related to either the interaction of hydrogen bond in hydroxyl groups of hemicellulose, lignin and crystalline cellulose that found in the WH stem, bleached cellulose, and CNCs or the adsorbed moisture content by the samples. The spectra associated with C-H stretching appeared in all three samples at wavenumber of 3000 - 2800cm^{-1}. The peak appeared at 1758cm^{-1} in Figure 4.3 (a) attributed to C-O bond which is normally found in the linkages of esters and aromatic ring in the hemicellulose and lignin components. However, this peak was disappeared in the spectra of bleached cellulose and CNCs. It confirms the hemicellulose and lignin materials were effectively removed from WH stem through bleaching and acid hydrolysis process (Sundari and Ramesh, 2012).

The peaks at 1621 and 1627cm^{-1} in Figure 4.3(b) and (c) indicated the vibration of water molecules absorbed in cellulose and CNCs, respectively. The absorption peaks at 1364 and 1218cm^{-1} in Figure 4.3 (b) belongs to the stretching and bending vibrations of -CH_2 and –CH bonds in bleached cellulose. The observed peaks at 1032cm^{-1} in Figure 4.3 (c) was associated with the presence of strong S=O stretching sulfoxide groups in CNCs, which resulted from acid hydrolysis process (Asrofi et al., 2018). The peak at 1032, 983 and 1014cm^{-1} in Figure 4.3 (a), (b) and (c) , respectively associated with β-glycosidic linkage in cellulose structure (Hidayah and Wusko, 2020).

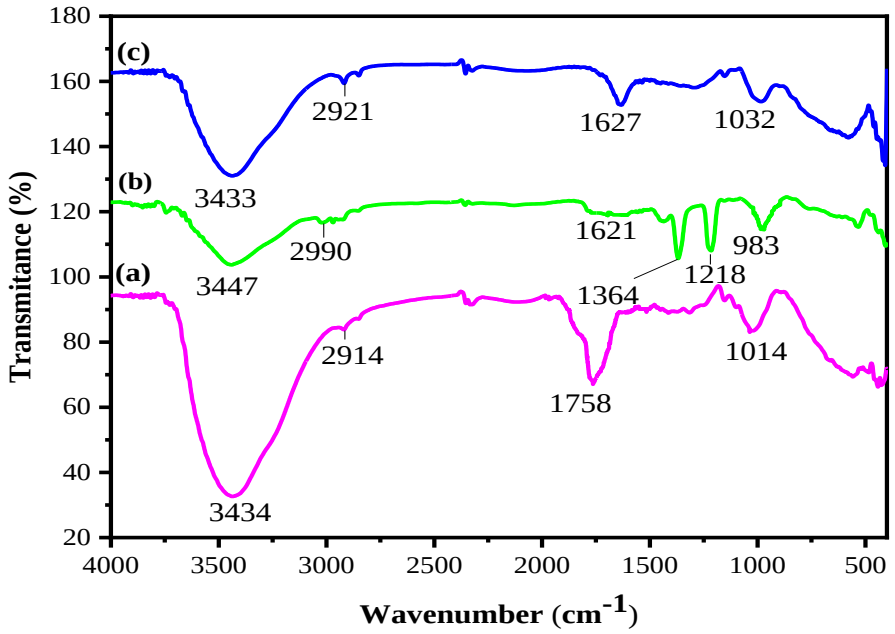

Figure 4.3 The FTIR spectra. (a) WH stem, (b) Bleached cellulose, and (c) CNCs

Furthermore, the FTIR spectra of CNCs, WH leave extracts, Ag@ZnO NPs, and CNCs/Ag@ZnO (1:1), CNCs/Ag@ZnO (1:0.5) and CNCs/Ag@ZnO (0.5:1) BNCs were given in Figure 4.4. The wide peak in the range of 3500 – 3300cm^{-1} in Figure 4.4 (b), (c), (d), (e) and (f) indicates the -OH functional group of phenolic and flavonoids components (Wolverton and Mcdonald, 2018). This components mainly found in WH leaves and these components actively involved in bio-reduction occurrence during doping of Ag onto ZnO nanostructures (Ahmad and Jaffri, 2018). The peaks at 1632 and 1620cm^{-1} in Figure 4.4 (c) and (f) indicate O-H stretch and N-H bends, respectively.

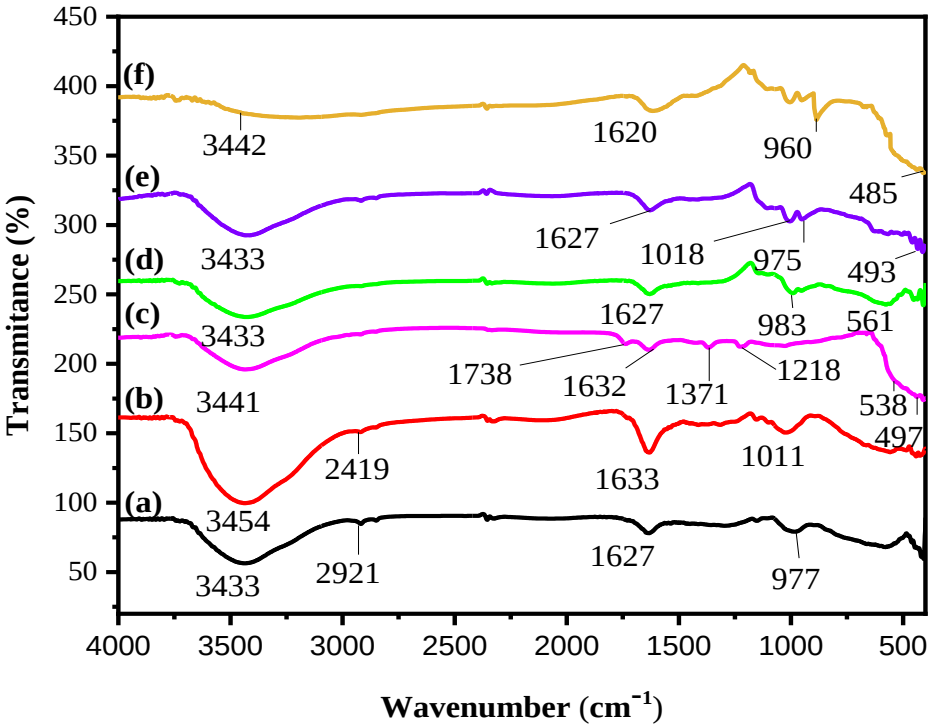

Figure 4.4 The FTIR spectra (a) CNCs, (b) WH leave extracts, (c) Ag@ZnO NPs, (d) CNCs/Ag@ZnO (1:1) BNC, (e) CNCs/Ag@ZnO (1:0.5) BNC and (f) CNCs/Ag@ZnO (0.5:1) BNC.

The peaks around 1371 and 1218cm^{-1} in Figure 4.4 (c) assigned to the C-O-C and O-H bonds owing to the deformations of the C-OH groups in Ag@ZnO NPs. The spectrum peak in range of 960 - 990cm^{-1} was appeared (Figure 4.4 (d), (e) and (f)) due to the presence of crystalline structure of CNCs in the three synthesized BNCs. The characteristic stretching of Zn-O and Ag-O bonds are assigned to the significant bands at 497 and 538cm^{-1} (Figure 4. 4 (c)). It confirms the doping of Ag into the ZnO nanostructure was successfully. The peaks at 485, 493, and 561cm^{-1}

(Figure 4.4 (d), (e) and (f)) were indicated that Ag@ZnO NPs appeared on the surface of each synthesized BNCs. According to the above FTIR spectra, each BNC consist both CNCs and NPs functional groups, which confirms the developed bio-based photocatalyst was successfully synthesized.

4.4 X-ray Diffraction Analysis

The crystallinity index, crystalline size and the distance between the lattices of WH stem, bleached cellulose, CNCs, Ag@ZnO NPs, and CNCs/Ag@ZnO (1:1), CNCs/Ag@ZnO (1:0.5) and CNCs/Ag@ZnO (0.5:1) were investigated using X-ray diffractometer (XRD) and the results were given in Figure 4.5. Generally, the strong diffraction peak in XRD analysis indicates the good crystalline structure of the materials. From this study, the XRD pattern of WH stem has two characteristic peaks at 2θ =14.52° and 21.74° (see Figure 4.5 (a)) that corresponds to the presence of high amount of amorphous and weak crystalline region of WH stem, respectively. In addition, the peaks at 2θ =22.1°, and 22.37° in Figure 4.5 (b) and (c) indicates the crystalline region of bleached cellulose and CNCs, respectively. Moreover, in Figure 4.5 (b) and (c) the peak at 2θ =14.52° was disappeared due to the removal of amorphous regions (hemicellulose and lignin components) from the raw WH stem after alkaline treatment, bleaching and acid hydrolysis process (Mustikaningrum et al., 2021).

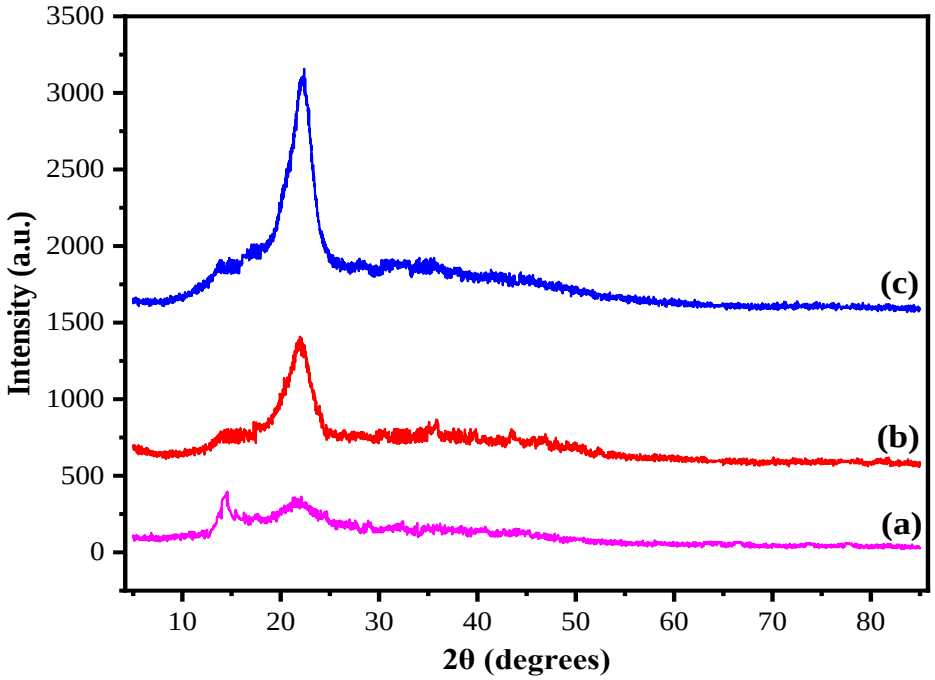

Figure 4.5 XRD Patterns. (a) WH stem, (b) Bleached Cellulose and (c) CNCs

The diffraction peak at 22.37° for CNCs was relatively sharper and narrower than WH stem and bleached cellulose. This phenomenon was due to the penetration of hydronium ions (H_3O^+) into cellulose components which breaks β-1, 4-glycosidic linkages within the cellulose chains, and thereby led to the release of individual crystallites. Therefore, the degree of crystallinity was increased after treating the cellulose using acid hydrolysis method (Asrofi et al., 2018). Therefore; the XRD analysis confirms the obtained CNCs were successfully synthesized and efficient for BNCs synthesis.

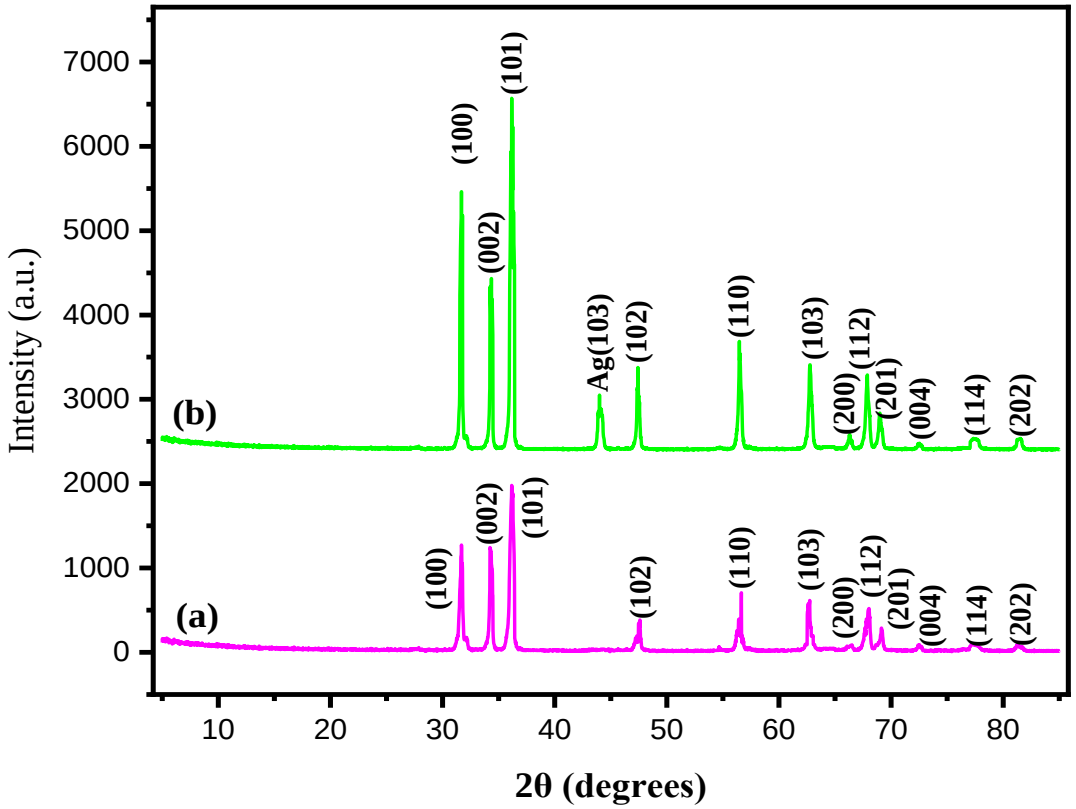

Figure 4.6 XRD patterns (a) ZnO and (b) Ag@ ZnO NPs

Furthermore, the diffraction peaks of pure ZnO and Ag@ZnO NPs were exhibited in Figure 4.6. According to the result, the WH leaf extract reduce the particle size to increase the surface area and inhibit the over-growth of ZnO and Ag@ZnO NPs (Javed et al., 2020). The strong and broad pattern of diffraction peaks of pure ZnO in Figure 4.6 (a) confirmed a characteristic peaks of hexagonal wurtzite structure at 32.03°, 34.29°, 36. 2°,47.47°,56.71°, 62.84°, 66.28°, 68.27°, 69.11°, 72.72°, 77.59°, and 81.66°. The reflection planes of the above listed peak values were (100), (002), (101), (102), (110), (103), (200), (112), (201), (004), (114) and (202), respectively.

In ZnO structure, the oxygen atoms organized in hexagonal tight packing and zinc atoms filling half of the tetrahedral sites. The atoms of zinc and oxygen are tetrahedrally coordinated to occupy an analogous location. After doping of Ag in to ZnO structure, additional peaks were induced in the XRD spectra at an angle of 32.03° (100), 34.29° (002), and 36. 2° (101) shown in Figure 4.6 (b). It confirms the presence of Ag particles in the grain borders of ZnO crystallites. As a substitute for Zn^{2+}, Ag dopant aids in obtaining a close peak shift in the XRD (Kwon and Kim, 2020). The peak clearly illustrates that adding Ag dopant causes a considerable decrease in crystallite size (Chitradevi et al., 2019). The peak at 43.85° (103) indicates the presence of silver (Ag), and no other impurities were observed. This result confirms the products consisted of pure phases. Furthermore, the diffraction peaks were more intensive and narrower, implying a good crystalline nature of Ag@ZnO nanocomposite products.

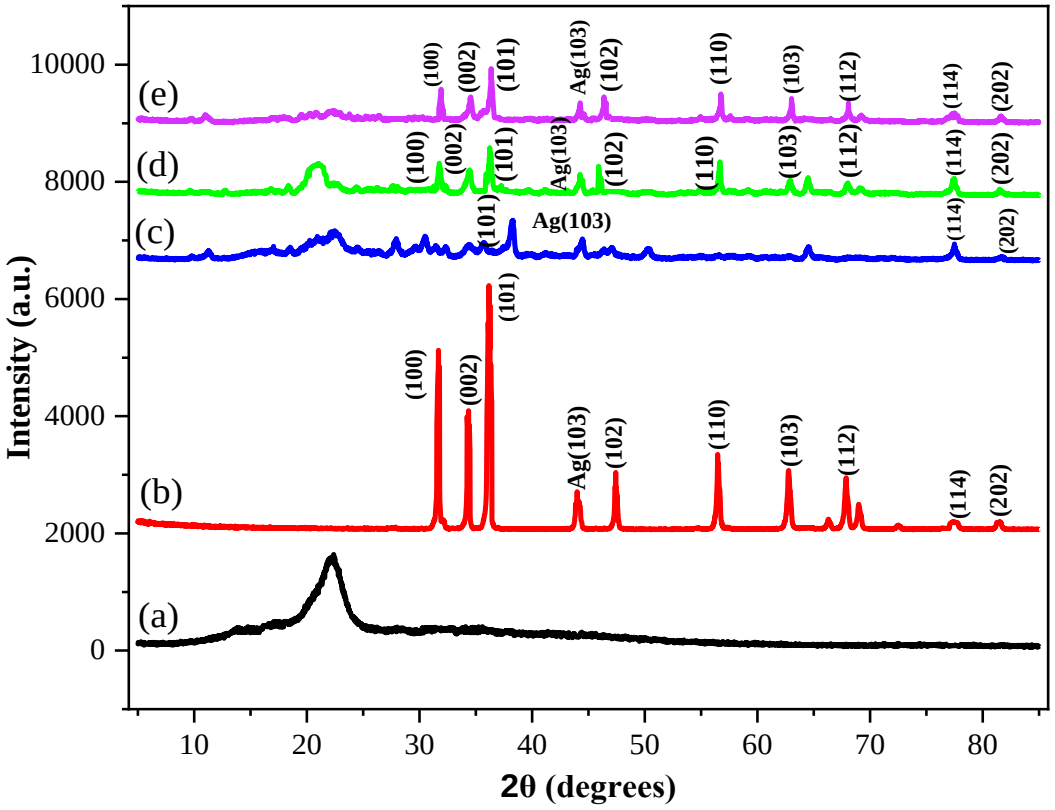

Figure 4.7 The XRD patterns (a) CNCs, (b) Ag@ZnO NPs, (c) CNCs/Ag@ZnO (1:1) BNC , (d) CNCs/Ag@ZnO (1:0.5) BNC, and (e) CNCs/Ag@ZnO (0.5:1) BNC.

In addition, the XRD patterns in the 2θ range of 10° - 80° for CNCs, Ag@ZnO NPs, and CNCs/Ag@ZnO (1:1), CNCs/Ag@ZnO (1:0.5) and CNCs/Ag@ZnO (0.5:1) BNCs were shown

in Figure 4.7. The peaks in the 2θ = 22.53° and 21.95° in Figure 4.7 (c) and (d) were almost the same as compared with pure CNCs XRD pattern. It confirms CNCs/Ag@ZnO (1:1) and CNCs/Ag@ZnO (1:0.5) BNC did not change their structural uniformity of the polymer matrix after incorporation of Ag@ZnO NPs. In Figure 4.7 (e) the weak CNCs characteristic was exhibited with the same region due to the concentration of Ag@ZnO NPs greater than CNCs in the CNCs/Ag@ZnO (0.5:1) BNC. In addition, the diffraction peaks ranging from 30.98° to 80° in Figure 4.7 (d) and (e) were neither the peaks were shifted nor a new peak appeared and those have the same diffraction patterns compared with the pure NPs, which indicates Ag@ZnO NPs were sucessfully incorporated in the CNCs/Ag@ZnO (1:0.5) and CNCs/Ag@ZnO (0.5:1) BNC.

The crystallinity index, average crystallite size and interplanar spacing (d-spacing) of WH stem, bleached cellulose, CNCs, Ag@ZnO NPs and the three synthesized BNCs were determined by using Eq. (9), (10) and (11) respectively and the detail calculation was given in Appendix-E. The crystallinity index of WH stem was found to be lower (see Table 4.2) and higher after acid hydrolysis process due to the elimination of the amorphous regions from the sample. In addition, the crystallinity of the CNCs was increased after combining of Ag@ZnO NPs. The obtained crystalline index, Crystallite size and d-spacing of each sample were given below in Table 4.2.

Table 4.2 The crystallinity index, crystallite size and interplanar spacing (d-spacing) results

Sample	Crystalline index (%)	Crystallite size (nm)	d-spacing (nm)
WH stem	29.82	0.31	0.081
Bleached cellulose	63.6	1.91	0.082
CNCs	84.3	2.08	0.083
Pure ZnO NPs	88.6	36.3	10.45
Ag doped ZnO NPs	91.75	24.54	5.776
CNCs/Ag@ZnO (1:1) BNC	87.34	9.8	0.3871
CNCs/Ag@ZnO (1:0.5) BNC	85.78	11.4	3.76
CNCs/Ag@ZnO (0.5:1) BNC	89.67	10.5	2.5

4.5 Thermo Gravimetric Analysis

The thermal stability of the samples was analyzed using thermo gravimetric analysis (TGA) under an inert atmosphere. The results of all samples illustrate similar behavior with three regions of thermal degradation as shown below in Figure 4.8. The first region in range from 10-100 ^{0}C (Region-I) attributed to the vaporization of moisture absorbed by all samples and in Figure 4.8 (a) the slight weight loss at the temperature range from 100-220 ^{0}C. It indicates the decomposition of hemicellulose structure in WH stem. In fact, the hemicellulose structure of WH has low thermal stability due to the presence of amorphous saccharides, which is easily converted to volatiles (CO, CO_2, and hydrogen carbon) at low temperature (Bronzato et al., 2017).

Furthermore, all samples exhibited the main stage of thermal degradation at a temperature range of 220-400 ^{0}C (Region-II). This region confirmed the cellulose experienced stronger de-polymerization, decarboxylation, and decomposition of glycosidic linkages. Cellulose is a linear polysaccharide polymer with a high order of arrangement and higher molecular weight, making it more stable than hemicellulose at high temperature (Thiripura Sundari and Ramesh, 2012). But the lower thermal resistance was exhibited for CNCs in the same region that related to the longer interaction between cellulose and sulfuric acid under hydrolysis. This resulted in more negatively charged sulfate groups on the CNCs surface resulting in decreased thermal resistance (Pandi et al., 2021).

The third region (Region-III) was above 400 ^{0}C, which particularly demonstrated that the decomposition of the remaining cellulose and lignin materials that found in all samples. The highest total weight loss was exhibited in CNCs due to the formation of a dense crystalline structure of the cellulose and the absence of any resistant materials (i.e. Hemicellulose, and lignin) in its structure. Moreover, lignin decomposes in a wider temperature range than hemicelluloses and cellulose (200-600 °C) because its structure comprises various functional oxygen groups with different thermal stabilities, such as; aromatic carbons, phenolics, and hydroxyphenolics (Song et al., 2019).

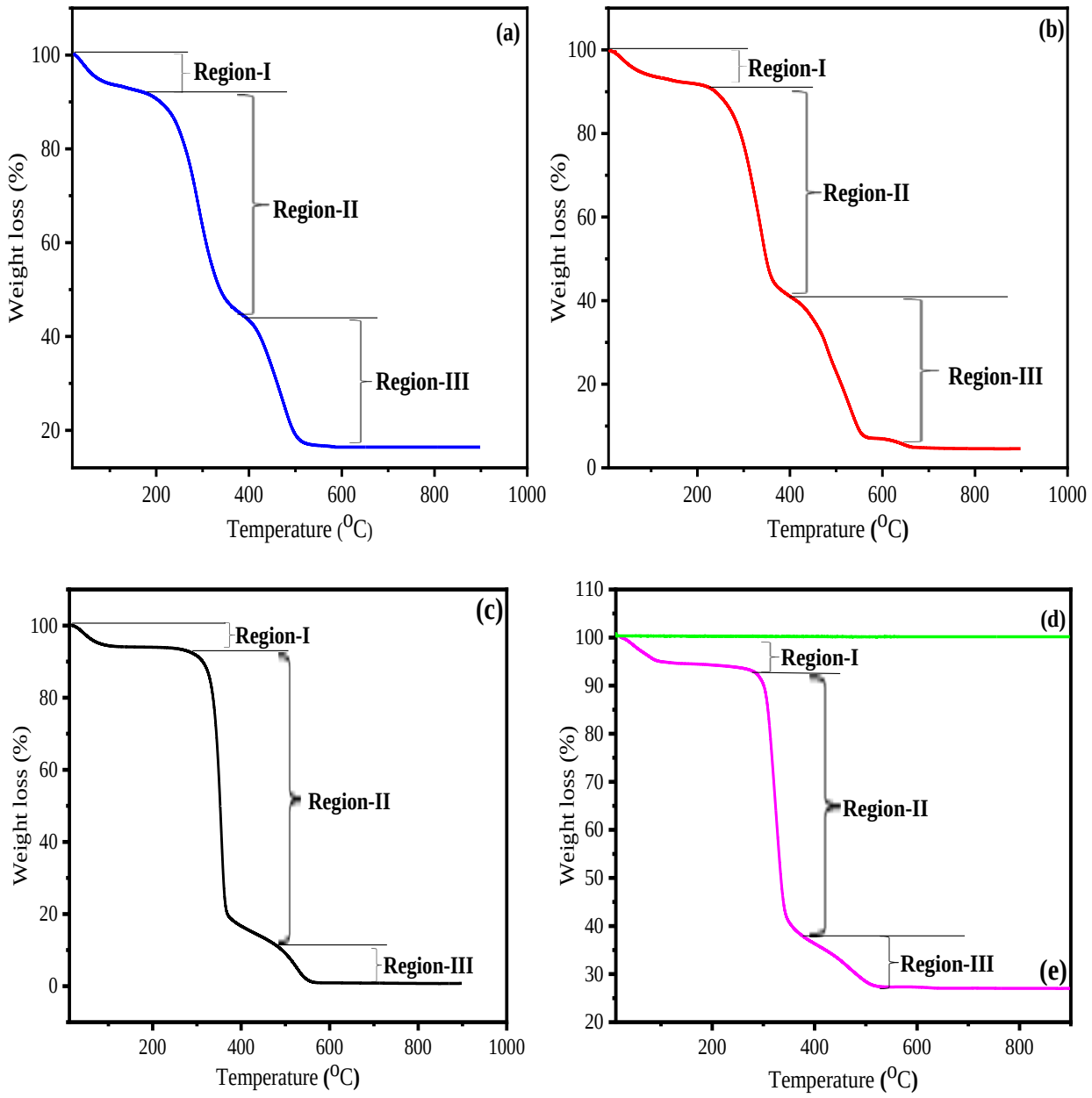

Figure 4.8 TGA curves (a) WH stem, (b) Bleached cellulose, (C) CNCs, (d) Ag@ZnO NPs and (e) CNCs/Ag@ZnO (1:0.5) BNC.

In addition, the TGA results of Ag@ZnO NPs and CNCs/Ag@ZnO (1:0.5) BNC were exhibited in Figure 4.8 (d) and (e), respectively. According to the result, the Ag@ZnO NPs has high thermal stability throughout a given temperature ranges (Figure 4.8 (d)) due to having large surface area to volume ratio and the excellent thermal resistance at high temperature. In addition, CNCs/Ag@ZnO (1:0.5) BNC has higher thermal stability than CNCs (see Figure 4.8 (c)) due to the appearance of strong interfacial adhesion between CNCs and Ag@ZnO NPs. Moreover, the

combination of NPs with CNCs not only influences the decomposition temperature but also increases the amount of the left residues after thermal degradation. Generally, the percentage of weight loss in each thermal degradation region and total percentage of weight loss of the samples were given below in Table 4.3.

Table 4.3 Weight loss of the samples in each thermal region

Sample Name	Weight loss in Region-I (%)	Weight loss in Region-II (%)	Weight loss in Region-III (%)	Total weight loss (%)
WH stem	6.201	45.335	27.173	78.709
Bleached Cellulose	8.253	49.049	37.421	94.723
CNCs	5.266	76.906	16.673	98.845
CNCs/Ag@ZnO (1:0.5) BNC	4.856	56.529	11.06	72.545

4.6 Brunauer Emmett Teller Analysis

The surface area, pore volume and pore size of CNCs, and CNCs/Ag@ZnO (1:1), CNCs/Ag@ZnO (1:0.5) and CNCs/Ag@ZnO (0.5:1) BNCs were investigated using Brunauer Emmett Teller (BET) analyzer. The detail BET analysis results of each sample were listed in Appendix-F. According to the results, CNCs/Ag@ZnO (1:0.5) BNC has large surface area, pore volume and narrow pore-size distribution than CNCs, and CNCs/Ag@ZnO (1:1) and CNCs/Ag@ZnO (0.5:1) BNCs. It makes an optimal choice for the application of MB dye degradation from synthetic and real textile wastewater using light irradiation as activation energy. Generally, the number of active sites of the photocatalyst increase with increasing of surface area thus, the dye degradation efficiency of BNCs becomes higher. In addition, the large pore volume allows the BNC photocatalyst to hold a large amount of dye solution that supports to capture and degrade the organic pollutant (i.e. MB dye compounds) effectively. Moreover, it can be observed that an addition of Ag@ZnO NPs in CNCs matrix increased the surface area and pore volume by narrowing the pore diameter of the synthesized BNC. The summarized BET results of the samples were given below in Table 4.4.

Table 4.4 Surface area, pore volume and pore size of the synthesized materials.

Sample Name	Surface Area (m^2/g)	Pore Volume (cm^3/g)	Pore Size (nm)
CNCs	436.8	0.023	0.49
CNCs/Ag@ZnO (1:1) BNC	564.6	0.086	0.26
CNCs/Ag@ZnO (1:0.5) BNC	687.7	1.85	0.12
CNCs/Ag@ZnO (0.5:1) BNC	639.5	0. 94	0.16

4.7 Dynamic Light Scattering Analysis

The particle size distribution graph of WH stem, bleached cellulose, CNCs, Ag@ZnO NPs, and CNCs/Ag@ZnO (1:1), CNCs/Ag@ZnO (1:0.5) and CNCs/Ag@ZnO (0.5:1) BNCs was given in Appendix-G. According to DLS results, CNCs has small particle size than raw WH stem and bleached cellulose as shown in Appendix-G (a), (b) and (c). It indicates the non-cellulosic materials (i.e. hemicellulose, lignin, and extractive components) were removed after acid hydrolysis process (Leng, 2019). In addition, Ag@ZnO NPs has small (32.3 nm) particle size (see Appendix-G (d)) which confirmed the WH leaves extract effectively inhibited the over-growth of the NPs. The DLS results of the three synthesized BNCs were also given in Appendix-G (e), (f) and (g). It confirmed CNCs/Ag@ZnO (1:0.5) BNC has small particle size than CNCs/Ag@ZnO (1:1) and CNCs/Ag@ZnO (1:0.5) BNC due to the presence of high quantity of Ag@ZnO NPs in its structure. Generally, the DLS results of each sample were summarized below in Table 4.5.

Table 4.5 DLS results of the samples

Sample Name	Z-Average (nm)	PDI	Particle Size (nm)	% Intensity	St. Dev (nm)
WH stem	125.7	0.672	139.2	53	3.958
Bleached Cellulose	109.2	0.466	78.9	22.1	3.667
CNCs	84	0.243	63.23	40	3.641
Ag@ZnO NPs	69.5	0.215	32.3	58	3.456
CNCs/Ag@ZnO (1:1) BNC	120.67	0.251	94.3	100	3.690
CNCs/Ag@ZnO (1:0.5) BNC	76.56	0.225	47.41	56.6	3.461
CNCs/Ag@ZnO (0.5:1) BNC	78.45	0.265	55.72	58.7	3.895

4.8 Scanning Electron Microscopy Analysis

The scanning electron microscope (SEM) was conducted to evaluate the morphological properties of WH stem, bleached cellulose, CNCs, Ag@ZnO NPs and CNCs/Ag@ZnO (1:0.5) as shown in Figure 4.9. The morphology of the untreated WH stem (Figure 4.9 (a)) has a smooth appearance due to the micro fibrils are tightly linked with adhesive substances i.e. amorphous components, waxes and oils (Sundari and Ramesh, 2012). After bleaching process the surface roughness of the sample was increased as shown in Figure 4.9 (b), which indicates the non-cellulosic contents i.e. lignin, hemicellulose, wax, and oil has been removed.

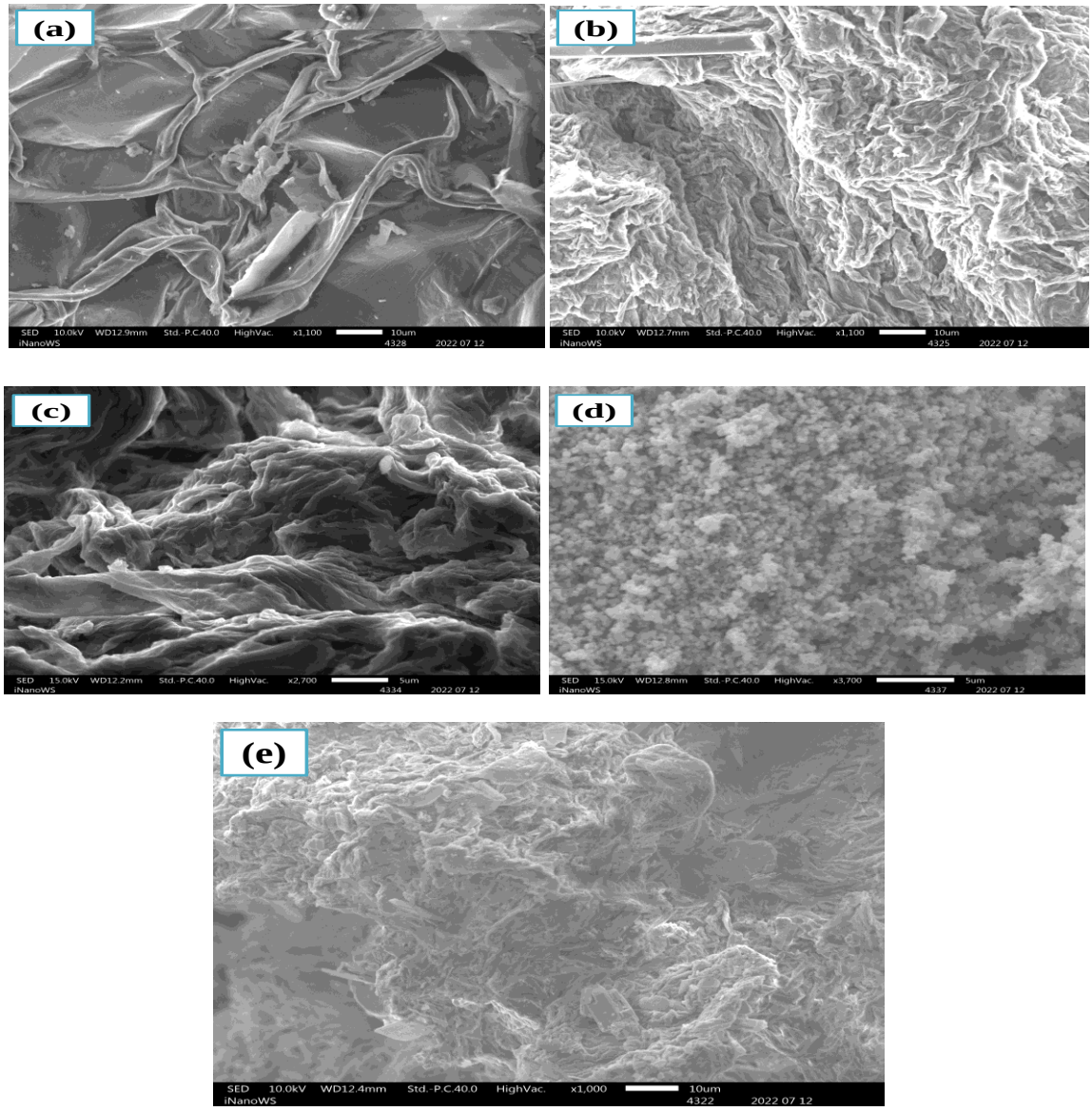

Figure 4.9 SEM images (a) WH stem, (b) Bleached cellulose, (c) CNCs, (d) Ag@ZnO NPs and (e) CNCs/Ag@ZnO (1:0.5) BNC.

In Figure 4.9(c), the SEM images clearly shown the synthesized CNCs has high surface porosity and it have a whisker-shaped structure due to the depolymerization of β-1,4 glycosidic bonds in solid crystalline cellulose. In addition, Figure 4.9 (b), and (c) clearly exhibits the formation of weak and strong fibril nano crystals, respectively. It confirms after each chemical treatments (i.e. alkaline treatment, bleaching process and acid hydrolysis), the surface roughness of the sample was increase and the nano crystals in the cellulose were released. Moreover, the surface morphology of Ag@ZnO NPs was shown in Figure 4.9 (d). According to the SEM micrographs, when Ag^+ ions are added to the reaction solution, Ag^+ and OH^- will first interact to generate AgOH precipitation, which consumes part of the alkaline ions in the solution, and then the ZnO tends to grow in wurtzite hexagonal structure. Also it decreases the agglomeration and regular organization of ZnO using Ag as a dopant. This can enhance the photocatalytic activity of the ZnO NPs under light irradiation. The shape of the Ag@ZnO NP_S obtained from SEM image also coincided with XRD results. Furthermore, the properties of both Ag@ZnO NPs and CNCs were clearly exhibited in CNCs/Ag@ZnO (1:0.5) BNC (Figure 4.9 (e)). It indicates the Ag@ZnO NPs uniformly dispersed in CNCs matrix.

Furthermore, the elemental compositions of WH stem, bleached cellulose, CNCs, Ag@ZnO NPs, and CNCs/Ag@ZnO (1:0.5) were examined by energy dispersive X-ray spectroscopy (EDX) (see Figure 4.10). The EDX result in Figure 4.10 (a) exhibits the presence of C (48.4%), O (40.7%), K (8%), Ca (1.5%), Na (1%), and Mg (0.5%) in WH stem. After bleaching process the composition of K and Mg were disappeared as shown in Figure 4.10 (b). In Figure 4.10 (c) except C (50.2%) and O (49.8) no other elementals are observed in the CNCs EDX spectra that confirm the synthesized samples were very pure. Figure 4.10 (d) represents the EDX spectra of Ag@ZnO NPs and it reveals the presence of Ag, Zn and O in the nanocomposite, which confirms the Ag ions successfully doped on ZnO nanostructure. The elements (i.e. C (45.6%), O (42.3%), Zn (9.8%), Na (0.9%) and Ag (1.4%)) were found in the CNCs/Ag@ZnO (1:0.5) BNC, it confirm the CNCs and Ag@ ZnO NPs were effectively incorporated.

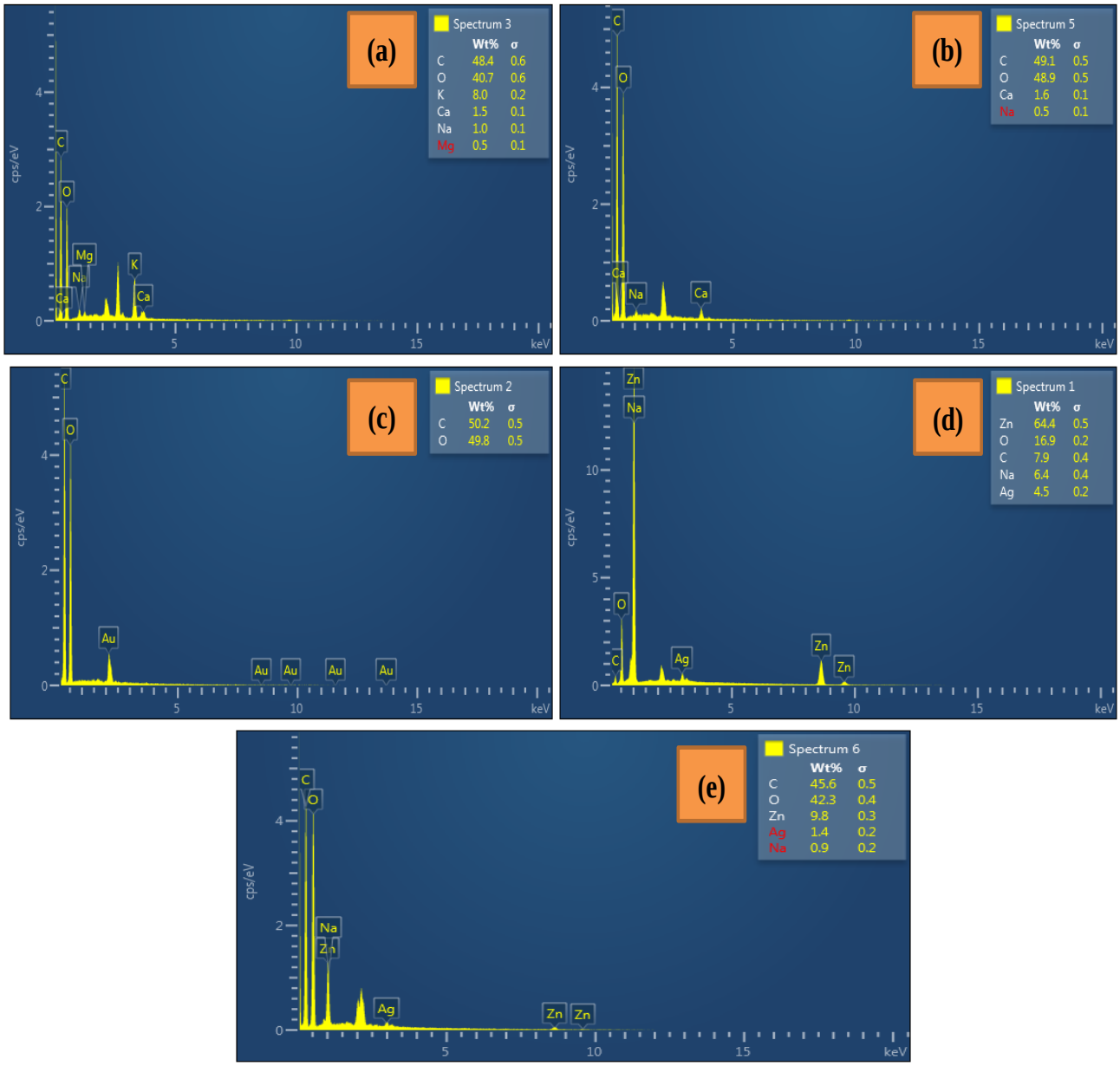

Figure 4.10 EDX analysis results (a) WH stem, (b) Bleached cellulose, (c) CNCs, (d) Ag@ZnO NPs, and (e) CNCs/Ag@ZnO (1:0.5) BNC

Furthermore, the EDX mapping of WH stem, bleached cellulose, CNCs, Ag@ZnO NPs and CNCs/Ag@ZnO NPs (1:0.5) were shown in Figure 4.11. According to the results, the concentration of carbon and oxygen in each samples (i.e. WH stem, bleached cellulose, CNCs, Ag@ZnO NPs, and CNCs/Ag@ZnO NPs (1:0.5) BNC) were higher than other elements. In addition, in Figure 4.11 (e) the elemental composition of both CNCs and Ag@ZnO NPs clearly exhibited in CNCs/Ag@ZnO (1:0.5) that confirmed Ag@ZnO NPs successfully disperse in the CNCs matrix.

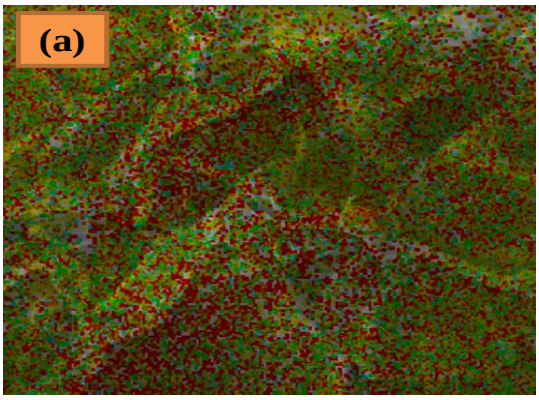

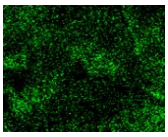
Carbon

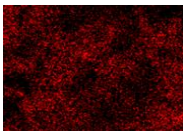
Oxygen

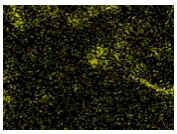
Potassium

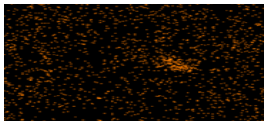
Calcium

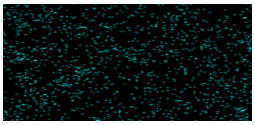
Sodium

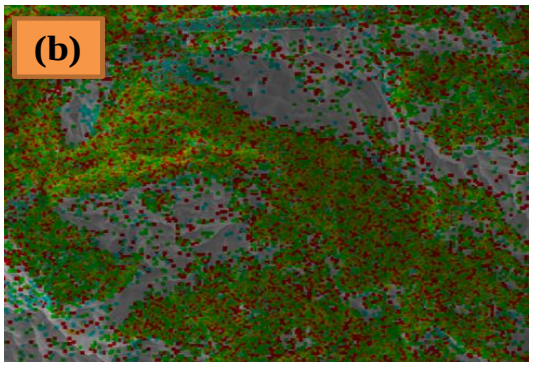

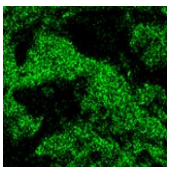
Carbon

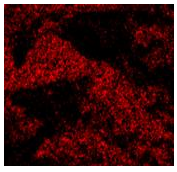
Oxygen

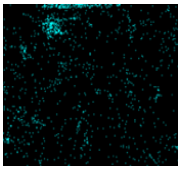
Calcium

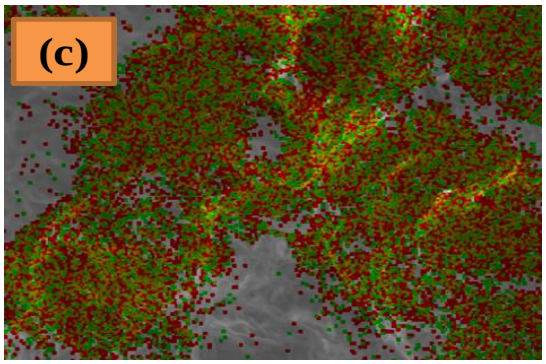

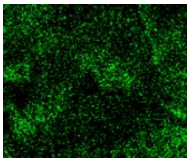
Carbon

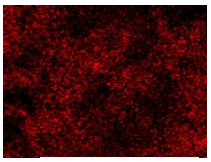
Oxygen

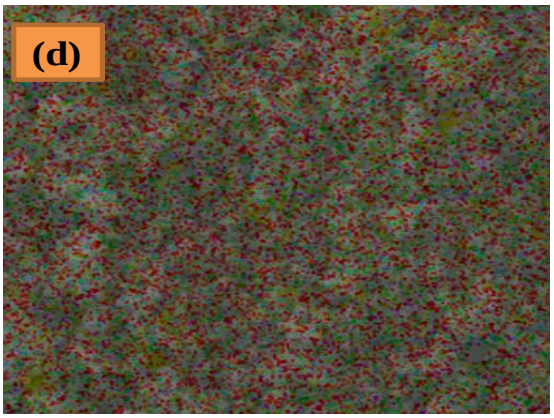

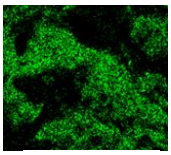
Carbon

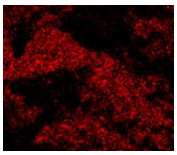
Oxygen

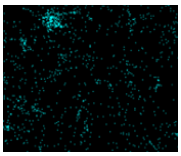
zinc

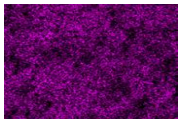
Sodium

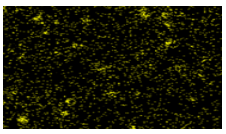
Silver

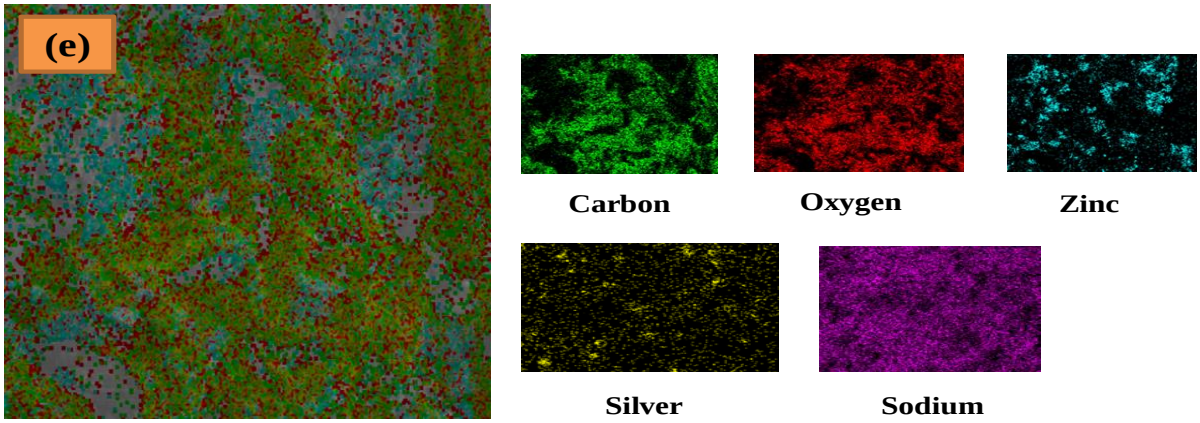

Figure 4.11 EDX maping results (a) WH stem, (b) Bleached cellulose, (c) CNCs, (d) Ag@ZnO NPs, and (e) CNCs/Ag@ZnO NPs (1:0.5) BNC

4.9 Point of Zero Charge

The point of zero charge plots of CNCs, Ag@ZnO NPs, and CNCs/Ag@ZnO (1:1), CNCs/Ag@ZnO (1:0.5) and CNCs/Ag@ZnO (0.5:1) BNCs were shown in Figure 4.12 (a) and (b) and the obtained P_{zc} of each sample was 7.59, 7.23, 7.26, 7.67, and 7.42, respectively. The experimental analysis results were also given in Appendix-H.

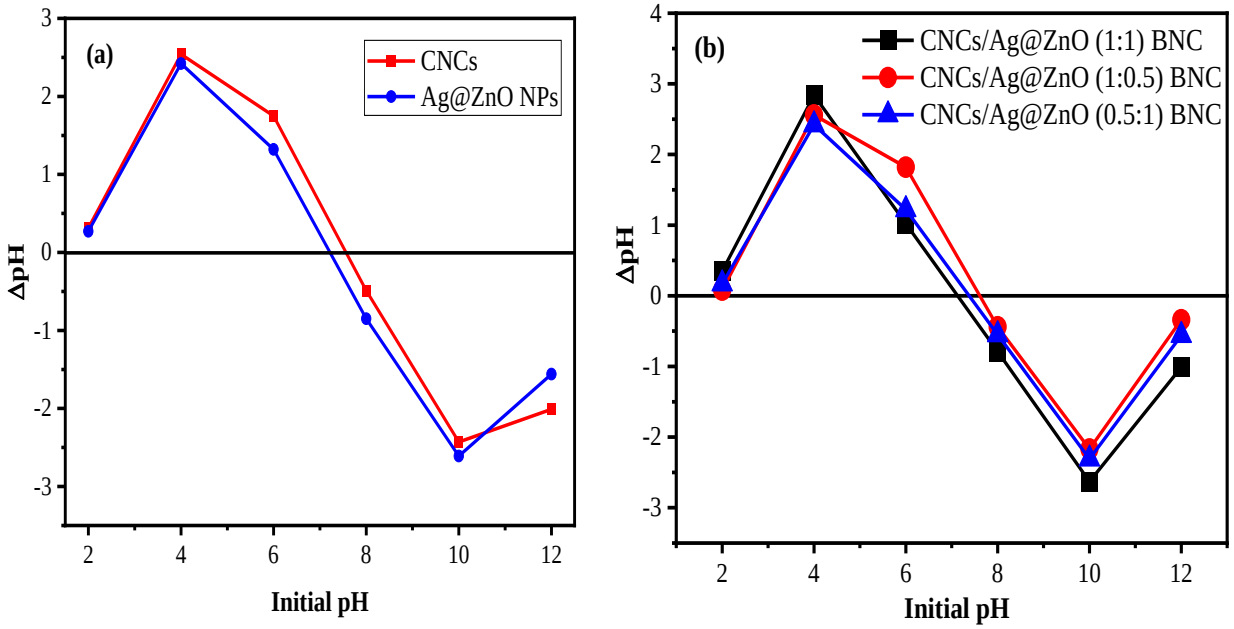

Figure 4.12 Point of zero charge (a) CNCs and Ag@ZnO NPs, (b) CNCs/Ag@ZnO (1:1), CNCs/Ag@ZnO (1:0.5) and CNCs/Ag@ZnO (0.5:1) BNC

Each P_{zc} graphs were confirms the surface charge of all samples were exhibited an ionic (negatively charged) property. If the pH of the solution become higher than P_{zc}, the surface of the material attracts cationic (positively charged) substance from a given solutions. Under these conditions, the cationic MB dye solution expected to degrade efficiently by anionic materials under light irradiation.

4.10 Photocatalytic Degradation Study

The photocatalytic performance of CNCs, Ag@ZnO NPs and CNCs/Ag@ZnO (1:1) BNC were investigated at different pH value under light irradiation (see Figure 4.13) to compare their degradation efficiency and for selecting the more efficient for further photocatalytic study. According to the results, CNCs, Ag@ZnO NPs and CNCs/Ag@ZnO (1:1) BNC exhibits 78.5%, 92.5% and 96.68% of dye degradation efficiency, at pH=10. This indicates CNCs/Ag@ZnO (1:1) BNC has higher dye degradation efficiency than CNCs and pure Ag@ZnO NPs.

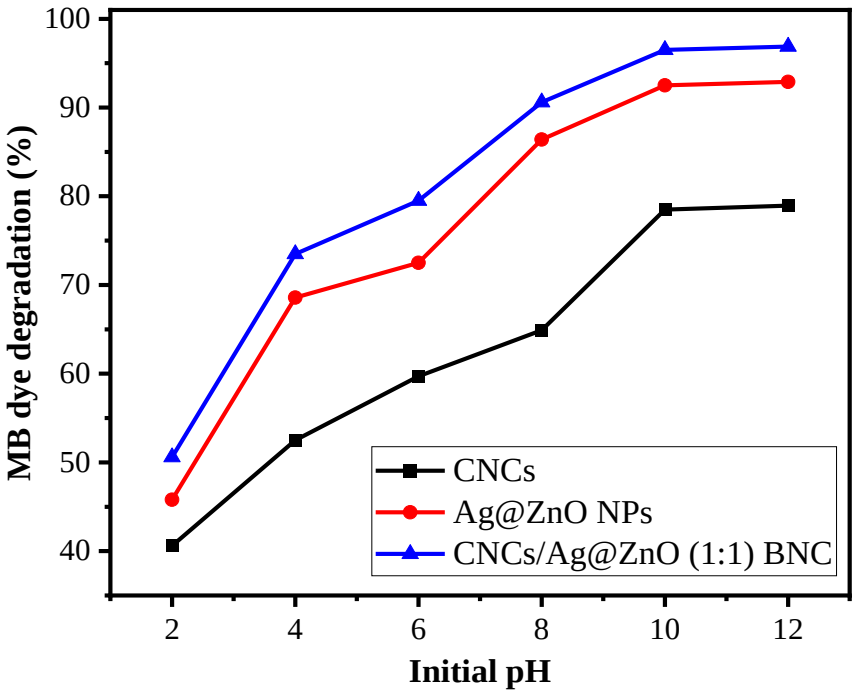

Figure 4.13 Comparison of photodegradation efficiency of CNCs, Ag@ZnO NPs and CNCs/Ag@ZnO NPs (1:1) BNC

In addition, at the minimum pH of the dye solution the degradation efficiency of CNCs, Ag@ZnO NPs and CNCs/Ag@ZnO NPs (1:1) BNC were lower due to the presence of excess HO_3^+ ion that resulted from the addition of HCl for pH adjustment. At the higher pH, an ionic

surface of each sample was able to capture cationic dye. But, further addition of pH of dye solution doesn't affect the dye degradation efficiency. From photocatalysis results, the incorporation of CNCs with Ag@ZnO NPs improves the photocatalytic performance of CNCs. In addition, the synthesized BNC contains multiphase nanostructures out of which one phase would be biological and rest of them would be inorganic compound that provides good physical stability and increase biodegradability performance. Therefore, CNCs/Ag@ZnO BNC was selected for further photocatalytic studies with different composite ratios (i.e. CNCs/Ag@ZnO (1:1), CNCs/Ag@ZnO (1:0.5) and CNCs/Ag@ZnO (0.5:1) BNCs). The obtained each experimental result was given in Appendix-I-1.

4.10.1 Effect of pH

In the photocatalytic degradation process, the pH of the aqueous solution potentially affects the photocatalytic efficiency of the synthesized BNCs. According to the results, all BNCs have high MB dye degradation percentage at pH=10 (see Appendix I-2.1). At this optimum pH the degradation efficiency of CNCs/Ag@ZnO (1:1), CNCs/Ag@ZnO (1:0.5) and CNCs/Ag@ZnO (0.5:1) BNC were 86.85%, 89.46% and 88.5%, respectively as shown in Figure 4.14.

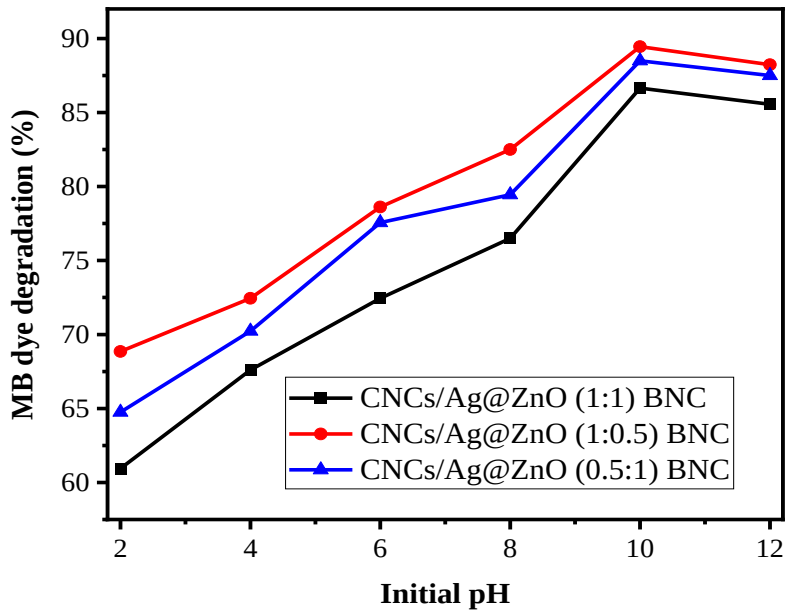

Figure 4.14 Effect of pH on the MB dye degradation efficiency of BNCs

Generally, the higher pH value provide higher numbers of hydroxyl ions to react with holes to form hydroxyl radicals, which enhance the dye decolorization rate (Modi and Fulekar, 2020). If

the pH of the dye solution higher than the optimum pH value (pH=10), the excess hydroxyl (-OH) group was created in the solution due to the addition of base (NaOH) solution for the purpose of pH adjustment. Consequently, it reduced the production of free radicals on the surface of BNCs which affect the efficiency of dye degradation under light irradiation. Furthermore, if the pH of the solution is lower than the optimum pH condition result more positive surface charge might be competed with Cl^- ions obtained from HCl during pH adjustment. As a result, the surface of the BNCs becomes inefficient to capture the targeted organic compound (MB dye) therefore; the efficiency of dye degradation under sunlight irradiation become lower.

4.10.2 Effect of BNC Dosage

The effect of CNCs/Ag@ZnO (1:1), CNCs/Ag@ZnO (1:0.5) and CNCs/Ag@ZnO (0.5:1) BNC dosage on the photocatalysis of MB dye under light irradiation was shown in Figure 4.15. It was observed that the degradation percentage of the MB dye increased with the increase of the amount of BNCs (see Appendix I-2.2) and then attained a value at equilibrium. The obtained results exhibit the increasing of photocatalyst dosage from 5 to 20 mg/L, the percentage of dye degradation also increased.

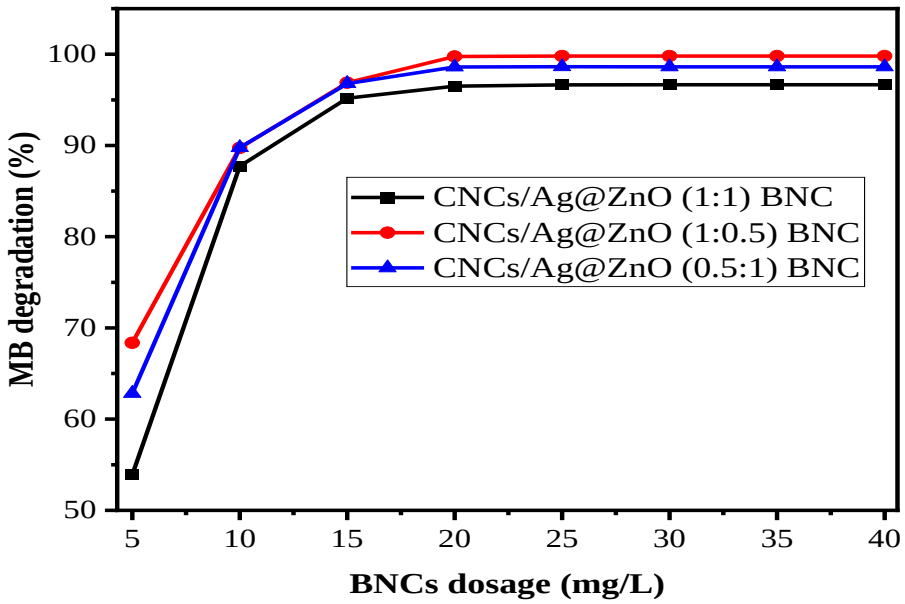

Figure 4.15 The effect of CNCs/Ag@ZnO (1:1), CNCs/Ag@ZnO (1:0.5) and CNCs/Ag@ZnO (0.5:1) BNC dosage on MB dye degradation efficiency

Further increasing in photocatalyst loading (i.e. 25, 30, 35 and 40 mg/L) does not affect the dye degradation efficiency due to the agglomeration of the photocatalyst particles (see Figure 4.15). It caused an increase in particle size and decrease in specific surface area of the BNCs, which leads to decrease the number of surface active sites (Shreema et al., 2021). From the study, 20mg/L of BNC dosage was taken as an optimum value for all BNCs ratio. In addition, at the optimum photocatalyst dosage and pH of the dye solution, the dye degradation efficiency of CNCs/Ag@ZnO (1:1), CNCs/Ag@ZnO (1:0.5) and CNCs/Ag@ZnO (0.5:1) BNCs were 96.5%, 99.95% and 98.6%, respectively. The highest dye degradation efficiency was achieved by CNCs/Ag@ZnO (1:0.5) BNC as compared to the others BNCs (i.e. CNCs/Ag@ZnO (1:1) and CNCs/Ag@ZnO (0.5:1)).

4.10.3 Effect of MB Concentration

The effect of MB dye concentration on the dye degradation efficiency of BNCs was investigated and the results were given in Figure 4.16. The dye degradation efficiency of CNCs/Ag@ZnO (1:1), CNCs/Ag@ZnO (1:0.5) and CNCs/Ag@ZnO (0.5:1) BNCs was decreases as increase of MB dye concentration. From this study, 15mg/L of MB dye concentration was an optimal value and at this concentration the degradation efficiency of CNCs/Ag@ZnO (1:1), CNCs/Ag@ZnO (1:0.5) and CNCs/Ag@ZnO (0.5:1) BNCs were 95.25%, 98.85% and 97.68%, respectively. The detail calculations were given in Appendix I-2.3.

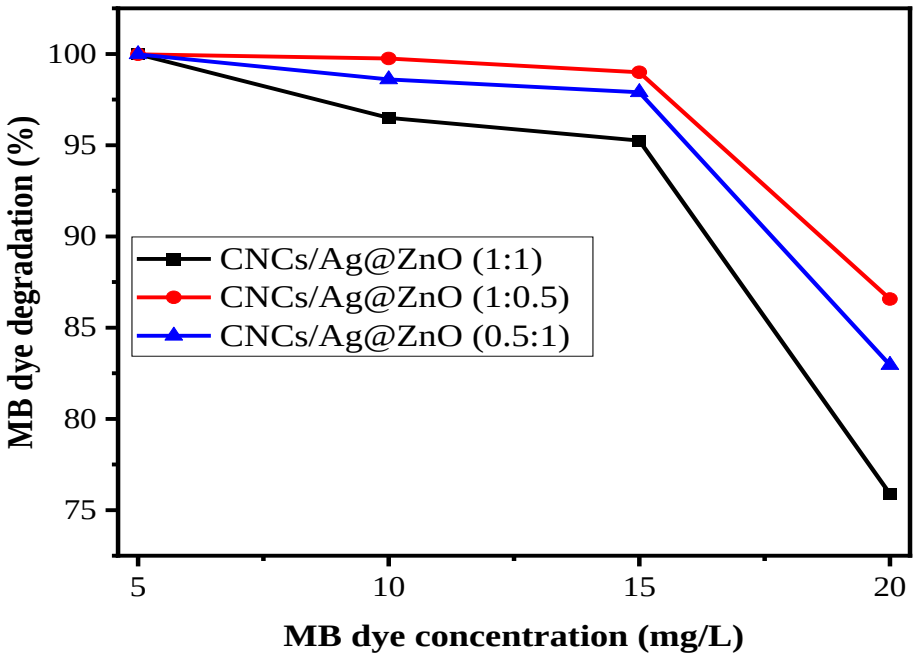

Figure 4.16 The effect of MB dye concentration on the dye degradation efficiency of CNCs/Ag@ZnO (1:1), CNCs/Ag@ZnO (1:0.5) and CNCs/Ag@ZnO (0.5:1) BNC

According to the results, CNCs/Ag@ZnO (1:0.5) BNC has the highest photocatalytic performance compared to CNCs/Ag@ZnO (1:1) and CNCs/Ag@ZnO (0.5:1) BNCs (see Figure 4.16). Generally, increasing of MB dye concentration leads to decreasing of dye degradation efficiency of the BNCs. This is due to lack of sufficient surface area (active sites) on the surface of the BNCs for the effective photocatalytic reaction process (Rahman and Neethu, 2017).

4.10.4 Effect of Irradiation Time

Figure 4.17 represents the variation of dye degradation efficiency of CNCs/Ag@ZnO (1:1), CNCs/Ag@ZnO (1:0.5) and CNCs/Ag@ZnO (0.5:1) BNCs at a given irradiation time (i.e. 0, 30, 60, 90, 120, 150 and 180min). Until 30min of irradiation time, low dye degradation efficiency was exhibited in all BNCs (see Appendix I-2.4) due to slower diffusion of solute onto BNCs surfaces. Significantly, at further increase of irradiation time the dye degradation efficiency was increase due to the number of free active sites of the BNCs was efficiently contact with MB dye molecules (see Figure 4.17).

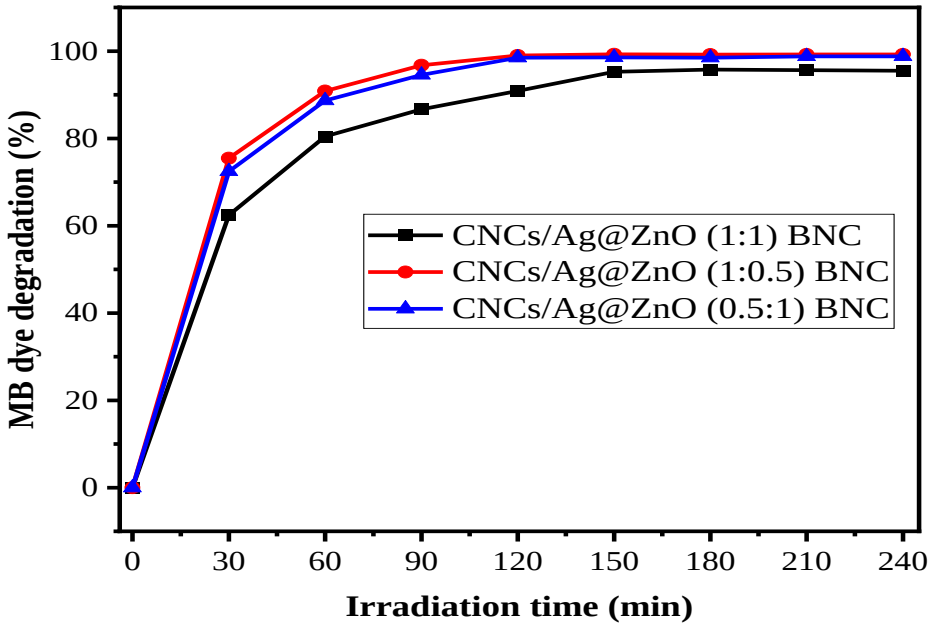

Figure 4.17 The effect of irradiation time on the degradation efficiency of CNCs/Ag@ZnO (1:1), CNCs/Ag@ZnO (1:0.5) and CNCs/Ag@ZnO (0.5:1) BNC.

However, after optimum irradiation time the degradation efficiency become constant due to the photocatalyst active sites were deactivated by strong by-products deposition on the surface of BNC (Ahmad et al., 2019). In this study, the optimum irradiation time for CNCs/Ag@ZnO (1:1), CNCs/Ag@ZnO (1:0.5) and CNCs/Ag@ZnO (0.5:1) BNC were 150 min, 120 min and 120 min, respectively. The dye degradation efficiency of CNCs/Ag@ZnO (1:1), CNCs/Ag@ZnO (1:0.5) and CNCs/Ag@ZnO (0.5:1) BNCs at optimal irradiation time were 95.8%, 98.8% and 98.25%, respectively. From the result, CNCs/Ag@ZnO (1:0.5) BNC required small irradiation time for degrading 15mg/L of MB dye concentration as compared to CNCs/Ag@ZnO (1:1) and CNCs/Ag@ZnO (0.5:1) BNCs.

4.10.5 Kinetics Study of MB Dye Degradation

The degradation kinetics of MB dye was investigated using CNCs/Ag@ZnO (1:1), CNCs/Ag@ZnO (1:0.5) and CNCs/Ag@ZnO (0.5:1) BNC, at optimum pH value (pH=10) and BNCs dosage (20mg/L) and the obtained results were given in Figure 4.18. After each degradation process, the residual MB dye concentration was determined by UV-Vis spectrophotometer at λmax = 664nm. All the kinetics plots were linear with R^2 (correlation coefficient) values (see Figure 4.18) this confirms the applicability of the pseudo-first-order reaction kinetic model for the photocatalytic degradation of MB dye. From the kinetic study, the dye degradation rate was decreased with increasing of the MB dye concentration from 5 to 20mg/L under light irradiation (see detail experimental analysis in Appendix-J).

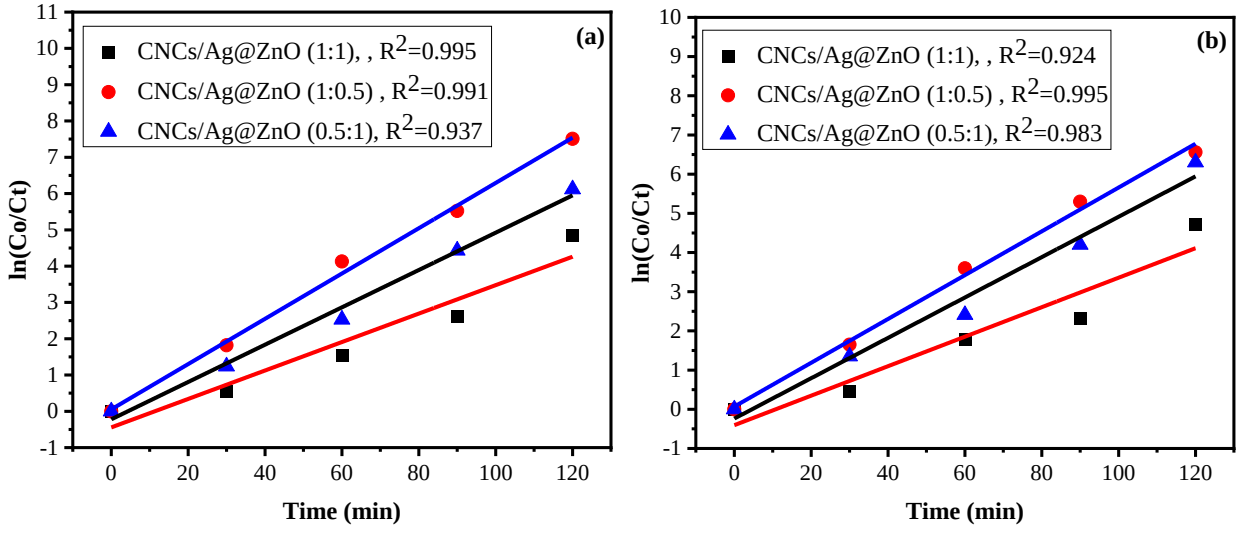

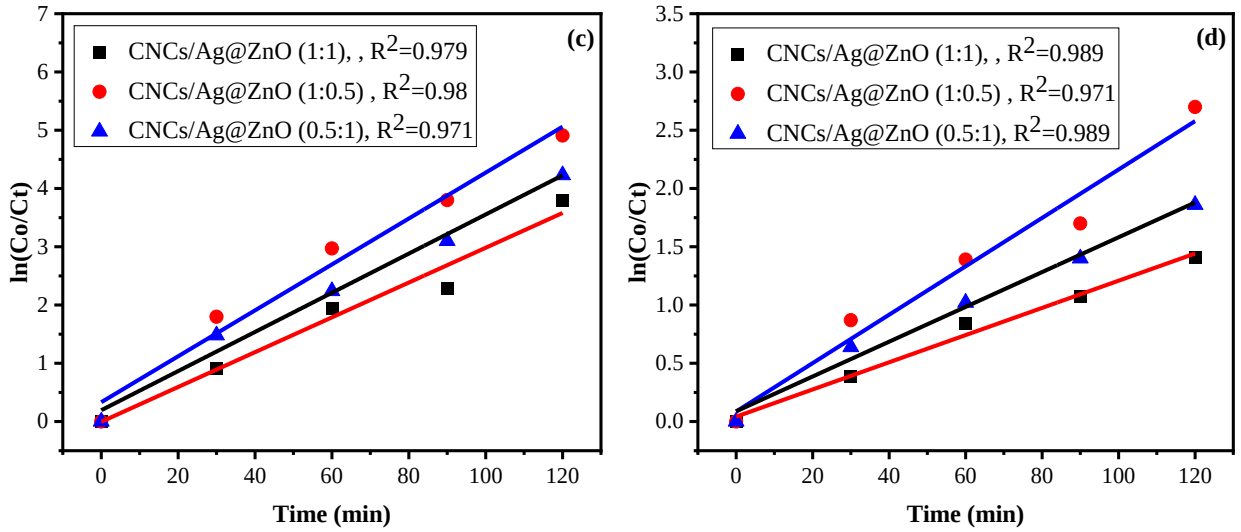

Figure 4.18 The pseudo first order kinetics model of MB dye degradation (a) 5mg/L , (b) 10mg/L, (c) 15mg/L and (d) 20mg/L of MB dye concentration.

4.10.6 Photocatalytic Performance Study under Dark Region

In different contact time, the obtained dye degradation efficiency of CNCs, Ag@ZnO NPs, and CNCs/Ag@ZnO (1:1), CNCs/Ag@ZnO (1:0.5) and CNCs/Ag@ZnO (0.5:1) BNCs under dark condition was exhibited in Figure 4.19. At optimum process conditions (i.e. pH of the dye solution = 10, BNCs dosage = 20mg/L, and MB dye concentration = 15mg/L), the dye degradation efficiency of CNCs, Ag@ZnO NPs, and CNCs/Ag@ZnO (1:1), CNCs/Ag@ZnO (1:0.5) and CNCs/Ag@ZnO (0.5:1) BNCs were 68.61%, 69.46%, 72.2%, 84.8%, and 83.29%, respectively. According to the results, CNCs/Ag@ZnO (1:0.5) BNC has high dye degradation efficiency under dark conditions than the other samples. The detail photocatalysis mechanism under dark region was explained in Appendix-K. This result can open the possibility of using CNCs/Ag@ZnO (1:0.5) BNC in both light and dark conditions.

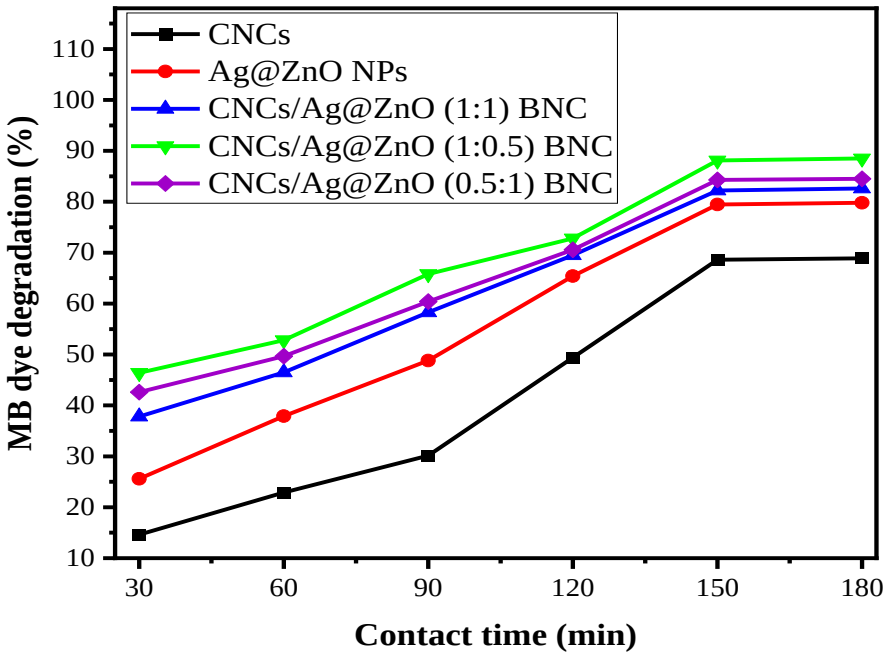

Figure 4.19 MB dye degradation under dark condition using CNCs, Ag@ZnO NPs, and CNCs/Ag@ZnO (1:1), CNCs/Ag@ZnO (1:0.5) and CNCs/Ag@ZnO (0.5:1) BNCs.

4.11 Response Surface Methodology-Box Behnken Design

During photocatalysis reaction, optimizations of the process variables using statistical approaches are crucial for the proper management of resources and time (Senthilkumar et al., 2012). In this study, the Response Surface Methodology-Box Behnken Design (RSM-BBD) approach was used to optimize the process conditions in the photocatalytic degradation of MB dye using the highest performance BNC (i.e. CNCs/Ag@ZnO (1:0.5)). Twenty nine experiments were performed according to the RSM-BBD generated as given in Table 4.6.

Table 4.6 RSM-BBD experimental design matrix and response data

Std	Run	Factors				MB degradation (%)	
		A:pH	B:CNC/Ag@ZnO (1:0.5) dosage (mg/L)	C:MB Con. (mg/L)	D:Time (min)	Actual value	Predicted value
9	1	2	17.5	12.5	30	18.9	15.34
5	2	6	17.5	5	30	40.6	43.62
12	3	10	17.5	12.5	180	98.89	103.13
11	4	2	17.5	12.5	180	15.9	16.48
24	5	6	30	12.5	180	56.5	57.55
27	6	6	17.5	12.5	105	90.5	87.92
8	7	6	17.5	20	180	64.4	60.36
4	8	10	30	12.5	105	98.5	95.84
26	9	6	17.5	12.5	105	84.6	87.92
21	10	6	5	12.5	30	17.4	17.78
14	11	6	30	5	105	93.6	92.56
13	12	6	5	5	105	60.3	58.37
1	13	2	5	12.5	105	16.5	18.14
22	14	6	30	12.5	30	46.4	48.12
6	15	6	17.5	20	30	42.4	41.83
17	16	2	17.5	5	105	46.4	46.83
20	17	10	17.5	20	105	92.5	93.50
10	18	10	17.5	12.5	30	47.4	46.41
19	19	2	17.5	20	105	27.4	28.88
3	20	2	30	12.5	105	38.6	38.03
16	21	6	30	20	105	55.5	57.01
7	22	6	17.5	5	180	83.4	82.96
23	23	6	5	12.5	180	66.5	66.22
29	24	6	17.5	12.5	105	87.5	87.92
15	25	6	5	20	105	68.9	69.53
2	26	10	5	12.5	180	86.5	86.06
25	27	6	17.5	12.5	105	88.4	87.92
28	28	6	17.5	12.5	105	88.6	87.92
18	29	10	17.5	5	105	99.99	99.94

4.11.1 Statistical Analysis

The quadratic model was chosen from the several possible models of Design-Expert 13 for the prediction of a given yield. The model equation that relates the MB dye degradation with process parameters in terms of actual factors was given in Equation (17). This equation was significant for predicting the given percentage of dye degradation and effect of each parameter. The final coded equation generated from MB dye degradation using CNC/Ag@ZnO (1:0.5) BNC was found to be well fitted to the quadratic model is:

MB degradation (Y) = + 87.92 + 29.43A + 5.42B – 6.10C + 14.47D – 4.52AB + 2.88AC +
13.9AD – 11.67BC – 9.75BD – 5.20CD – 16.24 A^2 – 14.16 B^2
– 4.39C^2 – 26.34D^2……..…… (17)

Where: A = pH

B = CNC/Ag@ZnO (1:0.5) BNC

C = MB dye concentration

D = Irradiation time

4.11.2 Model Summary Statistics

Model summary statistics focused on the model maximizing the Adjusted R^2 and the Predicted R^2. Predicted R-squared and standard deviation shows the closeness of the factors and the difference between each and grouped factors, respectively. The value of predicted R-square approaches to one indicates good fit for selected model. For this study, Quadratic model was suggested by the software. The application of RSM gives an empirical relationship between the response function and the independent variables. The recommended model for this study with Adjusted R^2 and the Predicted R^2 value were shown in Table 4.7.

Table 4.7 Suggested model for the design

Source	Std. Dev.	R^2	Adjusted R^2	Predicted R^2	PRESS	
Linear	18.06	0.6365	0.5759	0.5043	10672.54	
2FI	18.11	0.7257	0.5734	0.4254	12370.64	
Quadratic	**2.59**	**0.9956**	**0.9913**	**0.9785**	**462.88**	**Suggested**
Cubic	2.04	0.9988	0.9946	0.9550	969.81	Aliased

In particular, 99.99% of MB dye degradation by CNC/Ag@ZnO (1:0.5) BNC can be described by the proposed quadratic model. The standard deviation indicates the difference between each factors and grouped factor difference. According to model summary statistics, the closer to the unity of the R^2 (0.9956) implies that the experimental data are well fitted to the quadratic BBD model. The value shows that the predicted R-square of 0.9785 is in reasonable agreement with the adjusted R-square of 0.9913 i.e., the difference is less than 0.2. The 0.9956 value of R-square showed that 99.56% of total variation in the percentage of MB dye degradation is attributed to experimental variables studied. The model sequential sum of squares was given in Table 4.8.

Table 4.8 Sequential model sum of squares

Source	Sum of Squares	df	Mean Square	F-value	p-value	
Mean v_s Total	$1.137*10^5$	1	$1.137*10^5$			
Linear v_s Mean	13704.28	4	3426.07	10.51	< 0.0001	
2FI v_s Linear	1921.22	6	320.20	0.9761	0.4692	
Quadratic v_s 2FI	**5810.84**	**4**	**1452.71**	**216.64**	**< 0.0001**	**Suggested**
Cubic v_s Quadratic	68.80	8	8.60	2.06	0.1975	Aliased
Residual	25.08	6	4.18			
Total	$1.353*10^5$	29	4664.12			

4.11.3 Model Adequacy Test by Analysis of Variance

The developed model presented in Equation (16) was tested by analysis of variance (ANOVA) whether it is statistically significant or not and the obtained result from the quadratic BBD model shown in Table 4.9. The adequacy of the model was tested depending on F-value and P-value. F-value is important for comparing model variance with residual variance and P-value can be calculated by dividing model mean square to residual mean square. According to the ANOVA data in Table 4.9, the obtained f-value was 228.34, which implies the model is significant. P-values of model and all parameters were less than 0.0500 which indicates the model terms are significant. In this case, A, B, C, D, AB, AC, AD, BC, BD, CD, A^2, B^2, C^2, and D^2 are significant model terms. This implies the process parameters (i.e. pH of the dye solution, CNC/Ag@ZnO (1:0.5) BNC dosage, MB dye concentration, irradiation time) and their interactions are significant.

Table 4.9 ANOVA for Response Surface Quadratic Model

Source	Sum of Squares	df	Mean Square	F-value	p-value	
Model	21436.34	14	1531.17	228.34	< 0.0001	significant
A-pH	10394.68	1	10394.68	1550.15	< 0.0001	significant
B-Composite Dosage	352.08	1	352.08	52.51	< 0.0001	significant
C-MB Concentration	446.40	1	446.40	66.57	< 0.0001	significant
D-Time	2511.12	1	2511.12	374.48	< 0.0001	significant
AB	81.90	1	81.90	12.21	0.0036	significant
AC	33.12	1	33.12	4.94	0.0432	significant
AD	772.56	1	772.56	115.21	< 0.0001	significant
BC	545.22	1	545.22	81.31	< 0.0001	significant
BD	380.25	1	380.25	56.71	< 0.0001	significant
CD	108.16	1	108.16	16.13	0.0013	significant
A^2	1710.91	1	1710.91	255.15	< 0.0001	significant
B^2	1301.19	1	1301.19	194.05	< 0.0001	significant
C^2	124.98	1	124.98	18.64	0.0007	significant
D^2	4500.15	1	4500.15	671.11	< 0.0001	significant
Residual	93.88	14	6.71			
Lack of Fit	75.33	10	7.53	1.62	0.3387	not significant
Pure Error	18.55	4	4.64			
Cor Total	21530.22	28				

Additionally, the “lack of fit F-value” of 1.62 (see Table 4.10) implies there is 33.87 % chance that a “lack of fit F-value” this large could occur due to noise.

Table 4.10 Lack of fit tests summary

Source	Sum of Squares	df	Mean Square	F-value	p-value	
Linear	7807.39	20	390.37	84.19	0.0003	
2FI	5886.17	14	420.44	90.67	0.0003	
Quadratic	**75.33**	**10**	**7.53**	**1.62**	**0.3387**	**Suggested**
Cubic	6.53	2	3.27	0.7045	0.5469	Aliased
Pure Error	18.55	4	4.64			

Adequate precision compares the range of predicted values at design points to the average prediction error and measures signal to noise ratio (S/N ratio). In this system, the adequate precision was 47.1416 as shown in Table 4.11, it is greater than 4. This confirms the model prediction was adequately accurate and applicable. Furthermore, a lower value of coefficient of variation (CV = 4.14%) indicates the precision and consistency of the conducted experiment. Similarly, the obtained predicted residual sum of squares (PRESS) statistic (see Table 4.11) shows the better data points fit the model.

Table 4.11 Model statics of the design

Std. Dev.	2.59	R^2	0.9956
Mean	62.62	Adjusted R^2	0.9913
C.V. %	4.14	Predicted R^2	0.9785
PRESS	462.88	Adeq. Precision	47.1416

4.11.4 Diagnostic Plot of the Model

A normal plot of residuals between the normal probability (%) and the internally studentized residuals was used to determine how well the model satisfies the assumptions of ANOVA. Figure 4.20 (a) shows the relationship between the normal probability (%) and the internally studentized residuals. The experimental data points in the plots show fitted to the straight line that confirms the quadratic polynomial model satisfies the analysis of the assumptions of variance. In addition, Figure 4.20 (b) showed the predicted vs. actual value plots of the response parameters that judge the suitability of the model. The plots confirms the sufficient agreement

between real data and the outputs from the models. Figure 4.20 (c) shows the residuals versus run number plot that a random scattering nearby zero with a change of ± 4.0. It confirms the data were usually dispersed in the model responses. Moreover, Figure 4.20 (d) also confirms that the difference of the studentized residuals versus predicted has no individual form. Thus, it can be concluded that the achieved residuals have the usual scattering and the adequacy of the proposed model (Abolhasani et al., 2019).

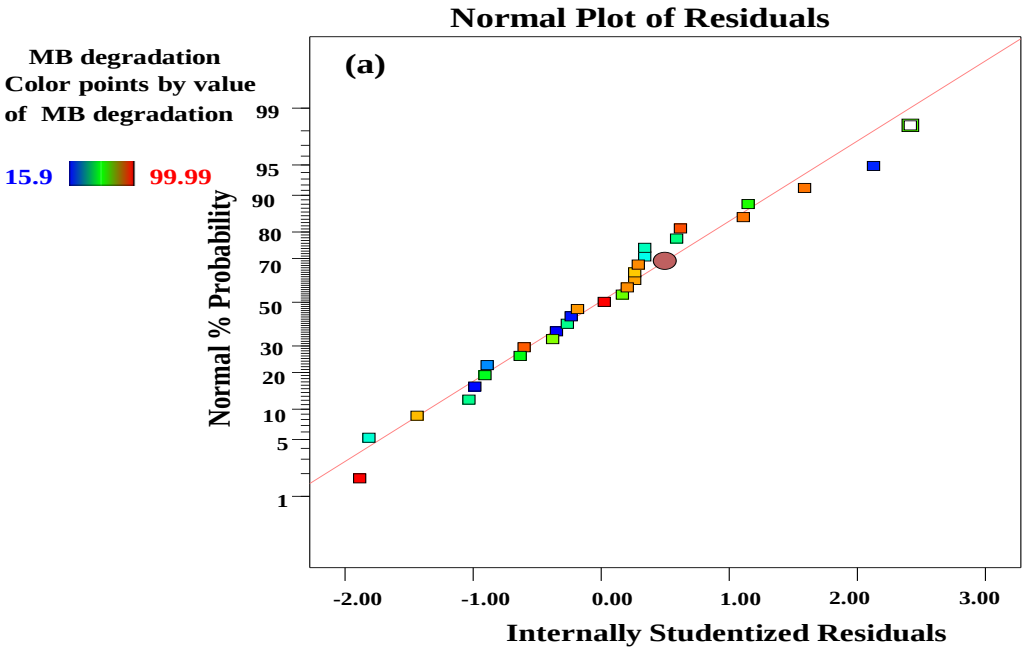

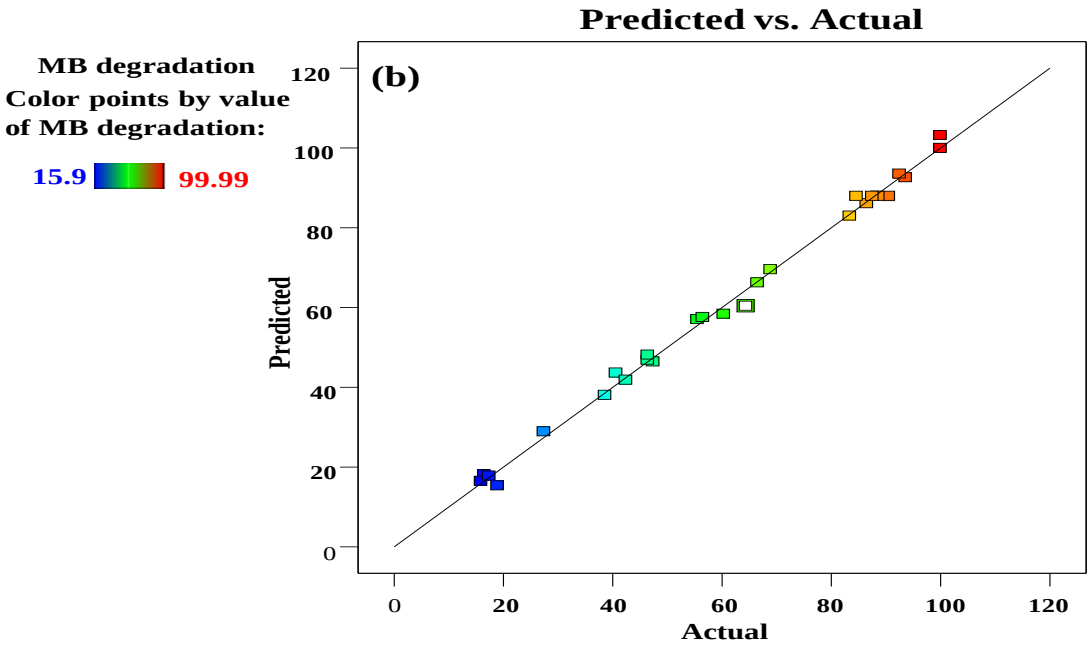

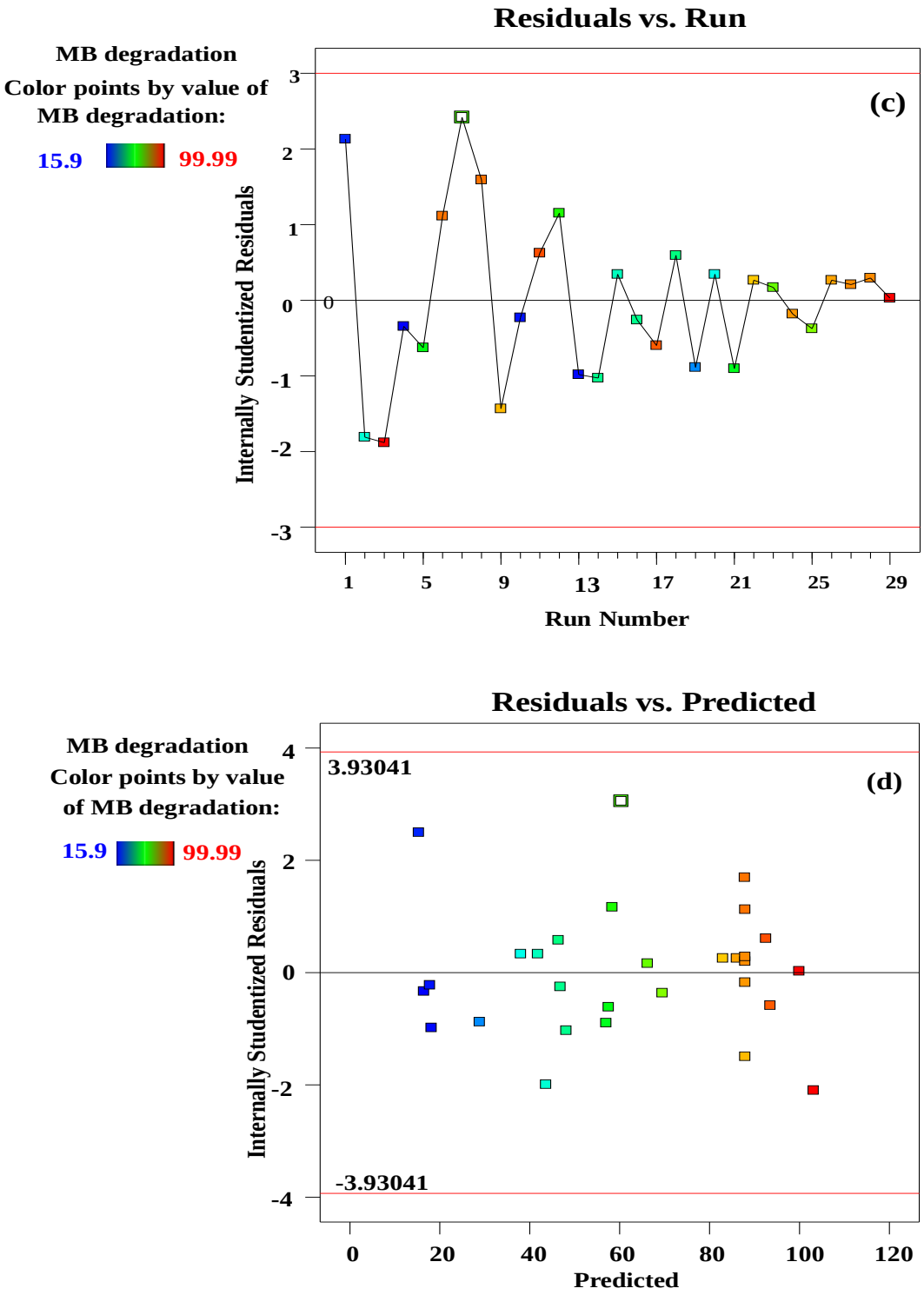

Figure 4.20 (a) Normal % probability Vs Residual, (b) Predicted Vs Actual, (c) Residual Vs Run number, and (d) Residual Vs Predicated amount for the photodegradation performance of CNCs/Ag@ZnO (1:0.5) BNC.

4.11.5 Multi- Parameters Effect Study

4.11.5.1 Effect of pH and BNC dosage

The pH of dye solution and CNCs/Ag@ZnO (1:0.5) BNC dosage has significant effect on the efficiency of MB dye degradation as shown Figure 4.21 (a) and (b). The response surface (3D) plot (Figure 4.21 (b)) clearly exhibits the MB dye degradation efficiency was increased (up to 99.98%) with increasing of pH of dye solution and CNCs/Ag@ZnO (1:0.5) BNC dosage until they were reached at optimum points. At lower pH and CNCs/Ag@ZnO (1:0.5) BNC dosage, efficiency of dye degradation was small (see Figure 4.21 (a)). However, the interaction of CNCs/Ag@ZnO (1:0.5) BNC dosage and pH of the solution have significant effect on the efficiency of MB dye degradation.

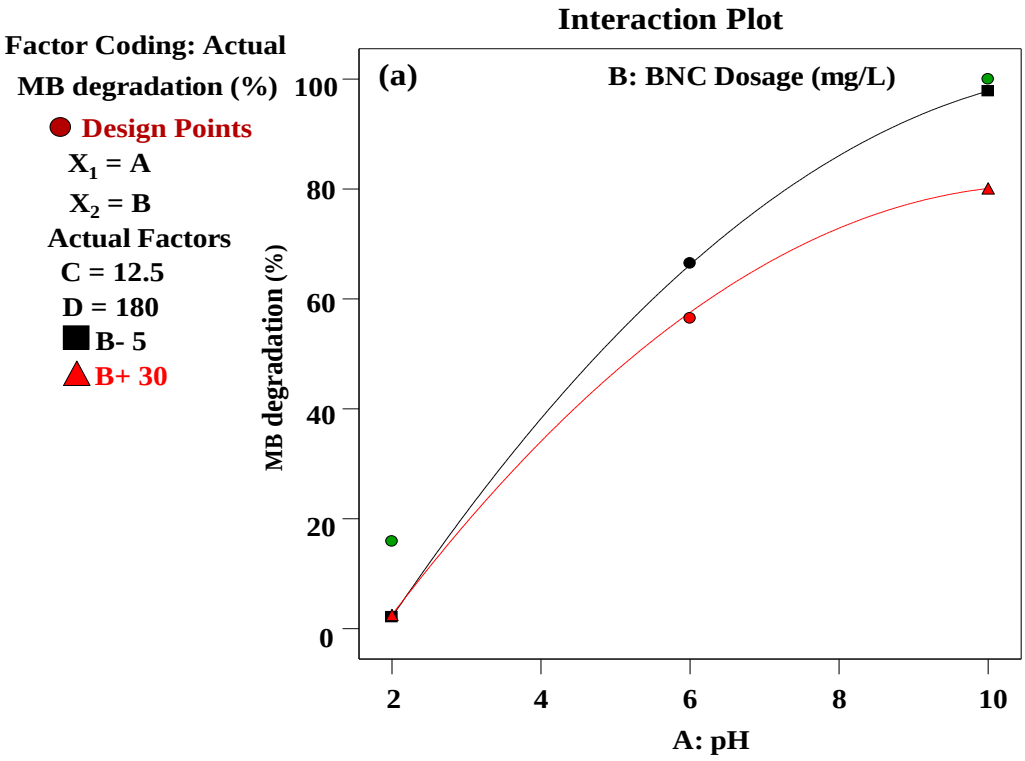

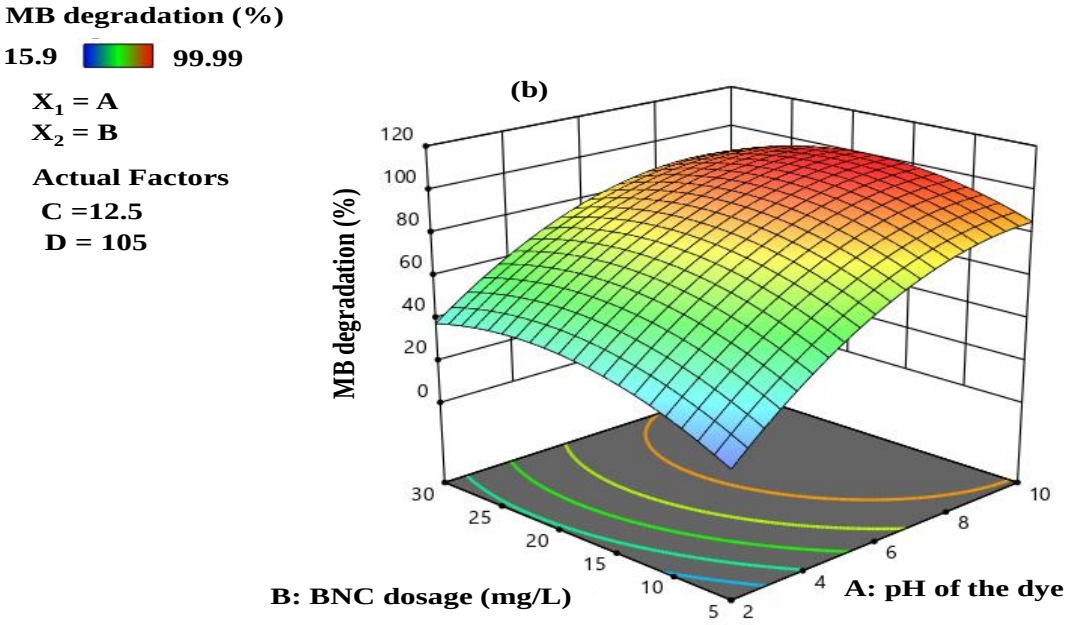

Figure 4.21 (a) Interaction and (b) 3D surface plot of the effects of pH of the solution (A) and CNCs/Ag@ZnO (1:0.5) BNC dosage (B) on the efficiency of MB dye degradation

4.11.5.2 Effect of pH and MB dye concentration

The interaction curves and 3D surface plot of pH of the dye solution and MB dye concentration shown in Figure 4.22 (a) and (b) are nearly parallel to each other. It confirms the interaction of pH of the dye solution and MB dye concentration not highly significant effect on the efficiency of MB dye degradation at a constant CNCs/Ag@ZnO (1:0.5) BNC dosage and irradiation time.

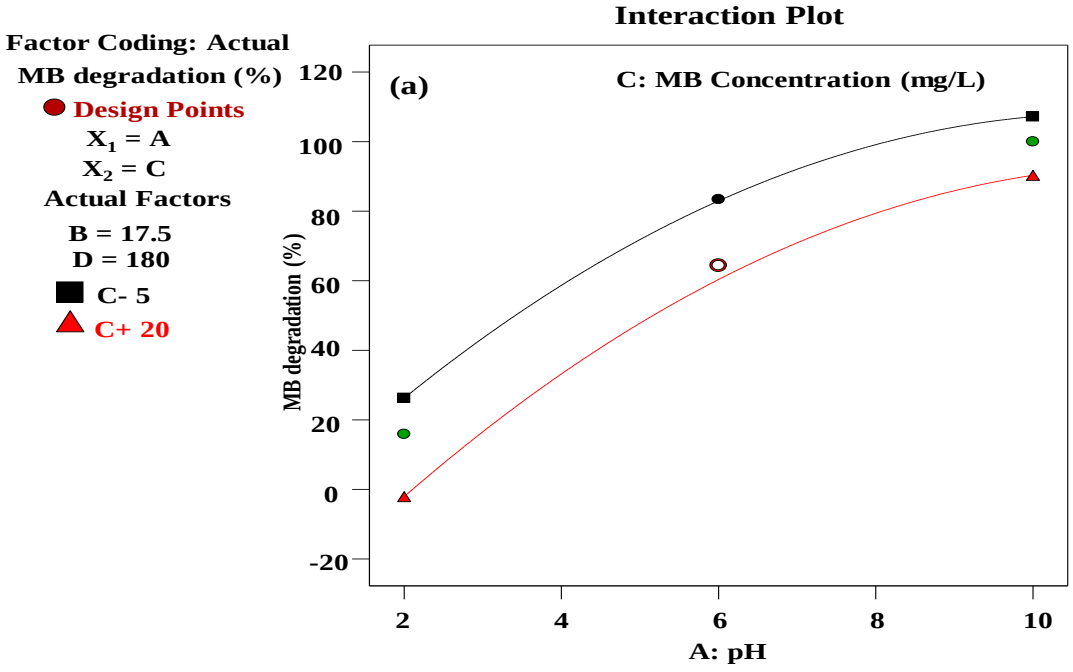

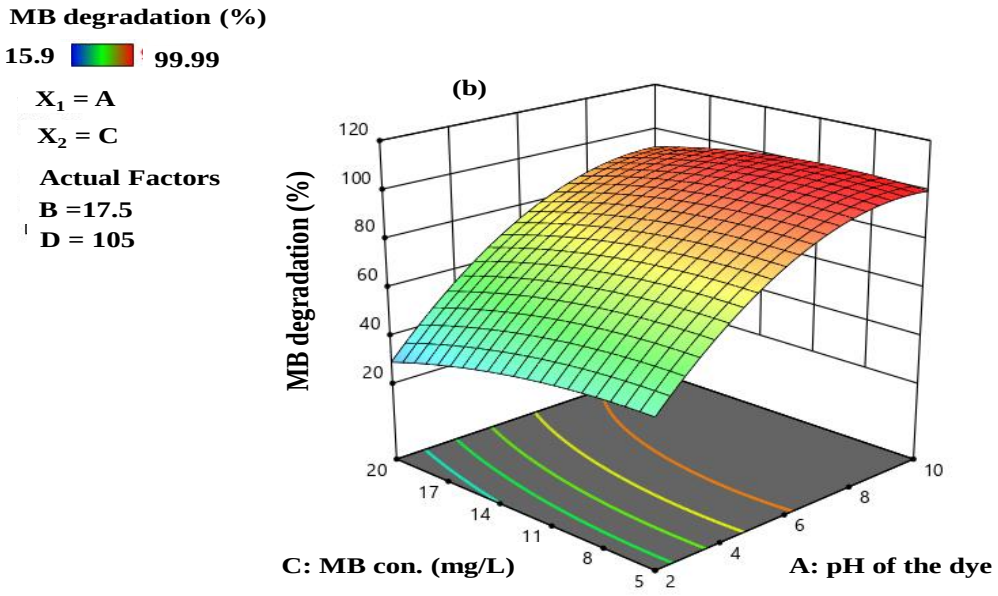

Figure 4.22 (a) Interaction curves and (b) 3D surface plot of the effects of pH of the solution (A) and MB dye concentration on the efficiency of MB dye degradation.

4.11.5.3 Effect of pH of the solution and Irradiation time

The effect of pH of the dye solution and irradiation time negatively affects the efficiency of MB dye degradation after reached optimum point as shown in Figure 4.23 (a) and (b). It was observed that at lower level of pH and irradiation time, gives lower degradation efficiency and vice versa. After optimum values the degradation efficiency becomes decreased. However, at lower pH of the dye solution the variation of irradiation time has no significant effect.

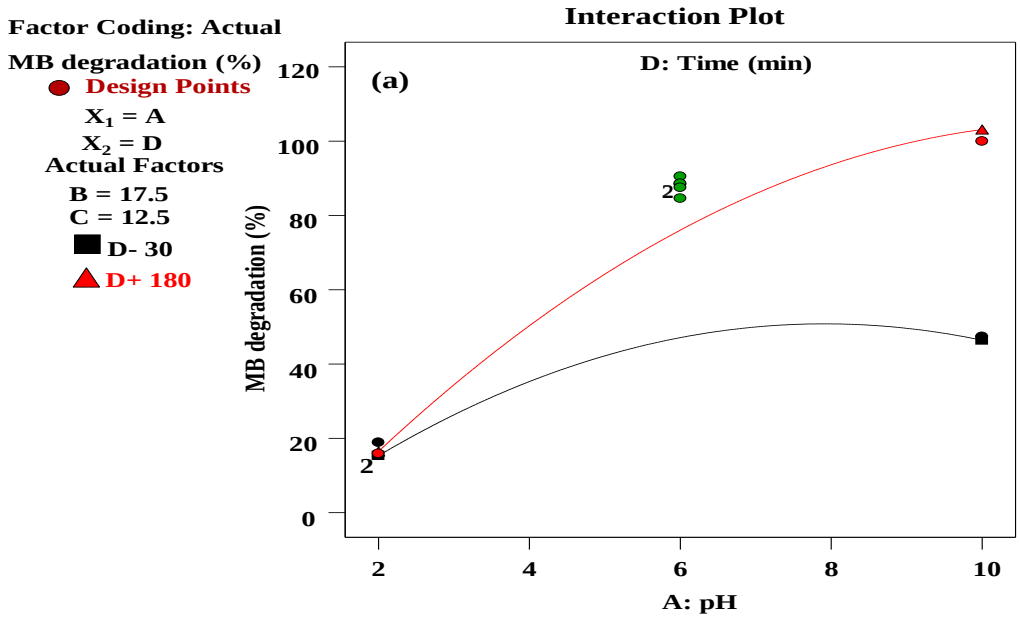

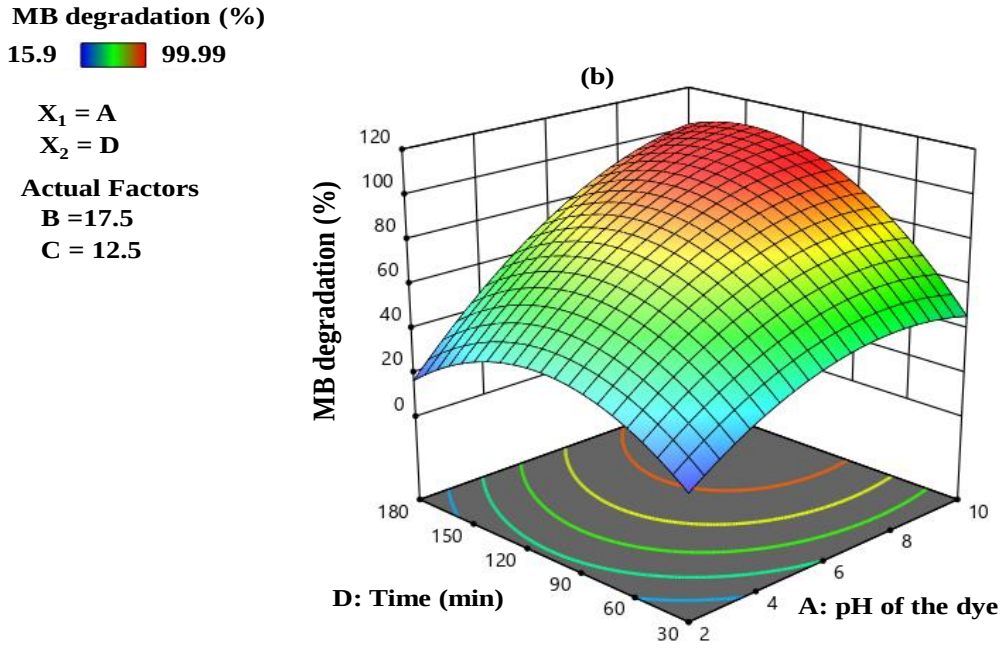

Figure 4.23 (a) Interaction and (b) 3D surface plot of the effects of pH of the dye solution (A) and irradiation time (D) on the MB dye degradation efficiency.

4.11.5.4 Effect of BNC dosage and MB dye concentration

The interaction of CNCs/Ag@ZnO (1:0.5) BNC dosage and MB dye concentration has significant effect on the efficiency of MB dye degradation as shown in Figure 4.24 (a). It was observed that the dye degradation efficiency was increased with increasing CNCs/Ag@ZnO (1:0.5) BNC dosage from 5 to 17.5 mg/L and lower MB dye concentration (5 -10 mg/L). After optimal points CNCs/Ag@ZnO (1:0.5) BNC dosage =17.5 mg/L and MB dye concentration = 12.5) the degradation efficiency decreased. It confirms the excessive amount of CNCs/Ag@ZnO (1:0.5) BNC forms agglomeration in the dye solution. In addition, further addition of MB dye concentration reduced the dye degradation efficiency. This is happened due to the availability of the active sites on the surface of BNC was not sufficiently enough for photocatalysis. The 3D surface as shown in Figure 4.24 (b) also confirms the dye degradation efficiency highly affected by the variation of BNC dosage and the amount of added MB dye molecules.

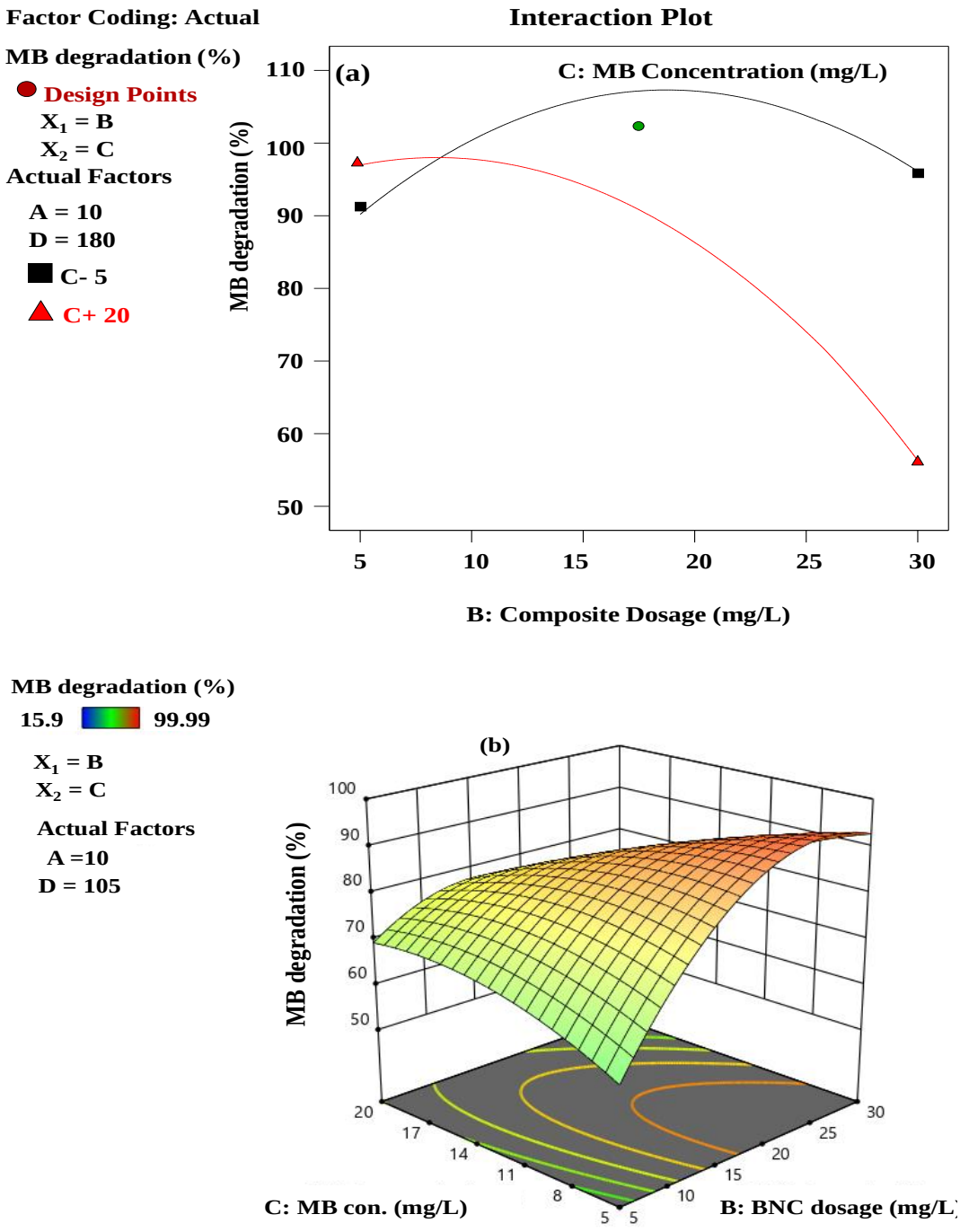

Figure 4.24 (a) Interaction and (b) 3D surface plot of the effects of CNCs/Ag@ZnO (1:0.5) BNC dosage (B) and MB dye concentration (C) on the efficiency of MB dye degradation

4.11.5.5 Effect of BNC Dosage and Iraddiation Time

Figure 4.25 (a) and (b) exhibits the interaction effect of CNCs/Ag@ZnO (1:0.5) BNC dosage and irradiation time on MB dye degradation efficiency. There is an increase in the dye

degradation efficiency with an increase of CNCs/Ag@ZnO (1:0.5) BNC dosage and irradiation time until it reached at optimal points. After further increasing of both process parameters the dye degradation efficiency was decreased.

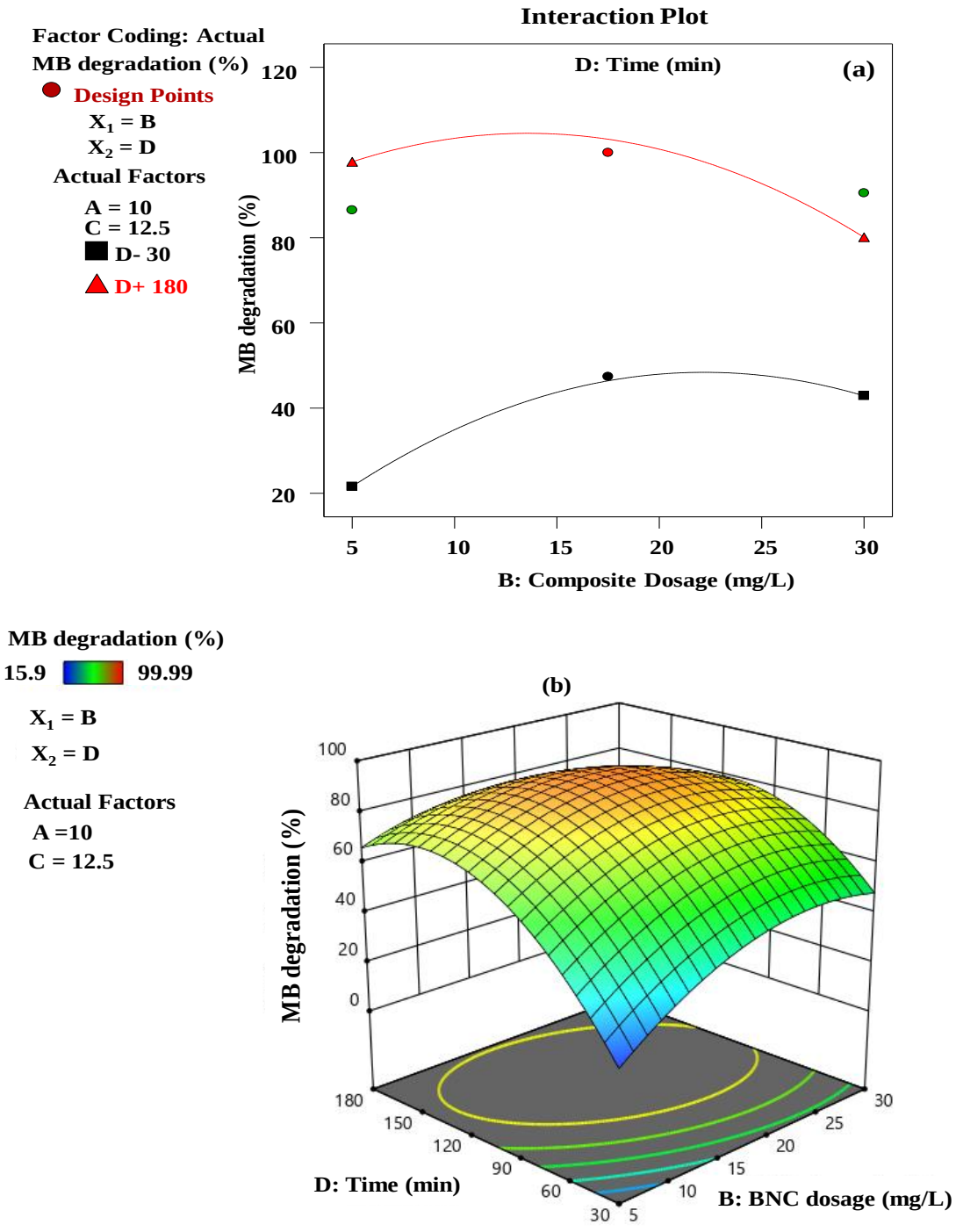

Figure 4.25 (a) Interaction and (b) 3D plot of the effects of CNCs/Ag@ZnO (1:0.5) BNC dosage (B) and irradiation time (D) on the efficiency of MB dye degradation

4.11.5.6 Effect of MB Dye Concentration and Irradiation Time

The effects of MB dye concentration and irradiation time interaction on dye degradation efficiency was clearly shown in Figure 4.26 (a) and (b). It exhibits at lower dye concentration the degradation efficiency gradually increases with increasing irradiation time.

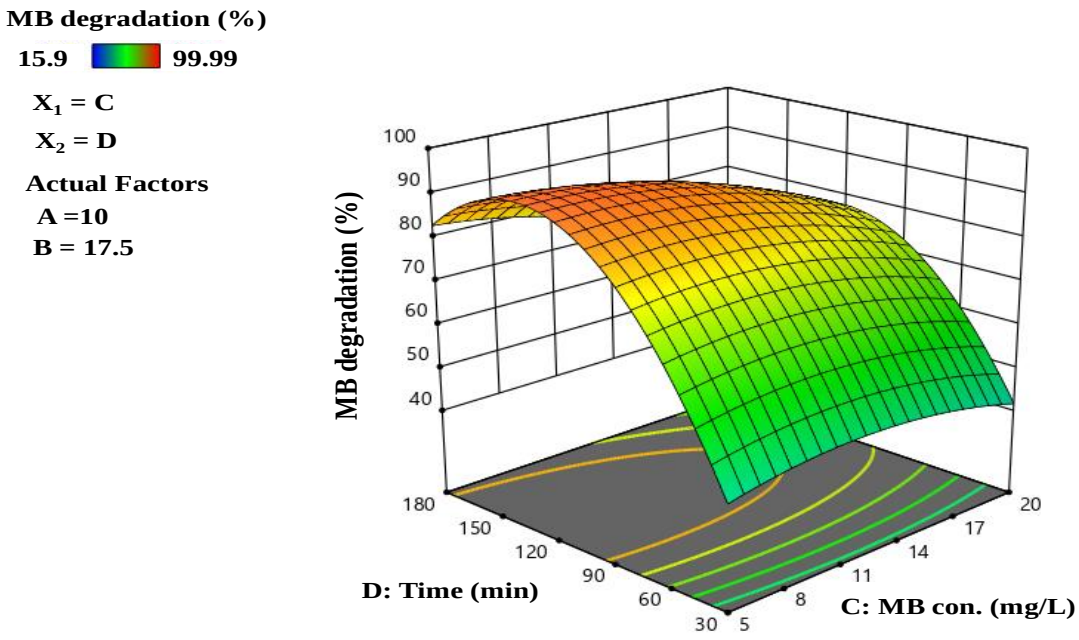

Figure 4.26 3D surface plot of the effects of MB dye concentration (C) and irradiation time (D) on the efficiency of MB dye degradation.

However, the trend of degradation efficiency was decreased at higher level of dye concentration and irradiation time. As a conclusion, the dye degradation efficiency significantly decreases when MB dye concentration and irradiation time were too high.

4.11.5 Optimization of the Process Parameters

The objective of optimization was to maximizing MB dye degradation efficiency in a given design space and range of process parameters. Optimization of different combination of process variables was conducted depending on desirability (D). The RSM-BBD optimization with other scenarios gives maximum dye degradation percentage, and based on considering the available resource it is possible to adapt different combinations of pH of the dye solution, CNCs/Ag@ZnO (1:0.5) BNC dosage, MB dye concentration and contact time. Numerical optimization and graphical optimization are most common ways for finding optimum response with optimum operating conditions. For this study numerical optimization was selected and the criteria set for the four factors were shown in the Table 4.12.

Table 4.12 Adjusted process parameters to maximize the dye degradation efficiency

Name	Goal	Lower Limit	Upper Limit	Lower Weight	Upper Weight	Importance
A:pH	Maximize	2	10	1	1	3
B:CNCs/Ag@ZnO (1:1) Dosage	In Range	5	30	1	1	3
C:MB Concentration	In Range	5	20	1	1	3
D:Time	In Range	30	180	1	1	3
MB degradation	Maximize	15.9	99.99	1	1	3

The desirability value helps to identify the maximum and stable response of the experiment. Additionally, obtaining a point in which a maximum MB dye degradation percentage occurred and low value of parameters was important to identify the optimum point (Hasanpour et al., 2021). According to numerical optimization solution, the maximum percentage of dye degradation of 99.040 % was achieved as shown in Appendix-L at the interaction parameters of pH= 10, 18.075 mg/L of CNCs/Ag@ZnO (1:0.5) BNC dosage, 17.468 mg/L of MB dye concentration and 111.855 min of irradiation time.

Table 4.13 Point prediction optimization of process parameter and response

Factor	Name	Level	Low Level	High Level	Std. Dev	Coding	
A	pH	10	2	10	0	Actual	
B	BNC Dosage (mg/L)	18.0751	5	30	0	Actual	
C	MB Con. (mg/L)	17.4679	5	20	0	Actual	
D	Contact Time (min)	111.855	30	180	0	Actual	
Response (%)	Prediction 102.04	SE mean 1.15807	95% CI low 85.4362	95% CI high 90.4038	SE Pred 2.83667	95% PI low 81.8359	95% PI high 94.004

After optimization, Experiments were conducted to determine whether the predicted results by the models are attainable. The experiments were carried out in triplicate (see Apendex-L-1) at predicted process parameters (i.e. pH = 10, CNCs/Ag@ZnO (1:0.5) BNC dosage =18.075 mg/L, MB dye concentration = 17.468 mg/L and Irradiation time = 111.855 min). The obtained degradation efficiency was listed in Table 4.14 and the average degradation efficiency was 98.85. From this result, it is observed that the responses predicted through the regression models and measured from the experiments were in close agreement. This implies that the obtained optimal process parameters from RSM-BBD analysis were reliable and applicable in real dye removal process and wastewater treatment.

Table 4.14 Experimental results

No. of conducted experiment	MB dye degradation efficiency (%)
Exp.1	98.82
Exp.1	99.3
Exp.1	98.43
Average	98.85

In addition, the obtained optimum values of process parameters i.e. pH of the dye solution, CNCs/Ag@ZnO (1:0.5) BNC dosage, MB dye concentration and irradiation time in the single effect study were agree with multiple effect-study through DoE. Generally, attaining of high degradation efficiency at lower photocatalyst dosage and operating time with high dye concentration is more feasible and has low operating cost. Moreover, MB dye degradation efficiency of CNCs/Ag@ZnO (1:1) and CNCs/Ag@ZnO (0.5:1) BNC were examined at optimum process parameters value (Apendix-L-2) and the obtained dye degradation percentage was 83.8% and 96.8% respectively. It confirms the synthesized CNCs/Ag@ZnO (1:0.5) BNC has high photocatalytic efficiency than CNCs/Ag@ZnO (1:1) and CNCs/Ag@ZnO (0.5:1) BNC.

4.12 Photodegradation Study on Real Textile Wastewater

The textile wastewater mainly contains considerable amounts of hazardous pollutants, where MB dye is very common. From the study, the pH of wastewater, color, COD and absorbance of the real textile wastewater were 9.8, blue color, and 0.264, respectively. It confirms the released sample was highly basic and has high concentration of MB dye, which potentially damages the human and environmental health during it discharged directly into nearby water bodies. In

addition, Figure 4.27 exhibits the calibration curve of known MB dye concentration (5-45mg/L) to determine the molar absorptivity coefficient and unknown dye concentration of the real sample.

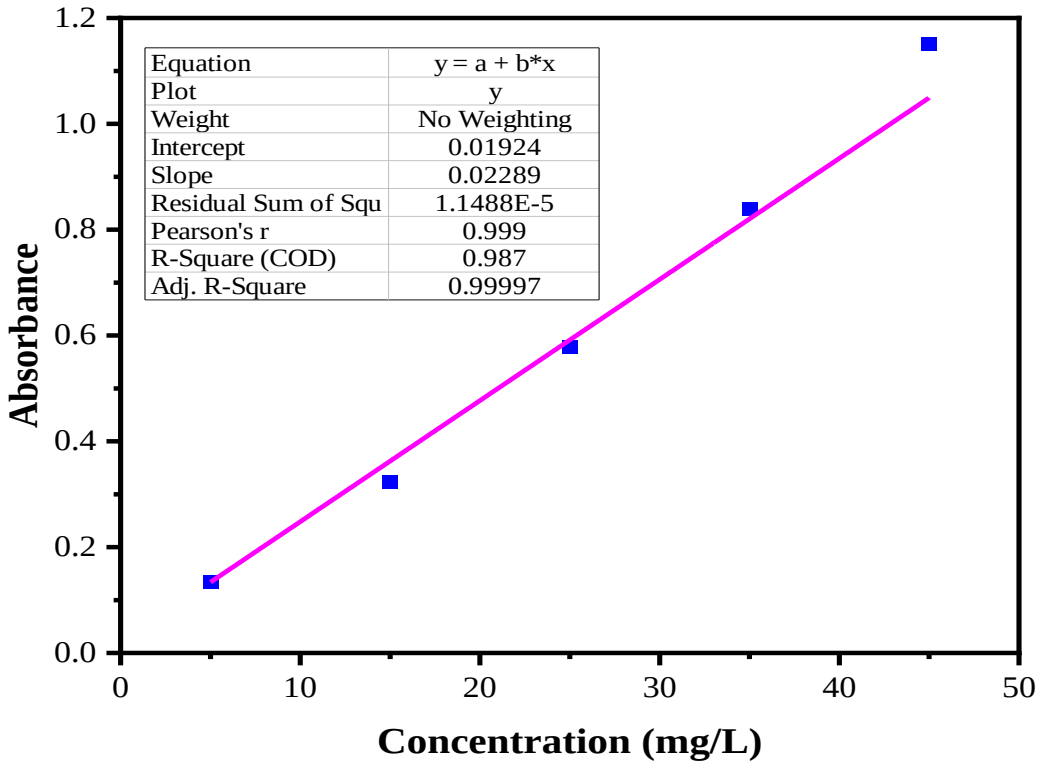

Figure 4.27 Calibration curve using known MB dye concentration (5-45mg/L)

From the curve, the molar absorptivity coefficient was $2.289*10^{-2}$ L mol^{-1} cm^{-1}. According to Beer's law equation the unknown MB dye concentration present in textile wastewater was 11.53 mg/L. The calculation part was given in Appendix-M. The obtained result indicates the high amount of MB dye molecule released from the company into nearby water bodies that potentially damage the aquatic ecology and surrounding lives. In addition, at optimum process parameters (i.e. pH = 10, CNCs/Ag@ZnO (1:0.5) BNC dosage =18.075 mg/L, MB dye concentration = 17.468 mg/L and Irradiation time = 111.855 min) the MB dye degradation efficiency of CNCs/Ag@ZnO (1:1), CNCs/Ag@ZnO (1:0.5) and CNCs/Ag@ZnO (1:0.5) BNC were 97.73%, 99.24% and 98.86%, respectively (see Appendix-O). The results confirm CNCs/Ag@ZnO (1:0.5) BNC has high photocatalytic efficiency in degradation of MB dyes from synthetic solution and real textile wastewater.

4.13 Reusability study

The possibility of reusing of the photocatalyst was examined to see the cost effectiveness of the method. At pH = 10, CNCs/Ag@ZnO (1:0.5) BNC dosage =18.075 mg/L, MB dye concentration = 17.468 mg/L and Irradiation time = 111.855 min (see Figure 4.28) the recyclability study was carried out.

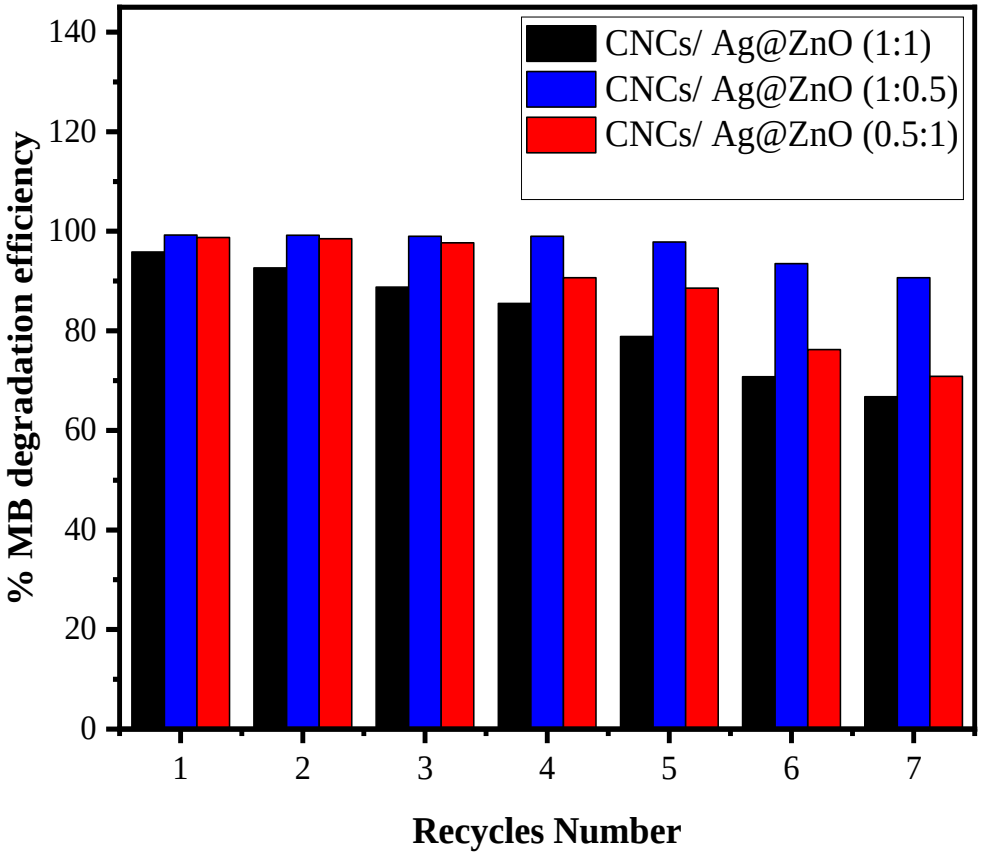

Figure 4.28 Reusability Study

From the results, it was observed the photodegradation efficiency of the three synthesized BNC was high, especially CNCs/Ag@ZnO (1:0.5) BNC at the first five degradation cycle. After five cycles, the degradation efficiency of each BNC slightly decreased due to the accumulation of the pollutant particles over the surface of the photocatalysts. Since the degradation efficiency of CNCs/Ag@ZnO (1:0.5) BNC did not decrease significantly after seven cycles, it was confirmed that composite improved stability and anti-photo corrosive nature. The degradation efficiency of CNCs/Ag@ZnO (1:1), CNCs/Ag@ZnO (1:0.5) and CNCs/Ag@ZnO (1:0.5) at seventh cycle was 66.75%, 90.67% and 70.85%, respectively (see Appendix-N). Therefore, CNCs/Ag@ZnO (1:0.5) has high recyclability efficiency.

CHAPTER FIVE

5. Conclusions and Recommendations

5.1 Conclusions

In this study, proximate and chemical composition analyses of raw WH stem were determined. From proximate analysis, the air dried powder WH stem has 15.21wt% moisture and 21.6wt% ash content. According to chemical composition analysis, the WH stem contains 19.33wt% extractives, 27.24wt% hemicellulose, 5.27wt% lignin, 48.16wt% cellulose. High value-added CNCs (36.5wt%) were successfully extracted from WH stem through acid hydrolysis process. The purified cellulose was isolated from WH stem by applying different chemical process (i.e. solvent extraction, alkaline treatment, bleaching process and acid hydrolysis process). In addition, WH leaves extract mediated Ag@ZnO NPs were effectively developed through green synthesis method. The synthesized CNCs and Ag@ZnO NPs were combined to develop BNC with different composite ratios (i.e. CNCs/Ag@ZnO (1:1), CNCs/Ag@ZnO (1:0.5) and CNCs/Ag@ZnO (0.5:1)) to attain the optimum composite.

Characterization of the samples was performed and the results confirm the developed CNCs, Ag@ZnO NPs, and the three BNCs were successfully synthesized. The UV-Visible spectrophotometry analysis exhibits the band gap of Ag@ZnO NPs become narrower (3.08 eV) than pure ZnO NPs (3.37 eV) due to the Ag particles form an intermediate levels in ZnO structure. From XRD and FTIR analysis, the crystallinity and functional groups of the samples were modified in each steps of chemical treatment, respectively. The TGA results confirms Ag@ZnO NPs have high thermal stability throughout a given temperature ranges and the thermal stability of CNCs was increased after combination with Ag@ZnO NPs. In addition, the BET analysis exhibits CNCs/Ag@ZnO (1:0.5) BNC has large surface area (687.7m^2/g) and pore volume (1.85cm^3/g) and small pore size (0.12 nm) than CNCs/Ag@ZnO (1:1) and CNCs/Ag@ZnO (0.5:1) BNCs. From DLS and SEM-EDX analysis the particle size and morphological entity of the samples were improved after each stage of chemical treatment, respectively.

The photocatalytic performance of each developed BNCs was examined through single and multiple process parameter effects and the obtained result indicates at optimal process conditions CNCs/Ag@ZnO (1:0.5) BNC has high dye degradation efficiency than the other BNCs. From

multiple effect study a 3-level quadratic model can effectively show the interaction of parameters. This was validated by both regression (R^2 = 0.9956 and adjusted R^2 = 0.9913) and ANOVA ($P < 0.0001$) analyses. Furthermore, the photocatalytic efficiency of the three developed BNCs were examined using real MB dye containing textile wastewater and the founded efficiency were 97.73%, 99.24% and 98.86%, respectively. It confirms the photocatalytic performance of CNCs/Ag@ZnO (1:0.5) BNC was high and could be applied to more effectively treat wastewaters containing both MB dye and organic compounds than those containing a single species only. The recyclability study also investigated and the result indicates even though it has been conducted until the 7^{th} round, CNCs/Ag@ZnO (1:0.5) BNC still has high photocatalytic efficiency (90.67%). This indicates CNCs/Ag@ZnO (1:0.5) BNC is economical feasible and it can be applied as fruitful photocatalytic material on industrial scale for the exploitation of structurally stable and complex dyestuff. In addition, this developed bio-based photocatalyst can be used in both day and night conditions. Generally, this study suggested that this study offers a green and non-toxic method containing biomaterials to synthesize various nanomaterials using this eco-friendly preparation route which could be extend to use other natural sources.

5.2 Recommendations

In this research only the WH stem and leaves were utilized as a source of cellulose and reducing agent (during Ag@ZnO NPs synthesis), respectively. However, the left weed parts specially, the root also a source of cellulose and has the capability of up taking heavy metals from wastewater. Therefore, it is recommended that the root and other parts of this weed should be test to develop productive materials. On the other hand, bio-based composite is the interest of many research areas that can fully or partially replace the existing synthetic material, which cannot be degraded and causing the global environmental crisis. Therefore, most of the current researchers turn their finding to new green and degradable materials as an alternative option. In addition, the following works are not included in this paper but it is important to address in the future studies.

- In the photocatalytic study only MB dye was used as an organic pollutant. But it is suggested that in the future studies the efficiency of the high performance BNC (i.e. CNC/Ag@ZnO (1:0.5)) should be investigate using other toxic textile dyes i.e. Congo Red, Methylene Red, etc. and heavy metals.
- A detailed economic feasibility study in the production process is recommended since it is critical for the rational of commercialization.
- The detail photocatalytic performance study of the developed CNCs/Ag@ZnO BNCs under dark condition was necessary.

REFERENCES

A, R., & M, I. T. (2022). SYNTHESIS OF SILVER (Ag) DOPED ZINC OXIDE (ZnO) NANOPARTICLES AS EFFICIENTPHOTOCATALYTIC ACTIVITY FOR DEGRADATION METHYLENE BLUE DYE. *Journal of Advanced Scientific Research*, *13*(02), 129–135. https://doi.org/10.55218/jasr.202213217

Abera Hailu Degaga. (2018). *Water Hyacinth (Eichhornia crassipes) Biology and its Impacts on Ecosystem , Biodiversity , Economy and*. *8*(6), 94–100.

Agengo. (2013). *Effects of water hyacinth on economic activities of the Community around Lake Victoria: a case of dung a beach in Kisumu-Kenya*. 99. http://erepository.uonbi.ac.ke/bitstream/handle/11295/62920/Ageng'o_Effects Of Water Hyacinth On Economic Activities Of The Community Around Lake Victoria A Case Of Dunga Beach In.pdf?isAllowed=y&sequence=3

Ahmad, I., Ahmed, E., & Ahmad, M. (2019). The excellent photocatalytic performances of silver doped ZnO nanoparticles for hydrogen evolution. *SN Applied Sciences*, *1*(4). https://doi.org/10.1007/s42452-019-0331-9

Ahmad, K. S., & Jaffri, S. B. (2018). Phytosynthetic Ag doped ZnO nanoparticles: Semiconducting green remediators: Photocatalytic and antimicrobial potential of green nanoparticles. *Open Chemistry*, *16*(1), 556–570. https://doi.org/10.1515/chem-2018-0060

Akendo, I. C. O., Gumbe, L. O., & Gitau, A. N. (2008). Dewatering and Drying Characteristics of Water Hyacinth (Eichhornia crassipes) Petiole. Part I. Dewatering Characteristics. *Agricultural Engineering International: CIGR Ejournal*, *X*, 1–11.

Akram, T. M., Ahmad, N., & Shaikh, I. A. (2016). Photocatalytic degradation of synthetic textile effluent by modified sol-gel, synthesized mobilized and immobilized TiO2, and ag-doped TiO2. *Polish Journal of Environmental Studies*, *25*(4), 1391–1402. https://doi.org/10.15244/pjoes/62102

Aragaw, S. G., Sabir, F. K., Andoshe, D. M., & Zelekew, O. A. (2020). Green synthesis of p-Co3O4/n-ZnO composite catalyst with Eichhornia crassipes plant extract mediated for methylene blue degradation under visible light irradiation. *Materials Research Express*, *7*(9). https://doi.org/10.1088/2053-1591/abb90e

Ashebir, M. E., Tesfamariam, G. M., Nigussie, G. Y., & Gebreab, T. W. (2018). Structural, optical, and photocatalytic activities of Ag-Doped and Mn-Doped ZnO Nanoparticles.

Journal of Nanomaterials, *2018*. https://doi.org/10.1155/2018/9425938

Asheville, U. N. C., Chapter, Y., & Moments, D. (2018). *N Λ = 2 D Sin Θ*. *February*, 1–18.

Asrofi, M., Abral, H., Kasim, A., Pratoto, A., Mahardika, M., Park, J. W., & Kim, H. J. (2018). Isolation of Nanocellulose from Water Hyacinth Fiber (WHF) Produced via Digester-Sonication and Its Characterization. *Fibers and Polymers*, *19*(8), 1618–1625. https://doi.org/10.1007/s12221-018-7953-1

Azam, M., Wabaidur, S. M., Khan, M. R., Al-Resayes, S. I., & Islam, M. S. (2022). Heavy Metal Ions Removal from Aqueous Solutions by Treated Ajwa Date Pits: Kinetic, Isotherm, and Thermodynamic Approach. *Polymers*, *14*(5). https://doi.org/10.3390/polym14050914

Azizi, S., Ahmad, M. Bin, Ibrahim, N. A., Hussein, M. Z., & Namvar, F. (2014). Preparation and properties of poly(vinyl alcohol)/chitosan blend bio-nanocomposites reinforced by cellulose nanocrystals. *Chinese Journal of Polymer Science (English Edition)*, *32*(12), 1620–1627. https://doi.org/10.1007/s10118-014-1548-0

Azzaz, A. A., Jellali, S., Hamed, N. B. H., El Jery, A., Khezami, L., Assadi, A. A., & Amrane, A. (2021). Photocatalytic treatment of wastewater containing simultaneous organic and inorganic pollution: Competition and operating parameters effects. *Catalysts*, *11*(7). https://doi.org/10.3390/catal11070855

Bailey, K., Basu, A., & Sharma, S. (2022). The Environmental Impacts of Fast Fashion on Water Quality: A Systematic Review. *Water (Switzerland)*, *14*(7). https://doi.org/10.3390/w14071073

Barbash, V. A., Yashchenko, O. V., & Vasylieva, O. A. (2019). Preparation and Properties of Nanocellulose from Miscanthus x giganteus. *Journal of Nanomaterials*, *2019*. https://doi.org/10.1155/2019/3241968

Bidu, J. M., van der Bruggen, B., Rwiza, M. J., & Njau, K. N. (2021). Current status of textile wastewater management practices and effluent characteristics in Tanzania. *Water Science and Technology*, *83*(10), 2363–2376. https://doi.org/10.2166/wst.2021.133

Bolorunduro, P. L. (n.d.). *Water Hyacinth Infestation : Nuisance or Nugget*. 111–122.

Bronzato, G. R. F., Ziegler, S. M., Silva, R. C., Cesarino, I., & Leão, A. L. (2017). Characterization of the pre-treated biomass of Eichhornia crassipes (water hyacinth) for the second generation ethanol production. *Molecular Crystals and Liquid Crystals*, *655*(1), 224–235. https://doi.org/10.1080/15421406.2017.1360696

Carneiro, M. T., Barros, A. Z. B., Morais, A. I. S., Carvalho Melo, A. L. F., Bezerra, R. D. S.,

Osajima, J. A., & Silva-Filho, E. C. (2022). Application of Water Hyacinth Biomass (Eichhornia crassipes) as an Adsorbent for Methylene Blue Dye from Aqueous Medium: Kinetic and Isothermal Study. *Polymers*, *14*(13). https://doi.org/10.3390/polym14132732

Chauhan, A., Verma, R., Kumari, S., Sharma, A., Shandilya, P., Li, X., Batoo, K. M., Imran, A., Kulshrestha, S., & Kumar, R. (2020). Photocatalytic dye degradation and antimicrobial activities of Pure and Ag-doped ZnO using Cannabis sativa leaf extract. *Scientific Reports*, *10*(1), 1–16. https://doi.org/10.1038/s41598-020-64419-0

Chitradevi, T., Jestin Lenus, A., & Victor Jaya, N. (2019). Structure, morphology and luminescence properties of sol-gel method synthesized pure and Ag-doped ZnO nanoparticles. *Materials Research Express*, *7*(1). https://doi.org/10.1088/2053-1591/ab5c53

Chonsakorn, S., Srivorradatpaisan, S., & Mongkholrattanasit, R. (2019). Effects of different extraction methods on some properties of water hyacinth fiber. *Journal of Natural Fibers*, *16*(7), 1015–1025. https://doi.org/10.1080/15440478.2018.1448316

Contreras, M., Grande-tovar, C. D., Vallejo, W., & Chaves-l, C. (2019). *Bio-Removal of Methylene Blue from Aqueous Solution by Galactomyces geotrichum KL20A*. 1–13. https://doi.org/10.3390/w11020282

Dey, S., & Islam, A. (2015). A review on textile wastewater characterization in Bangladesh. *Resources and Environment*, *5*(1), 15–44. https://doi.org/10.5923/j.re.20150501.03

Doner, L. W., Sweeney, G. A., & Hicks, K. B. (1997). Isolation of hemicellulose from corn fiber. *Cereal Chemistry*, *74*(2), 176–181. https://www.google.com/patents/US6147206

Dussán, K. J., Silva, D. D. V., Moraes, E. J. C., Arruda, P. V., & Felipe, M. G. A. (2014). Dilute-acid hydrolysis of cellulose to glucose from sugarcane bagasse. *Chemical Engineering Transactions*, *38*, 433–438. https://doi.org/10.3303/CET1438073

Eldeeb, T. M., El-Nemr, A., Khedr, M. H., & El-Dek, S. I. (2021). Novel bio-nanocomposite for efficient copper removal. *Egyptian Journal of Aquatic Research*, *47*(3), 261–267. https://doi.org/10.1016/j.ejar.2021.07.002

Enyew, B. G., Assefa, W. W., & Gezie, A. (2020). Socioeconomic effects of water hyacinth (Echhornia Crassipes) in Lake Tana, North Western Ethiopia. *PLoS ONE*, *15*(9), 1–21. https://doi.org/10.1371/journal.pone.0237668

Fahad, A., Saphira Mohamed, R. M., Radhi, B., & Al-Sahari, M. (2019). Wastewater and its Treatment Techniques: An Ample Review. *Indian Journal of Science and Technology*, *12*(25), 1–13. https://doi.org/10.17485/ijst/2019/v12i25/146059

Fang, Z., Li, B., Liu, Y., Zhu, J., Li, G., Hou, G., Zhou, J., & Qiu, X. (2020). Critical Role of Degree of Polymerization of Cellulose in Super-Strong Nanocellulose Films. *Matter*, *2*(4), 1000–1014. https://doi.org/10.1016/j.matt.2020.01.016

Farhat, W., Venditti, R., Quick, A., Taha, M., Mignard, N., Becquart, F., & Ayoub, A. (2017). Hemicellulose extraction and characterization for applications in paper coatings and adhesives. *Industrial Crops and Products*, *107*(January), 370–377. https://doi.org/10.1016/j.indcrop.2017.05.055

Fito, J., Abrham, S., & Angassa, K. (2020). Adsorption of Methylene Blue from Textile Industrial Wastewater onto Activated Carbon of Parthenium hysterophorus. *International Journal of Environmental Research*, *14*(5), 501–511. https://doi.org/10.1007/s41742-020-00273-2

Fobiri, G. K. (2022). Synthetic Dye Application in Textiles: A Review on the Efficacies and Toxicities Involved. *Textile and Leather Review*, *5*(May), 180–198. https://doi.org/10.31881/TLR.2022.22

Foo, K. Y., & Hameed, B. H. (2010). An overview of dye removal via activated carbon adsorption process. *Desalination and Water Treatment*, *19*(1–3), 255–274. https://doi.org/10.5004/dwt.2010.1214

G, A., S, B., K, M. P., G, S., & U, G. P. (2020). Extraction and molecular characterization of biological compounds from water hyacinth. *Journal of Medicinal Plants Studies*, *8*(5), 14–19. https://doi.org/10.22271/plants.2020.v8.i5a.1189

George, J., & Sabapathi, S. N. (2015). Cellulose nanocrystals: Synthesis, functional properties, and applications. *Nanotechnology, Science and Applications*, *8*, 45–54. https://doi.org/10.2147/NSA.S64386

Gopal, B. (1987). Water hyacinth. *Water Hyacinth.* https://doi.org/10.30843/nzpp.1951.4.7048

Gupta, A. (2017). *WATER POLLUTION-SOURCES , EFFECTS AND CONTROL WATER POLLUTION-SOURCES , EFFECTS AND CONTROL*. *January 2016*.

Gupta, V. K., Khamparia, S., Tyagi, I., Jaspal, D., & Malviya, A. (2015). Decolorization of mixture of dyes: A critical review. *Global Journal of Environmental Science and Management*, *1*(1), 71–94. https://doi.org/10.7508/gjesm.2015.01.007

Hailu, A., & Degaga, E. G. (2019). Water Hyacinth (Eichhornia crassipes) Biology and Its Impacts on Ecosystem, Biodiversity, Economy and Human Well-being. *Journal of Natural Sciences Research*, *March*. https://doi.org/10.7176/jnsr/9-12-04

Harun, I., Pushiri, H., Amirul-Aiman, A. J., & Zulkeflee, Z. (2021). Invasive water hyacinth: Ecology, impacts and prospects for the rural economy. *Plants*, *10*(8). https://doi.org/10.3390/plants10081613

Hasanpour, M., Motahari, S., Jing, D., & Hatami, M. (2021). Statistical analysis and optimization of photodegradation efficiency of methyl orange from aqueous solution using cellulose/zinc oxide hybrid aerogel by response surface methodology (RSM). *Arabian Journal of Chemistry*, *14*(11), 103401. https://doi.org/10.1016/j.arabjc.2021.103401

Hidayah, N., & Wusko, I. (2020). *Isolation of Cellulose Fiber from Water Hyacinth (Eichornia crassipes) by Bleaching-Alkalination Method*. https://doi.org/10.4108/eai.23-11-2019.2298330

Idrees, M., Adnan, A., & Qureshi, F. A. (2013). Optimization of sulfide/sulfite pretreatment of lignocellulosic biomass for lactic acid production. *BioMed Research International*, *2013*. https://doi.org/10.1155/2013/934171

Iravani, S. (2011). Green synthesis of metal nanoparticles using plants. *Green Chemistry*, *13*(10), 2638–2650. https://doi.org/10.1039/c1gc15386b

Isai, K. A., & Shrivastava, V. S. (2019). Photocatalytic degradation of methylene blue using ZnO and 2%Fe–ZnO semiconductor nanomaterials synthesized by sol–gel method: a comparative study. *SN Applied Sciences*, *1*(10), 1–11. https://doi.org/10.1007/s42452-019-1279-5

Istirokhatun, T., Rokhati, N., Rachmawaty, R., Meriyani, M., Priyanto, S., & Susanto, H. (2015). Cellulose Isolation from Tropical Water Hyacinth for Membrane Preparation. *Procedia Environmental Sciences*, *23*(Ictcred 2014), 274–281. https://doi.org/10.1016/j.proenv.2015.01.041

Javed, R., Zia, M., Naz, S., Aisida, S. O., Ain, N. ul, & Ao, Q. (2020). Role of capping agents in the application of nanoparticles in biomedicine and environmental remediation: recent trends and future prospects. *Journal of Nanobiotechnology*, *18*(1), 1–15. https://doi.org/10.1186/s12951-020-00704-4

Jemal, K., Sandeep, B. V., & Pola, S. (2017). Synthesis, Characterization, and Evaluation of the Antibacterial Activity of Allophylus serratus Leaf and Leaf Derived Callus Extracts Mediated Silver Nanoparticles. *Journal of Nanomaterials*, *2017*. https://doi.org/10.1155/2017/4213275

Journal, A. (2017). *Bionanocomposite : A Review Bionanocomposite : A Review*. *5*(December),

1–3. https://doi.org/1872-2121/08

Kamarulzaman, N., Kasim, M. F., & Rusdi, R. (2015). Band Gap Narrowing and Widening of ZnO Nanostructures and Doped Materials. *Nanoscale Research Letters*, *10*(1). https://doi.org/10.1186/s11671-015-1034-9

Kareem, M. A., Bello, I. T., Shittu, H. A., Sivaprakash, P., Adedokun, O., & Arumugam, S. (2022). Synthesis, characterization, and photocatalytic application of silver doped zinc oxide nanoparticles. *Cleaner Materials*, *3*(March), 100041. https://doi.org/10.1016/j.clema.2022.100041

Kargarzadeh, H., Ioelovich, M., Ahmad, I., Thomas, S., & Dufresne, A. (2017). Methods for Extraction of Nanocellulose from Various Sources. *Handbook of Nanocellulose and Cellulose Nanocomposites*, 1–49. https://doi.org/10.1002/9783527689972.ch1

Katheresan, V., Kansedo, J., & Lau, S. Y. (2018). Efficiency of various recent wastewater dye removal methods: A review. *Journal of Environmental Chemical Engineering*, *6*(4), 4676–4697. https://doi.org/10.1016/j.jece.2018.06.060

Kausar, A., Naeem, K., Tariq, M., Nazli, Z. I. H., Bhatti, H. N., Jubeen, F., Nazir, A., & Iqbal, M. (2019). Preparation and characterization of chitosan/clay composite for direct Rose FRN dye removal from aqueous media: Comparison of linear and non-linear regression methods. *Journal of Materials Research and Technology*, *8*(1), 1161–1174. https://doi.org/10.1016/j.jmrt.2018.07.020

Kay, S. H., Haller, W. T., & Garrard, L. A. (1984). Effects of heavy metals on water hyacinths (Eichhornia crassipes (Mart.) Solms). *Aquatic Toxicology*, *5*(2), 117–128. https://doi.org/10.1016/0166-445X(84)90003-1

Khan, I., Saeed, K., Zekker, I., Zhang, B., Hendi, A. H., Ahmad, A., Ahmad, S., Zada, N., Ahmad, H., Shah, L. A., Shah, T., & Khan, I. (2022). *and Photodegradation*.

Kharat, D. S. (2015). *TREATMENT OF TEXTILE INDUSTRY EFFLUENTS : August*.

Khodaie, M., Ghasemi, N., Moradi, B., & Rahimi, M. (2013). Removal of methylene blue from wastewater by adsorption onto znclactivated corn husk carbon equilibrium studies. *Journal of Chemistry*, *2013*. https://doi.org/10.1155/2013/383985

Kumaran, V., Sudhagar, P., Konga, A. K., & Ponniah, G. (2020). Photocatalytic degradation of synthetic organic reactive dye wastewater using GO-TiO2 nanocomposite. *Polish Journal of Environmental Studies*, *29*(2), 1683–1690. https://doi.org/10.15244/pjoes/109027

Kusmono, Listyanda, R. F., Wildan, M. W., & Ilman, M. N. (2020). Preparation and

characterization of cellulose nanocrystal extracted from ramie fibers by sulfuric acid hydrolysis. *Heliyon*, *6*(11), e05486. https://doi.org/10.1016/j.heliyon.2020.e05486

Kwon, D., & Kim, J. (2020). *Silver-doped ZnO for photocatalytic degradation of methylene blue*. *37*(7), 1226–1232. https://doi.org/10.1007/s11814-020-0520-7

Lara-Serrano, J. S., Rutiaga-Quiñones, O. M., López-Miranda, J., Fileto-Pérez, H. A., Pedraza-Bucio, F. E., Rico-Cerda, J. L., & Rutiaga-Quiñones, J. G. (2016). Physicochemical characterization of water hyacinth (Eichhornia crassipes (Mart.) Solms). *BioResources*, *11*(3), 7214–7223. https://doi.org/10.15376/biores.11.3.7214-7223

Lau, G. E., Abdullah, C. A. C., Ahmad, W. A. N. W., Assaw, S., & Zheng, A. L. T. (2020). Eco-friendly photocatalysts for degradation of dyes. *Catalysts*, *10*(10), 1–16. https://doi.org/10.3390/catal10101129

Lellis, B., Fávaro-polonio, C. Z., Pamphile, J. A., & Polonio, J. C. (2019). *Effects of textile dyes on health and the environment and bioremediation potential of living organisms*. https://doi.org/10.1016/j.biori.2019.09.001

Leng, T. (1990). Cellulose Nanocrystals: Particle Size Distribution and Dispersion in Polymer Composites. *Cesko-Slovenska Gynekologie*, *55*(3), 218–222.

Liu, X., Xu, W., & Pan, Y. (2015). Liu et al. suspect that Zhu et al. (2015) may have underestimated dissolved organic nitrogen (N) but overestimated total particulate N in wet deposition in China. *Science of The Total Environment*. https://doi.org/10.1016/j.scitotenv.2015.03.004

Lusiana, S. E., Srihardyastutie, A., & Masruri, M. (2019). Cellulose nanocrystal (CNC) produced from the sulphuric acid hydrolysis of the pine cone flower waste (Pinus merkusii Jungh et de Vriese). *Journal of Physics: Conference Series*, *1374*(1). https://doi.org/10.1088/1742-6596/1374/1/012023

Mahamadi C. (2012). Water hyacinth as a biosorbent: A review. *African Journal of Environmental Science and Technology*, *5*(13). https://doi.org/10.5897/ajestx11.007

Maynez-Navarro, O. D., & Sánchez-Salas, J. L. (2018). Focus on Zinc Oxide as a Photocatalytic Material for Water Treatment. *Int J Biorem Biodegrad*, *106*(November 2018). https://doi.org/10.29011/IJBB-106/100006

Mayyahi, A. Al, & Al-asadi, H. A. A. (2018). *Advanced Oxidation Processes (AOPs) for Wastewater Treatment and Reuse : A Brief Review*. *2*(3), 18–30.

Mehari, A. K., Gebremedhin, S., & Ayele, B. (2015). *Effects of Bahir Dar Textile Factory*

Effluents on the Water Quality of the Head Waters of Blue Nile River , Ethiopia. *2015*.

Mironga, J. M., Mathooko, J. M., & Onywere, S. M. (2014). Effects of spreading patterns of water hyacinth (Eichhornia crassipes) on zooplankton population in Lake Naivasha, Kenya. *International Journal of Development and Sustainability*, *3*(10), 1971–1987.

Modi, S., & Fulekar, M. H. (2020). Synthesis and characterization of zinc oxide nanoparticles and zinc oxide/cellulose nanocrystals nanocomposite for photocatalytic degradation of Methylene blue dye under solar light irradiation. *Nanotechnology for Environmental Engineering*, *5*(2), 1–12. https://doi.org/10.1007/s41204-020-00080-2

Mohamed, F., Hassaballa, S., Shaban, M., & Ahmed, A. M. (2022). Highly Efficient Photocatalyst Fabricated from the Chemical Recycling of Iron Waste and Natural Zeolite for Super Dye Degradation. *Nanomaterials*, *12*(2). https://doi.org/10.3390/nano12020235

Mondal, P., Baksi, S., & Bose, D. (2017). *Study of environmental issues in textile industries and recent wastewater treatment technology*. *61*(2), 94–105.

Morkoç, H., & Özgür, Ü. (2009). General Properties of ZnO. In *Zinc Oxide*. https://doi.org/10.1002/9783527623945.ch1

Mousa, M. H., Dong, Y., & Davies, I. J. (2016). Recent advances in bionanocomposites: Preparation, properties, and applications. *International Journal of Polymeric Materials and Polymeric Biomaterials*, *65*(5), 225–254. https://doi.org/10.1080/00914037.2015.1103240

Mulugeta, M., & Lelisa, B. (2014). *Removal of Methylene Blue (Mb) Dye from Aqueous Solution by Bioadsorption onto Untreated Parthenium hystrophorous Weed Modern Chemistry & Applications*. *2*(4). https://doi.org/10.4172/2329-6798.1000146

Muniz, F. T. L., Miranda, M. A. R., Morilla Dos Santos, C., & Sasaki, J. M. (2016). The Scherrer equation and the dynamical theory of X-ray diffraction. *Acta Crystallographica Section A: Foundations and Advances*, *72*(3), 385–390. https://doi.org/10.1107/S205327331600365X

Mustikaningrum, M., Cahyono, R. B., & Yuliansyah, A. T. (2021). Effect of NaOH Concentration in Alkaline Treatment Process for Producing Nano Crystal Cellulose-Based Biosorbent for Methylene Blue. *IOP Conference Series: Materials Science and Engineering*, *1053*(1), 012005. https://doi.org/10.1088/1757-899x/1053/1/012005

Ng, H. M., Sin, L. T., Tee, T. T., Bee, S. T., Hui, D., Low, C. Y., & Rahmat, A. R. (2015). Extraction of cellulose nanocrystals from plant sources for application as reinforcing agent in polymers. *Composites Part B: Engineering*, *75*, 176–200.

https://doi.org/10.1016/j.compositesb.2015.01.008

Nova, L., Nova, L., Mota, A. L. N., Albuquerque, L. F., Beltrame, L. T. C., Chiavone-Filho, O., Machulek Jr, A., Nascimento, C. A. O., Nova, L., Nova, L., Mota, A. L. N., Albuquerque, L. F., Beltrame, L. T. C., Chiavone-Filho, O., Machulek Jr, A., Nascimento, C. A. O., Jr., A. M., & Nascimento, C. A. O. (2009). Advanced oxidation processes and their application in the petroleum industry: a review. *Brazilian Journal of Petroleum and Gas*, *2*(3), 122–142. http://www.portalabpg.org.br/bjpg/index.php/bjpg/article/view/57

Omondi, E. A., Ndiba, P. K., & Njuru, P. G. (2019). Characterization of water hyacinth (E. crassipes) from Lake Victoria and ruminal slaughterhouse waste as co-substrates in biogas production. *SN Applied Sciences*, *1*(8). https://doi.org/10.1007/s42452-019-0871-z

Ong, C. B., Ng, L. Y., & Mohammad, A. W. (2018). A review of ZnO nanoparticles as solar photocatalysts: Synthesis, mechanisms and applications. *Renewable and Sustainable Energy Reviews*, *81*(March 2017), 536–551. https://doi.org/10.1016/j.rser.2017.08.020

Pandi, N., Sonawane, S. H., & Anand Kishore, K. (2021). Synthesis of cellulose nanocrystals (CNCs) from cotton using ultrasound-assisted acid hydrolysis. *Ultrasonics Sonochemistry*, *70*(September 2020), 105353. https://doi.org/10.1016/j.ultsonch.2020.105353

Parvin, S., Hossen, A., Rahman, W., Hossen, I., Halim, A., Biswas, B. K., & Khan, A. S. (2018). Uptake Hazardous Dye from Wastewater Using Water Hyacinth as Bio-Adsorbent. *European Journal of Sustainable Development Research*, *3*(1), 1–10. https://doi.org/10.20897/ejosdr/3917

Paul, S., Saha, D., Hosen, S. M. Z., & Bin, T. (2012). *Overview on Water Resources and Pollution*. *4*(3), 108–114.

Periyasamy, A. P., Ramamoorthy, S. K., Rwawiire, S., & Zhao, Y. (2018). *Sustainable Wastewater Treatment Methods for Textile Industry*. Springer Singapore. https://doi.org/10.1007/978-981-10-8591-8_2

Pham, T. A. T., Tran, V. A., Le, V. D., Nguyen, M. V., Truong, D. D., Do, X. T., & Vu, A. T. (2020). Facile Preparation of ZnO Nanoparticles and Ag/ZnO Nanocomposite and Their Photocatalytic Activities under Visible Light. *International Journal of Photoenergy*, *2020*. https://doi.org/10.1155/2020/8897667

Pratama, J. H., Amalia, A., Rohmah, R. L., & Saraswati, T. E. (2020). The extraction of cellulose powder of water hyacinth (eichhornia crassipes) as reinforcing agents in bioplastic. *AIP Conference Proceedings*, *2219*(May 2020). https://doi.org/10.1063/5.0003804

Punitha, S., Bhuvaneshwari, M., Nadu, T., Design, A., Nadu, T., Design, A., & Nadu, T. (2015). *Selection of Plant – Water Hyacinth*. *3*(8), 290–294.

Rahman, R., & Neethu, M. K. (2017). Degradation of Methylene Blue in Textile Waste Water Using Activated Sawdust and Eggshell Biosorbent. *International Journal of Advance Research and Innovative Ideas in Education*, *2*(4), 7–16. www.ijariie.com7

Ranganath, M. S., & Vipin, V. (2015). Surface Roughness Prediction Model for CNC Turning of EN-8 Steel Using Surface Roughness Prediction Model for CNC Turning of EN-8 Steel Using Response Surface Methodology. *International Journal of Emerging Technology and Advanced Engineering*, *5*(6), 135–143.

Sagadevan, S., Pal, K., Chowdhury, Z. Z., & Hoque, M. E. (2017). Structural, dielectric and optical investigation of chemically synthesized Ag-doped ZnO nanoparticles composites. *Journal of Sol-Gel Science and Technology*, *83*(2), 394–404. https://doi.org/10.1007/s10971-017-4418-8

Sahoo, C., Gupta, A. K., & Sasidharan Pillai, I. M. (2012). Photocatalytic degradation of methylene blue dye from aqueous solution using silver ion-doped TiO 2 and its application to the degradation of real textile wastewater. *Journal of Environmental Science and Health - Part A Toxic/Hazardous Substances and Environmental Engineering*, *47*(10), 1428–1438. https://doi.org/10.1080/10934529.2012.672387

Said, B., Souad M', R., & Ahmed, E. H. (2020). A review on classifications, recent synthesis and applications of textile dyes. *Inorganic Chemistry Communications*, *3*(March), 107891.

Sakamoto, M., Ahmed, T., Begum, S., & Huq, H. (2019). *Water Pollution and the Textile Industry in Bangladesh : Flawed Corporate Practices or Restrictive Opportunities ?* https://doi.org/10.3390/su11071951

Samadi, M., Zirak, M., Naseri, A., Khorashadizade, E., & Moshfegh, A. Z. (2016). Recent progress on doped ZnO nanostructures for visible-light photocatalysis. *Thin Solid Films*, *605*, 2–19. https://doi.org/10.1016/j.tsf.2015.12.064

Sang-aroon, W., Somseemee, O., Khammung, S., & Wongwilad, S. (2015). *Photocatalytic reduction of Cr (VI) in aqueous solution by silver doped zinc oxide under ultraviolet light irradiation*. *Vi*, 42–58. https://www.researchgate.net/publication/275960974

Senthilkumar, S., Perumalsamy, M., Prabhuy, H. J., Ahmedbasha, C., & Anantharaman, N. (2012). Response surface optimization for efficient dye removal by isolated strain Pseudomonas sp. *Central European Journal of Engineering*, *2*(3), 425–434.

https://doi.org/10.2478/s13531-012-0001-9

Setyaningsih, L., Satria, E., Khoironi, H., Dwisari, M., Setyowati, G., Rachmawati, N., Kusuma, R., & Anggraeni, J. (2019). Cellulose extracted from water hyacinth and the application in hydrogel. *IOP Conference Series: Materials Science and Engineering*, *673*(1). https://doi.org/10.1088/1757-899X/673/1/012017

Sharma, S., & Nain, K. S. (2017). Photodegradation of Real Textile Wastewater by Using ZnO catalyst. *International Journal of Emerging Technology and Advanced Engineering*, *7*(11), 202–207.

Shatnawi, M., Alsmadi, A. M., Bsoul, I., Salameh, B., Mathai, M., Alnawashi, G., Alzoubi, G. M., Al-Dweri, F., & Bawa'aneh, M. S. (2016). Influence of Mn doping on the magnetic and optical properties of ZnO nanocrystalline particles. *Results in Physics*, *6*(November 2016), 1064–1071. https://doi.org/10.1016/j.rinp.2016.11.041

Shchipunov, Y. (2012). Bionanocomposites: Green sustainable materials for the near future. *Pure and Applied Chemistry*, *84*(12), 2579–2607. https://doi.org/10.1351/PAC-CON-12-05-04

Shreema, K., Mathammal, R., Kalaiselvi, V., Vijayakumar, S., Selvakumar, K., & Senthil, K. (2021). Green synthesis of silver doped zinc oxide nanoparticles using fresh leaf extract Morinda citrifoliaand its antioxidant potential. *Materials Today: Proceedings*, *47*(May), 2126–2131. https://doi.org/10.1016/j.matpr.2021.04.627

Sievers, M. (2011). Advanced Oxidation Processes. *Treatise on Water Science*, *4*, 377–408. https://doi.org/10.1016/B978-0-444-53199-5.00093-2

Singh, R., Barman, P. B., & Sharma, D. (2017). Synthesis, structural and optical properties of Ag doped ZnO nanoparticles with enhanced photocatalytic properties by photo degradation of organic dyes. *Journal of Materials Science: Materials in Electronics*, *28*(8), 5705–5717. https://doi.org/10.1007/s10854-016-6242-2

Siva Vijayakumar, T., Karthikeyeni, S., Vasanth, S., Ganesh, A., Bupesh, G., Ramesh, R., Manimegalai, M., & Subramanian, P. (2013). Synthesis of Silver-Doped Zinc Oxide Nanocomposite by Pulse Mode Ultrasonication and Its Characterization Studies. *Journal of Nanoscience*, *2013*, 1–7. https://doi.org/10.1155/2013/785064

Šmelcerović, M. (2019). Industrial Wastewater. *KNOWLEDGE - International Journal*, *July 2013*, 595–599. https://doi.org/10.35120/kij3003595s

Song, K., Zhu, X., Zhu, W., & Li, X. (2019). Preparation and characterization of cellulose

nanocrystal extracted from Calotropis procera biomass. *Bioresources and Bioprocessing*, *6*(1). https://doi.org/10.1186/s40643-019-0279-z

Srithar, A., Kannan, J. C., & Senthil, T. S. (2017). Preparation and Characterization of Ag doped ZnO nanoparticles and its Antibacterial Applications Academic Discipline and Sub-Disciplines Nano technology TYPE (METHOD / APPROACH). *Journal of Advances in Chemistry*, *13*, 6273–6279.

Sukarni, S., Zakaria, Y., Sumarli, S., Wulandari, R., Ayu Permanasari, A., & Suhermanto, M. (2019). Physical and Chemical Properties of Water Hyacinth (Eichhornia crassipes) as a Sustainable Biofuel Feedstock. *IOP Conference Series: Materials Science and Engineering*, *515*(1). https://doi.org/10.1088/1757-899X/515/1/012070

Tamgadge, Y. S., Gedam, P. P., Ganorkar, R. P., Mahure, M. A., Pahurkar, V. G., & Muley, G. G. (2018). Synthesis and characterization of Ni doped ZnO nanoparticles. *AIP Conference Proceedings*, *1953*(5), 378–385. https://doi.org/10.1063/1.5032338

Tanpichai, S., Biswas, S. K., Witayakran, S., & Yano, H. (2019). Water Hyacinth: A Sustainable Lignin-Poor Cellulose Source for the Production of Cellulose Nanofibers. *ACS Sustainable Chemistry and Engineering*, *7*(23), 18884–18893. https://doi.org/10.1021/acssuschemeng.9b04095

Tarekegn, M. M., & Balakrishnan, M. (2021). *zerovalent iron , nanoclay and iron impregnated*. 30109–30131. https://doi.org/10.1039/d1ra03918k

Taye, M. T., Ntegeka, V., Ogiramoi, N. P., & Willems, P. (2011). Assessment of climate change impact on hydrological extremes in two source regions of the Nile River Basin. *Hydrology and Earth System Sciences*, *15*(1), 209–222. https://doi.org/10.5194/hess-15-209-2011

Tewabe, T. (2018). Prelacteal Feeding Practices among Mothers in Motta Town, Northwest Ethiopia: A Cross-sectional Study. *Ethiopian Journal of Health Sciences*, *28*(4), 393–402. https://doi.org/10.4314/ejhs.v28i4.5

Thakur, D., Sharma, A., Rana, D. S., Thakur, N., Singh, D., Tamulevicius, T., Andrulevicius, M., Tamulevicius, S., Shukla, S. K., & Thakur, S. (2020). Facile synthesis of silver-doped zinc oxide nanostructures as efficient scaffolds for detection of p-nitrophenol. *Chemosensors*, *8*(4), 1–15. https://doi.org/10.3390/chemosensors8040108

Thiripura Sundari, M., & Ramesh, A. (2012). Isolation and characterization of cellulose nanofibers from the aquatic weed water hyacinth - Eichhornia crassipes. *Carbohydrate Polymers*, *87*(2), 1701–1705. https://doi.org/10.1016/j.carbpol.2011.09.076

Uddin, M. N., Islam, M. T., & Das, S. (2014). A novel biosorbent, water-hyacinth, uptaking methylene blue from aqueous solution: Kinetics and equilibrium studies. *International Journal of Chemical Engineering*, *2014*. https://doi.org/10.1155/2014/819536

Wang, X., Jiang, J., & Gao, W. (2022). Reviewing textile wastewater produced by industries: characteristics, environmental impacts, and treatment strategies. *Water Science and Technology*, *85*(7), 2076–2096. https://doi.org/10.2166/wst.2022.088

Wolverton, B. C., & Mcdonald, R. C. (1978). Nutritional composition of water hyacinths grown on domestic sewage. *Economic Botany*, *32*(4), 363–370. https://doi.org/10.1007/BF02907930

Worku, M., & Sahile, S. (2017). Impact of Water Hyacinth, Eichhornia crassipes (Martius) (Pontederiaceae) in Lake Tana Ethiopia: A Review. *Journal of Aquaculture Research & Development*, *09*(01), 9–11. https://doi.org/10.4172/2155-9546.1000520

Yadav, V. K., Choudhary, N., Ali, D., Kumar, G., Gnanamoorthy, G., Khan, A. U., Kumar, P., & Kumar, S. H. (2022). *Determination of Adsorption of Methylene Blue Dye by Incense Stick Ash Waste and Its Toxicity on RTG-2 Cells*. *2022*.

Youssef, A. M., Assem, F. M., Abdel-Aziz, M. E., Elaaser, M., Ibrahim, O. A., Mahmoud, M., & Abd El-Salam, M. H. (2019). Development of bionanocomposite materials and its use in coating of Ras cheese. *Food Chemistry*, *270*, 467–475. https://doi.org/10.1016/j.foodchem.2018.07.114

Zayed, M., Othman, H., Ghazal, H., & Hassabo, A. G. (2021). Psidium Guajava leave extract as reducing agent for synthesis of zinc oxide nanoparticles and its application to impart multifunctional properties for cellulosic fabrics. *Biointerface Research in Applied Chemistry*, *11*(5), 13535–13556. https://doi.org/10.33263/BRIAC115.1353513556

Zelekew, O. A., Fufa, P. A., Sabir, F. K., & Duma, A. D. (2021). Water hyacinth plant extract mediated green synthesis of Cr2O3/ZnO composite photocatalyst for the degradation of organic dye. *Heliyon*, *7*(7), e07652. https://doi.org/10.1016/j.heliyon.2021.e07652

APPENDIXES

Appendix-A Pictures of SomeLaboratory Equipment used in the Study

Centrifuge

Electronic beam balance

Magnetic stirrer

Muffle furnace

Blast drying oven

Soxlet apparatus

Orbital shaker

Sample grinder

Heating mantle

Appendix-B Some Common Producers During Lab Work

Appendix-B-1 CNCs Synthesis

WH weed

Sample preparation and cleaning

Sample drying

Size reduction

Solvent extraction

Alkiline treatment

Bleaching process

Acid hydrolysis process

CNCs

Appendix-B-2 Ag@ZnO NPs Synthesis

WH leaves powder

Leaf extraction

Dissolution process

Ag@ZnO NPs synthesis

Dried Ag@ZnO NPs

Calcinate Ag@ZnO NPs

Appendix-B-3 CNCs/Ag@ZnO BNC Synthesis

CNCs/Ag@ZnO synthesis

Dried CNCs/Ag@ZnO synthesis

Appendix-C Estimation of Proximate Analysis Calculation Part

Appendix-C-1 Determination of Moisture Content

- Mass of air-dried sample = 5g
- Mass of oven dried = 4.338g

$$\text{Moisture (\%)} = \frac{S_1 - S_2}{S_2}$$

$$= \frac{5 - 4.34}{4.338} * 100 = \underline{15.21\%}$$

Appendix-C-2 Determination of Ash Content

- Mass of oven dried sample = 4.338g
- Mass of obtained ash = 0.937

$$\text{Ash content (\%)} = \frac{0.937}{4.338} * 100 = \underline{21.6\%}$$

Appendix-C-3 Determination of Extractive Content

- Mass of air-dried sample = 5g
- Mass of oven dried extracted sample = 4.19g

$$\text{Extractive content (\%)} = \frac{W_1 - W_2}{W_2} * 100$$

$$= \frac{5 - 4.19}{4.19} * 100 = \underline{19.33\%}$$

Appendix-C-4 Determination of Hemicellulose Content

- Mass of extracted sample = 4.19g
- Mass of oven dried alkaline treated sample = 3.293g

$$\text{Hemicellulose content (\%)} = \frac{\mathrm{M_d} - M_a}{M_a} * 100$$

$$= \frac{4.19 - 3.293}{3.293} * 100 = \underline{27.24\%}$$

Appendix-C-5 Determination of Lignin Content

- Mass of mass of dried alkaline treated sample =3.293g
- Mass of oven dried sample after bleaching process = 3.128g

$$\text{Lignin content (\%)} = \frac{M_1 - M_2}{M_2} * 100$$

$$= \frac{3.293 - 3.128}{3.128} * 100 = \underline{5.27\%}$$

Appendix-C-6 Determination of Cellulose Content

- Percentage of extractive content = 19.33%
- Percentage of hemicellulose content = 27.24%
- Percentage of lignin content = 5.27%

$$\text{Cellulose content (\%)} = 100 - (EC + HC + LC)$$

$$= 100 - (19.33\% + 27.24\% + 5.27\%)$$

$$= \underline{48.16\%}$$

Appendix-C-7 Determination of CNCs Content

- Mass of oven-dried whitish cellulose = 3.128g
- Mass of CNCs = 1.142

$$\text{Yield (\%)} = \frac{M_2}{M_1} * 100$$

$$= \frac{1.142}{3.128} * 100 = \underline{36.5\%}$$

Appendix-D Estimation of Band Gap Energy

$$E_g = \frac{1240}{\lambda}, \text{ where: } \lambda = 402\text{nm}$$

$$= \frac{1240}{402} = \underline{3.08\text{Ev}}$$

Appendix-E Determination of Crystallinity, Crystalline Size and d-Spacing

Appendix-E -1 Determination of Crystallinity

Appendix-E -1.1 Crystallinity of WH stem

- Area of crystalline peak-1 = 763.36
- Area of crystalline peak-2 = 1,469.34
- Total area = 7,488.06

$$\text{Crystallinity (CI \%)} = \frac{763.36 + 1469.34}{7488.06} * 100 = \underline{29.82\%}$$

Appendix-E -1.2 Crystallinity of Bleached Cellulose

- Area of crystalline peak = 7,274.25
- Total area = 11,437.5

$$\text{Crystallinity (CI \%)} = \frac{7274.25}{11437.5} * 100$$

$$= \underline{63.6\%}$$

Appendix-E -1.3 Crystallinity of CNCs

- Area of crystalline peak = 13,432.02
- Total area = 16,320.8

$$\text{Crystallinity (CI \%)} = \frac{13{,}432.02}{16{,}320.8} * 100$$

$$= \underline{84.3\%}$$

Appendix-E -1.4 Crystallinity of Ag@ZnO NPs

- Area of crystalline peaks = 6,275.65
- Total area = 6,839.95

$$\text{Crystallinity (CI \%)} = \frac{6{,}275.65}{6{,}839.95} * 100$$

$$= \underline{91.75\%}$$

Appendix-E -1.5 Crystallinity of CNCs/Ag@ZnO (1:1) BNC

- Area of crystalline peak = 7,663.23
- Total area = 8,774.02

$$\text{Crystallinity (CI \%)} = \frac{7{,}663.23}{8{,}774.02} * 100$$

$$= \underline{87.34\%}$$

Appendix-E -1.6 Crystallinity of CNCs/Ag@ZnO (1:0.5) BNC

- Area of crystalline peak = 6,018.87
- Total area = 7,016.64

$$\text{Crystallinity (CI \%)} = \frac{6{,}018.87}{7{,}016.64} * 100$$

$$= \underline{85.78\%}$$

Appendix-E -1.7 Crystallinity of CNCs/Ag@ZnO (0.5:1) BNC

- Area of crystalline peak = 5,281.33
- Total area = 5889.74

$$\text{Crystallinity (CI \%)} = \frac{5{,}281.33}{5889.74} * 100$$

$$= \underline{89.67\%}$$

Appendix-E -2 Determination of Crystalline Size

Appendix-E -2.1 Crystalline Size of WH stem

$$2\theta = Xc = 22.91419^0$$

$$\theta = \frac{22.91419}{2} = \underline{11.46}^0$$

$$\beta = FWHM = 27.58314^0$$

To convert degree to radian:

- $\theta = 11.46^0 * \frac{\pi}{180} = 0.200015$
- $\beta = 27.58314^0 * \frac{\pi}{180} = 0.4814166$

$D = \frac{k\lambda}{\beta\cos\theta}$, where: k = 0.94 and λ = 1.54178Å = 0.154178nm

$$= \frac{0.94 * 0.154178}{0.4814166 * \cos(0.2)} = \underline{0.31nm}$$

Appendix-E -2.2 Crystalline Size of Bleached Cellulose

$$2\theta = Xc = 21.7347^0$$

$$\theta = \frac{21.7347}{2} = \underline{10.86735}^0$$

$$\beta = FWHM = 4.42248^0$$

To convert degree to radian:

- $\theta = 10.86735^0 * \frac{\pi}{180} = 0.189$
- $\beta = 4.42248^0 * \frac{\pi}{180} = 0.0772$

$$D = \frac{k\lambda}{\beta\cos\theta}$$

$$= \frac{0.94*0.154178}{0.0772*\cos(0.189)} = \underline{1.91nm}$$

Appendix-E -2.3 Crystalline Size of CNCs

$$2\theta = Xc = 21.92917^0$$

$$\theta = \frac{21.92917}{2} = \underline{10.964585}^0$$

$$\beta = FWHM = 4.07187^0$$

To convert degree to radian:

- $\theta = 10.964585^0 * \frac{\pi}{180} = 0.192$
- $\beta = 4.07187^0 * \frac{\pi}{180} = 0.071067$

$$D = \frac{k\lambda}{\beta\cos\theta}$$

$$= \frac{0.94*0.154178}{0.071067*\cos(0.192)} = \underline{2.08nm}$$

Appendix-E -2.4 Crystalline Size of Ag@ZnO NPs

$$2\theta = Xc = 36.18473^0$$

$$\theta = \frac{36.18473}{2} = \underline{18.092365}^0$$

$$\beta = FWHM = 0.35613^0$$

To convert degree to radian:

- $\theta = 18.092365^0 * \frac{\pi}{180} = 0.32$
- $\beta = 0.35613^0 * \frac{\pi}{180} = 0.0062156$

$$D = \frac{k\lambda}{\beta\cos\theta}$$

$$= \frac{0.94*0.154178}{0.0062156*\cos(0.32)} = \underline{24.54nm}$$

Appendix-E -2.5 Crystalline Size of CNCs/Ag@ZnO (1:1) BNC

$$2\theta = Xc = 21.314^0$$

$$\theta = \frac{36.18473}{2} = \underline{10.65702}^0$$

$$\beta = FWHM = 0.84732299^0$$

To convert degree to radian:

- $\theta = 10.65702^0 * \frac{\pi}{180} = 0.186$
- $\beta = 0.84732299^0 * \frac{\pi}{180} = 0.0147886$

$$D = \frac{k\lambda}{\beta\cos\theta}$$

$$= \frac{0.94*0.154178}{0.0147886*\cos(0.186)} = \underline{9.8nm}$$

Appendix-E -2.6 Crystalline Size of CNCs/Ag@ZnO (1:0.5) BNC

$$2\theta = Xc = 22.3452^0$$

$$\theta = \frac{36.18473}{2} = \underline{11.1726}^0$$

$$\beta = FWHM = 0.7284^0$$

To convert degree to radian:

- $\theta = 11.1726 * \frac{\pi}{180} = 0.195$
- $\beta = 0.7284^0 * \frac{\pi}{180} = 0.012713$

$$D = \frac{k\lambda}{\beta\cos\theta}$$

$$= \frac{0.94*0.154178}{0.012713*\cos(0.195)} = \underline{11.4nm}$$

Appendix-E -2.7 Crystalline Size of CNCs/Ag@ZnO (0.5:1) BNC

$$2\theta = Xc = 22.68913^0$$

$$\theta = \frac{36.18473}{2} = \underline{11.34456}^0$$

$$\beta = FWHM = 0.790836^0$$

To convert degree to radian:

- $\theta = 11.34456^0 * \frac{\pi}{180} = 0.198$

- $\beta = 0.790836^0 * \frac{\pi}{180} = 0.01380268$

$$D = \frac{k\lambda}{\beta\cos\theta}$$

$$= \frac{0.94*0.154178}{0.01380268*\cos(0.198)} = \underline{10.5nm}$$

Appendix-E -3 Determination of d-spacing

Appendix-E -3.1 d-spacing of WH stem

$$2\theta = Xc = 14.58^0$$

$$\theta = 7.29^0$$

To convert degree to radian:

- $\theta = 7.29^0 * \frac{\pi}{180} = 1.2723$

$$d = \frac{n\lambda}{2\sin\theta}$$, where: n =1, and λ= 0.15406nm

$$= \frac{0.15406}{2*\sin(1.2723)} = \underline{0.081nm}$$

Appendix-E -3.2 d-spacing of Bleached Cellulose

$$2\theta = Xc = 21.96^0$$

$$\theta = 10.98^0$$

To convert degree to radian:

- $\theta = 10.98^0 * \frac{\pi}{180} = 1.916^0$

$$d = \frac{n\lambda}{2\sin\theta}$$

$$= \frac{0.15406}{2*\sin(1.916)} = \underline{0.082nm}$$

Appendix-E -3.3 d-spacing of CNCs

$$2\theta = Xc = 22.38^0$$

$$\theta = 11.19^0$$

To convert degree to radian:

- $\theta = 11.19^0 * \frac{\pi}{180} = 1.9526$

$$d = \frac{n\lambda}{2\sin\theta}$$

$$= \frac{0.15406}{2*\sin(1.9526)} = \underline{0.083nm}$$

Appendix-E -3.4 d-spacing of Ag@ZnO NPs

$$2\theta = Xc = 36.16^0$$

$$\theta = 18.08^0$$

To convert degree to radian:

- $\theta = 18.08^0 * \frac{\pi}{180} = 3.162$

$$d = \frac{n\lambda}{2\sin\theta}$$

$$= \frac{0.15406}{2*\sin(3.15496)} = \underline{5.77nm}$$

Appendix-E -3.5 d-spacing of CNCs/Ag@ZnO (1:1) BNC

$$2\theta = Xc = 38.3^0$$

$$\theta = 19.15^0$$

To convert degree to radian:

- $\theta = 19.15^0 * \frac{\pi}{180} = 3.342$

$$d = \frac{n\lambda}{2\sin\theta}$$

$$= \frac{0.15406}{2*\sin(3.342)} = \underline{0.3871nm}$$

Appendix-E -3.6 d-spacing of CNCs/Ag@ZnO (1:0.5) BNC

$$2\theta = Xc = 36.24^0$$

$$\theta = 18.12^0$$

To convert degree to radian:

- $\theta = 18.12^0 * \frac{\pi}{180} = 3.162$

$$d = \frac{n\lambda}{2\sin\theta}$$

$$= \frac{0.15406}{2*\sin(3.162)} = \underline{3.76nm}$$

Appendix-E -3.7 d-spacing of CNCs/Ag@ZnO (0.5:1) BNC

$2\theta = Xc = 36.36^0$

$\theta = 18.18$

To convert degree to radian:

- $\theta = 18.18^0 * \frac{\pi}{180} = 3.17241$

$d = \frac{n\lambda}{2\sin\theta}$, where: n =1, and λ= 0.15406nm

$= \frac{0.15406}{2*\sin(3.17242)} =$ 2.50097nm

Appendix- F BET Analysis Results

Appendix - F -1 BET Analysis Results of CNCs

Appendix - F -1.1 Surface Area of CNCs

Quantachrome NovaWin - Data Acquisition and Reduction
for NOVA instruments
©1994-2010, Quantachrome Instruments
version 11.0

Analysis Report
Operator:alex Date:2022/08/08 Operator:alex Date:8/8/2022
Sample ID: BE 5 A Filename: C:\QCdata\Physisorb\BE 5.qps
Sample Desc: Comment:
Sample weight: 0.04 g Sample Volume: 0.010256 cc Sample Density:3.9 g/cc
Outgas Time: 8.0 hrs OutgasTemp: 300.0 C
Analysis gas: Nitrogen Bath Temp: 77.3 K
Press. Tolerance:0.100/0.100 (ads/des)Equil time: 60/60 sec (ads/des) Equil timeout: 240/240 sec (ads/des)
Analysis Time: 74.8 min End of run: 2022/08/08 12:27:11 Instrument: Nova Station B
Cell ID: 2 F/W version: 0.00
Adsorbate Nitrogen Temperature 77.350K
Molec. Wt.: 28.013 g Cross Section: 16.200 Å² Liquid Density: 0.808 g/cc

Relative Pressure P/Po	Volume @ STP cc/g	1 / [W((Po/P) - 1)]
5.29350e-02	22.7503	1.9444e+00
1.12518e-01	47.1905	2.1651e+00

1.73623e-01	72.3557	2.4297e+00
2.35250e-01	97.8150	2.9344e+00
2.97372e-01	121.9711	2.5832e+00

BET summary

Slope = 3.183
Intercept = 1.887e+00
Correlation coefficient, r = 0.967659
C constant= 2.853

Surface Area = 436.8m²/g

Appendix –F-1.2 Pore Volume and Size of CNCs

Quantachrome NovaWin - Data Acquisition and Reduction
for NOVA instruments
©1994-2010, Quantachrome Instruments
version 11.0

Analysis Report
Operator:alex Date:2022/08/08 Operator:alex Date:8/8/2022
Sample ID: BE 5 A Filename: C:\QCdata\Physisorb\BE 5.qps
Sample Desc: Comment:
Sample weight: 0.04 g Sample Volume: 0.010256 cc Sample Density:3.9 g/cc
Outgas Time: 8.0 hrs OutgasTemp: 300.0 C
Analysis gas: Nitrogen Bath Temp: 77.3 K
Press. Tolerance:0.100/0.100 (ads/des) Equil time: 60/60 sec (ads/des) Equil timeout: 240/240 sec (ads/des)
Analysis Time: 74.8 min End of run: 2022/08/08 12:27:11 Instrument: Nova Station B
Cell ID: 2 F/W version: 0.00
Adsorbate Nitrogen Temperature 77.350K
Molec. Wt.: 28.013 g Cross Section: 16.200 Å² Liquid Density: 0.808 g/cc

Pore Volume Data

HK method cumulative pore volume	2.30e-02 cc/g
SF method cumulative pore volume	1.175e-01 cc/g
NLDFT method cumulative pore volume	1.658e-01 cc/g

Pore Size Data

HK method pore Radius (Mode)	4.9e+00 Å
SF method pore Radius (Mode)	1.666e+01 Å
NLDFT pore Radius (Mode)	1.324e+01 Å

Appendix –F-2 BET Analysis Results of CNCs/Ag@ZnO (1:1) BNC

Appendix –F-2.1 Surface Area of CNCs/Ag@ZnO (1:1) BNC

Quantachrome NovaWin - Data Acquisition and Reduction
for NOVA instruments
©1994-2010, Quantachrome Instruments
version 11.0

Analysis Report
Operator:alex Date:2022/08/08 Operator:alex Date:8/8/2022
Sample ID: BE 5 A Filename: C:\QCdata\Physisorb\BE 5.qps
Sample Desc: Comment:
Sample weight: 0.04 g Sample Volume: 0.010256 cc Sample Density:3.9 g/cc
Outgas Time: 8.0 hrs OutgasTemp: 300.0 C
Analysis gas: Nitrogen Bath Temp: 77.3 K
Press. Tolerance:0.100/0.100 (ads/des)Equil time: 60/60 sec (ads/des) Equil timeout: 240/240 sec (ads/des)
Analysis Time: 74.8 min End of run: 2022/08/08 12:27:11 Instrument: Nova Station B
Cell ID: 2 F/W version: 0.00
Adsorbate Nitrogen Temperature 77.350K
Molec. Wt.: 28.013 g Cross Section: 16.200 Å² Liquid Density: 0.808 g/cc

Relative Pressure P/Po	Volume @ STP cc/g	1 / [W((Po/P) - 1)]
5.34100e-02	22.5325	2.0036e+00
1.13320e-01	47.0502	2.1733e+00
1.74250e-01	71.6806	2.3554e+00
2.35668e-01	96.0033	2.5697e+00
2.97425e-01	120.2154	2.8176e+0

BET summary

Slope = 3.318
Intercept = 1.804e+00
Correlation coefficient, r = 0.997287
C constant= 2.839
Surface Area = 564.6 m²/g

Appendix –F-2.2 Pore Volume and Size of CNCs/Ag@ZnO (1:1) BNC

Quantachrome NovaWin - Data Acquisition and Reduction
for NOVA instruments
©1994-2010, Quantachrome Instruments
version 11.0

Analysis Report
Operator:alex Date:2022/08/08 Operator:alex Date:8/8/2022
Sample ID: BE 5 A Filename: C:\QCdata\Physisorb\BE 5.qps
Sample Desc: Comment:
Sample weight: 0.04 g Sample Volume: 0.010256 cc Sample Density:3.9 g/cc
Outgas Time: 8.0 hrs OutgasTemp: 300.0 C
Analysis gas: Nitrogen Bath Temp: 77.3 K
Press. Tolerance:0.100/0.100 (ads/des) Equil time: 60/60 sec (ads/des) Equil timeout: 240/240 sec (ads/des)
Analysis Time: 74.8 min End of run: 2022/08/08 12:27:11 Instrument: Nova Station B
Cell ID: 2 F/W version: 0.00
Adsorbate Nitrogen Temperature 77.350K
Molec. Wt.: 28.013 g Cross Section: 16.200 Å² Liquid Density: 0.808 g/cc

Pore Volume Data

HK method cumulative pore volume	8.6e-02 cc/g
SF method cumulative pore volume	1.075e-01 cc/g
NLDFT method cumulative pore volume	1.758e-01 cc/g

Pore Size Data

HK method pore Radius (Mode)	2.6e+00 Å
SF method pore Radius (Mode)	1.666e+01 Å
NLDFT pore Radius (Mode)	1.324e+01 Å

Appendix –F-3 BET Analysis Results of CNCs/Ag@ZnO (1:0.5) BNC

Appendix –F-3.1 Surface Area of CNCs/Ag@ZnO (1:0.5) BNC

Quantachrome NovaWin - Data Acquisition and Reduction
for NOVA instruments
©1994-2010, Quantachrome Instruments
version 11.0

Analysis Report
Operator:alex Date:2022/08/08 Operator:alex Date:8/8/2022
Sample ID: BE 5 A Filename: C:\QCdata\Physisorb\BE 5.qps

Sample Desc: Comment:
Sample weight: 0.04 g Sample Volume: 0.010256 cc Sample Density:3.9 g/cc
Outgas Time: 8.0 hrs OutgasTemp: 300.0 C
Analysis gas: Nitrogen Bath Temp: 77.3 K
Press. Tolerance:0.100/0.100 (ads/des)Equil time: 60/60 sec (ads/des) Equil timeout: 240/240 sec (ads/des)
Analysis Time: 74.8 min End of run: 2022/08/08 12:27:11 Instrument: Nova Station B
Cell ID: 2 F/W version: 0.00
Adsorbate Nitrogen Temperature 77.350K
Molec. Wt.: 28.013 g Cross Section: 16.200 Å² Liquid Density: 0.808 g/cc

Relative Pressure P/Po	Volume @ STP cc/g	1 / [W((Po/P) - 1)]
5.29350e-02	22.6503	1.9744e+00
1.12518e-01	47.2905	2.1451e+00
1.73623e-01	72.1557	2.3297e+00
2.35250e-01	97.1150	2.5344e+00
2.97372e-01	121.6711	2.7832e+00

BET summary
Slope = 3.283
Intercept = 1.781e+00
Correlation coefficient, r = 0.997659
C constant= 2.843
Surface Area = 687.723 m²/g

Appendix –F 3.2 Pore Volume and Size of CNCs/Ag@ZnO (1:0.5) BNC

Quantachrome NovaWin - Data Acquisition and Reduction
for NOVA instruments
©1994-2010, Quantachrome Instruments
version 11.0
Analysis Report
Operator:alex Date:2022/08/04 Operator:alex Date:8/4/2022
Sample ID: BE 6 A Filename: C:\QCdata\Physisorb\BE 66.qps
Sample Desc: Comment:
Sample weight: 0.04 g Sample Volume: 0.01026 cc Sample Density:3.9 g/cc
Outgas Time: 8.0 hrs OutgasTemp: 300.0 C
Analysis gas: Nitrogen Bath Temp: 77.3 K

Press. Tolerance:0.100/0.100 (ads/des)Equil time: 60/60 sec (ads/des) Equil timeout: 240/240 sec (ads/des)
Analysis Time: 80.7 min End of run: 2022/08/04 13:02:52 Instrument: Nova Station C
Cell ID: 2 F/W version: 0.00
Adsorbate Nitrogen Temperature 77.350K
Molec. Wt.: 28.013 g Cross Section: 16.200 Å² Liquid Density: 0.808 g/cc

Pore Volume Data

HK method cumulative pore volume	18.51e-01 cc/g
SF method cumulative pore volume	1.064e-01 cc/g
NLDFT method cumulative pore volume	1.736e-01 cc/g

Pore Size Data

HK method pore Radius (Mode)	1.224e+00 Å
SF method pore Radius (Mode)	1.679e+01 Å
NLDFT pore Radius (Mode)	1.324e+01 Å

Appendix –F-4 BET Analysis Results of CNCs/Ag@ZnO (0.5:1) BNC

Appendix –F-4.1 Surface Area of CNCs/Ag@ZnO (0.5:1) BNC

Quantachrome NovaWin - Data Acquisition and Reduction
for NOVA instruments
©1994-2010, Quantachrome Instruments
version 11.0
Analysis Report
Operator:alex Date:2022/08/08 Operator:alex Date:8/8/2022
Sample ID: BE 37A Filename: C:\QCdata\Physisorb\BE 7.qps
Sample Desc: Comment:
Sample weight: 0.04 g Sample Volume: 0.010256 cc Sample Density:3.9 g/cc
Outgas Time: 8.0 hrs OutgasTemp: 300.0 C
Analysis gas: Nitrogen Bath Temp: 77.3 K
Press. Tolerance:0.100/0.100 (ads/des)Equil time: 60/60 sec (ads/des) Equil timeout: 240/240 sec (ads/des)
Analysis Time: 81.5 min End of run: 2022/08/08 12:33:52 Instrument: Nova Station C
Cell ID: 2 F/W version: 0.00
Adsorbate Nitrogen Temperature 77.350K
Molec. Wt.: 28.013 g Cross Section: 16.200 Å² Liquid Density: 0.808 g/cc

Relative Pressure P/Po	Volume @ STP cc/g	1 / [W((Po/P) - 1)]
5.37690e-02	22.5925	2.0124e+00
1.14057e-01	47.1442	2.1849e+00
1.74258e-01	71.2942	2.3683e+00
2.35598e-01	95.6523	2.5781e+00
2.98050e-01	119.9244	2.8329e+00

BET summary

Slope = 3.336
Intercept = 1.811e+00
Correlation coefficient, r = 0.997332
C constant = 2.842
Surface Area = 676.620 m²/g

Appendix –F-4.2 Pore Volume and Size of CNCs/Ag@ZnO (0.5:1) BNC

Quantachrome NovaWin - Data Acquisition and Reduction

for NOVA instruments

©1994-2010, Quantachrome Instruments
version 11.0

Analysis Report
Operator:alex Date:2022/08/08 Operator:alex Date:8/8/2022
Sample ID: BE 37A Filename: C:\QCdata\Physisorb\BE 7.qps
Sample Desc: Comment:
Sample weight: 0.04 g Sample Volume: 0.010256 cc Sample Density:3.9 g/cc
Outgas Time: 8.0 hrs OutgasTemp: 300.0 C
Analysis gas: Nitrogen Bath Temp: 77.3 K
Press. Tolerance:0.100/0.100 (ads/des)Equil time: 60/60 sec (ads/des) Equil timeout: 240/240 sec (ads/des)
Analysis Time: 81.5 min End of run: 2022/08/08 12:33:52 Instrument: Nova Station C
Cell ID: 2 F/W version: 0.00
Adsorbate Nitrogen Temperature 77.350K
Molec. Wt.: 28.013 g Cross Section: 16.200 Å² Liquid Density: 0.808 g/cc

Pore Volume Data

HK method cumulative pore volume 9.431e-01 cc/g

SF method cumulative pore volume	1.058e-01 cc/g
NLDFT method cumulative pore volume	1.729e-01 cc/g

Pore Size Data

HK method pore Radius (Mode)	1.637e-01 Å
SF method pore Radius (Mode)	1.670e+01 Å
NLDFT pore Radius (Mode)	1.324e+01 Å

Appendix-G DLS Results

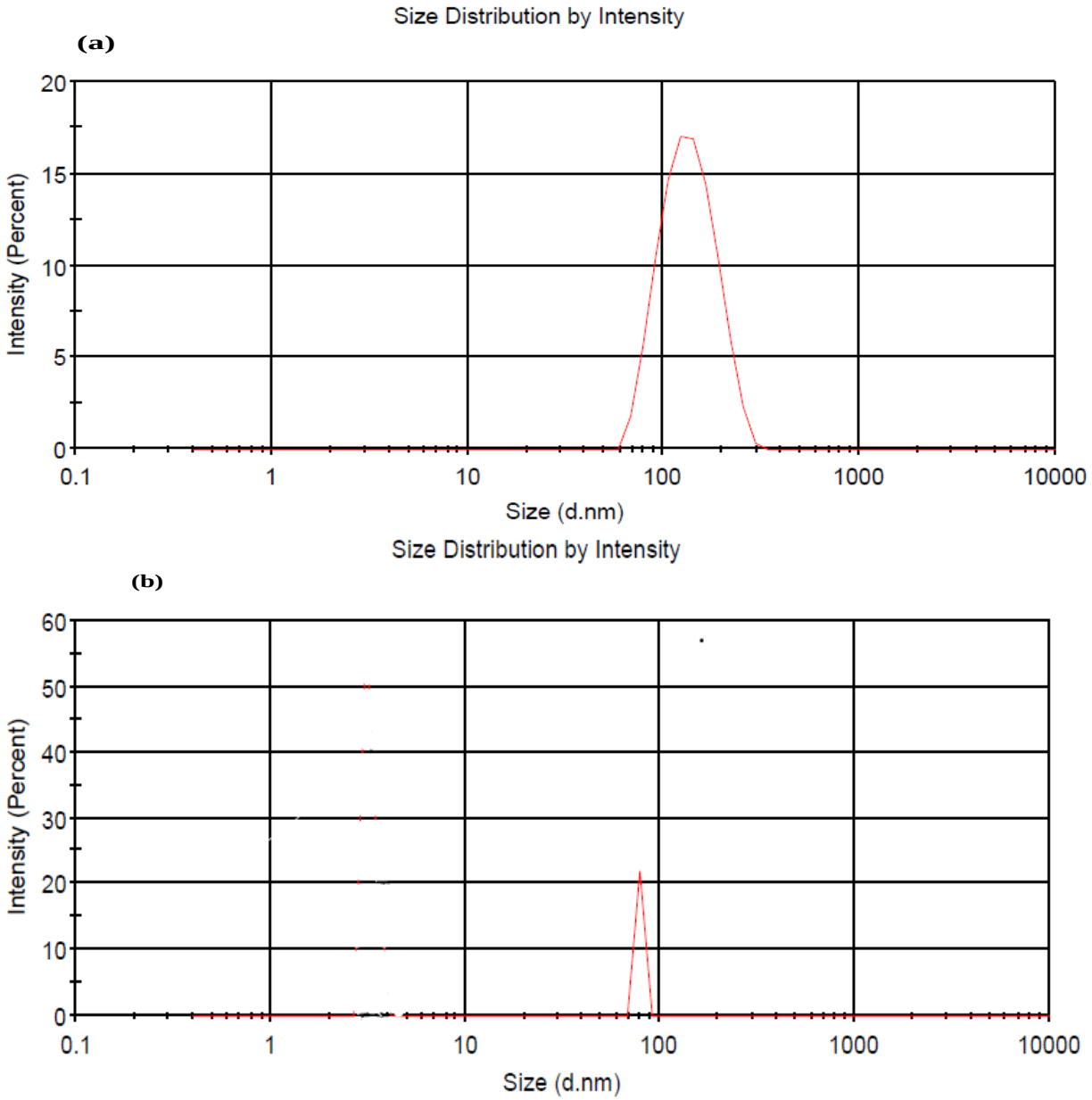

(c)

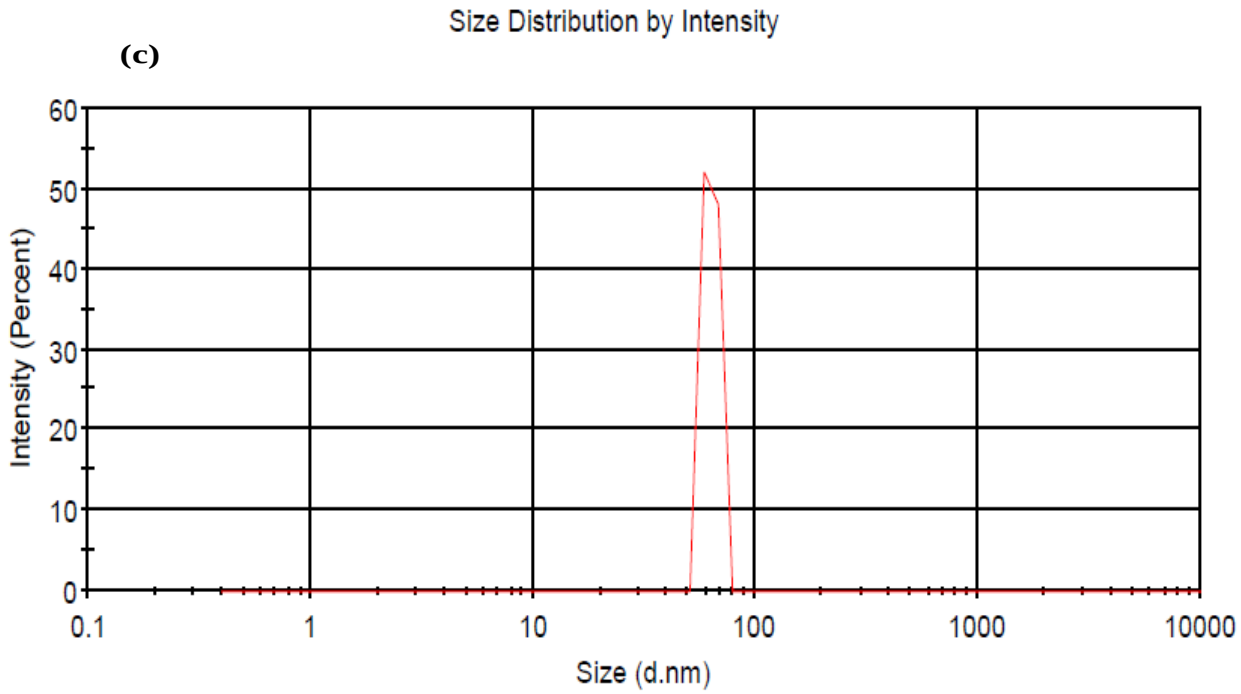
Size Distribution by Intensity
Intensity (Percent)
60
50
40
30
20
10
0
0.1
1
10
100
1000
10000
Size (d.nm)

(d)

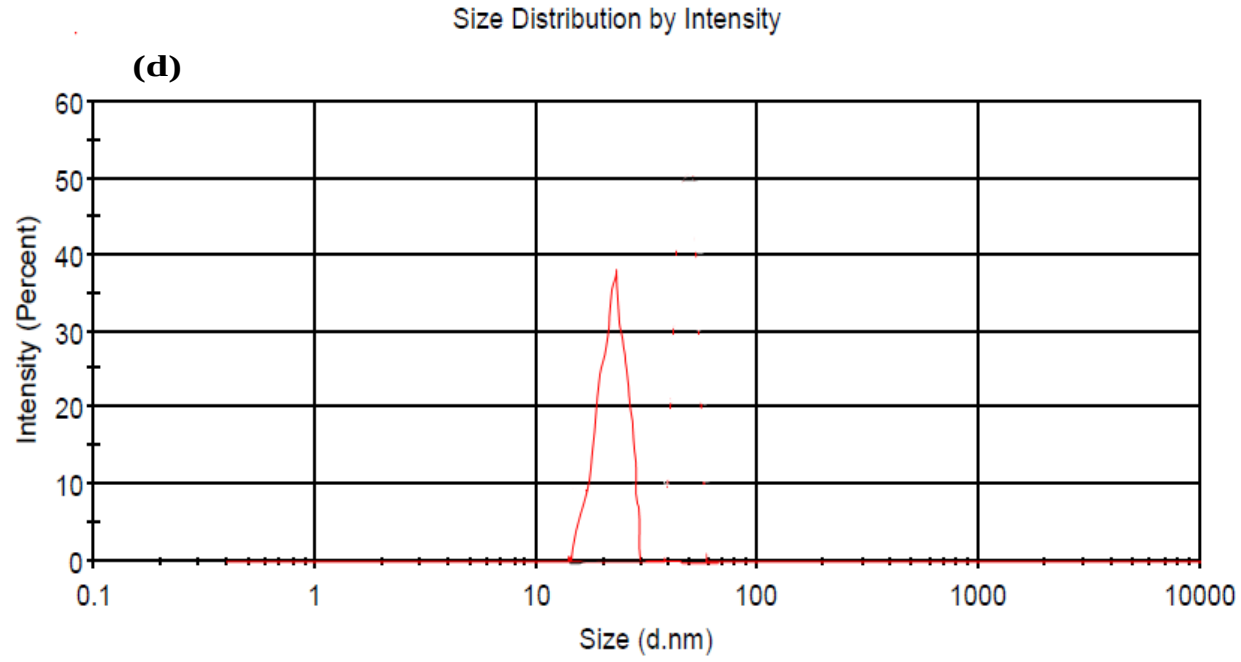
Size Distribution by Intensity
Intensity (Percent)
60
50
40
30
20
10
0
0.1
1
10
100
1000
10000
Size (d.nm)

(e)

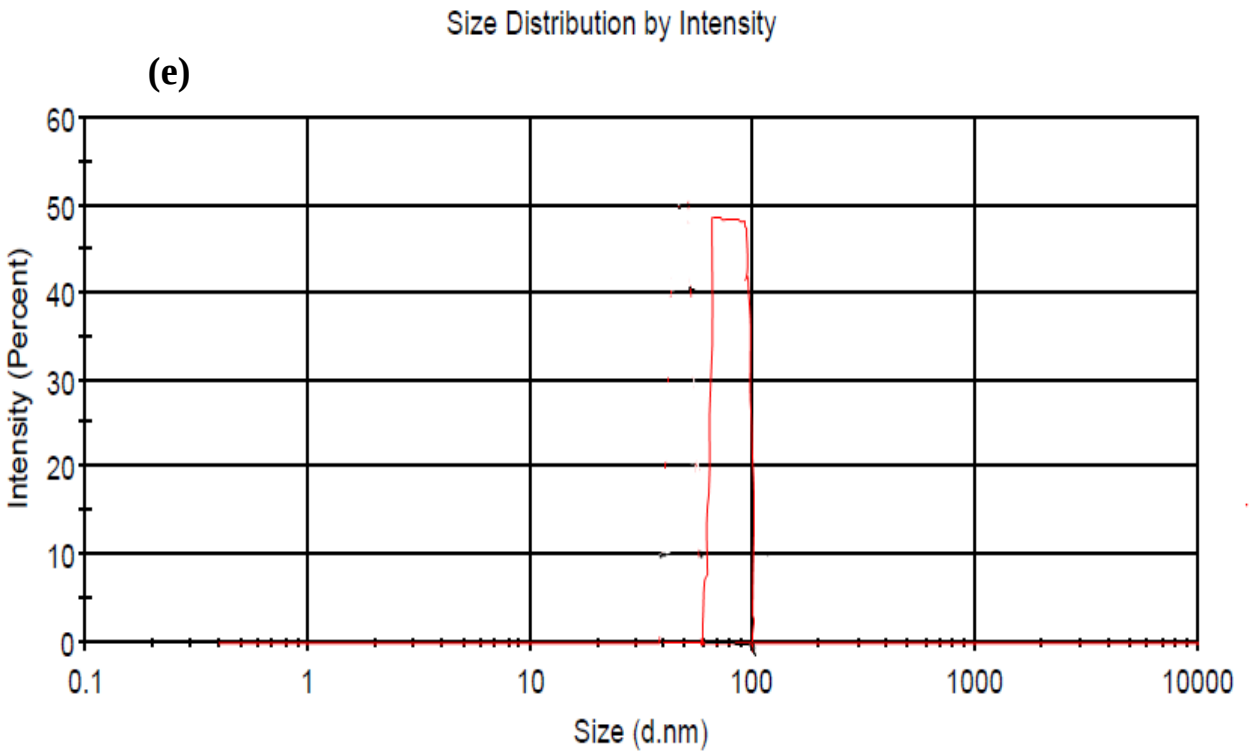
Size Distribution by Intensity
Intensity (Percent)
60
50
40
30
20
10
0
0.1
1
10
100
1000
10000
Size (d.nm)

(f)

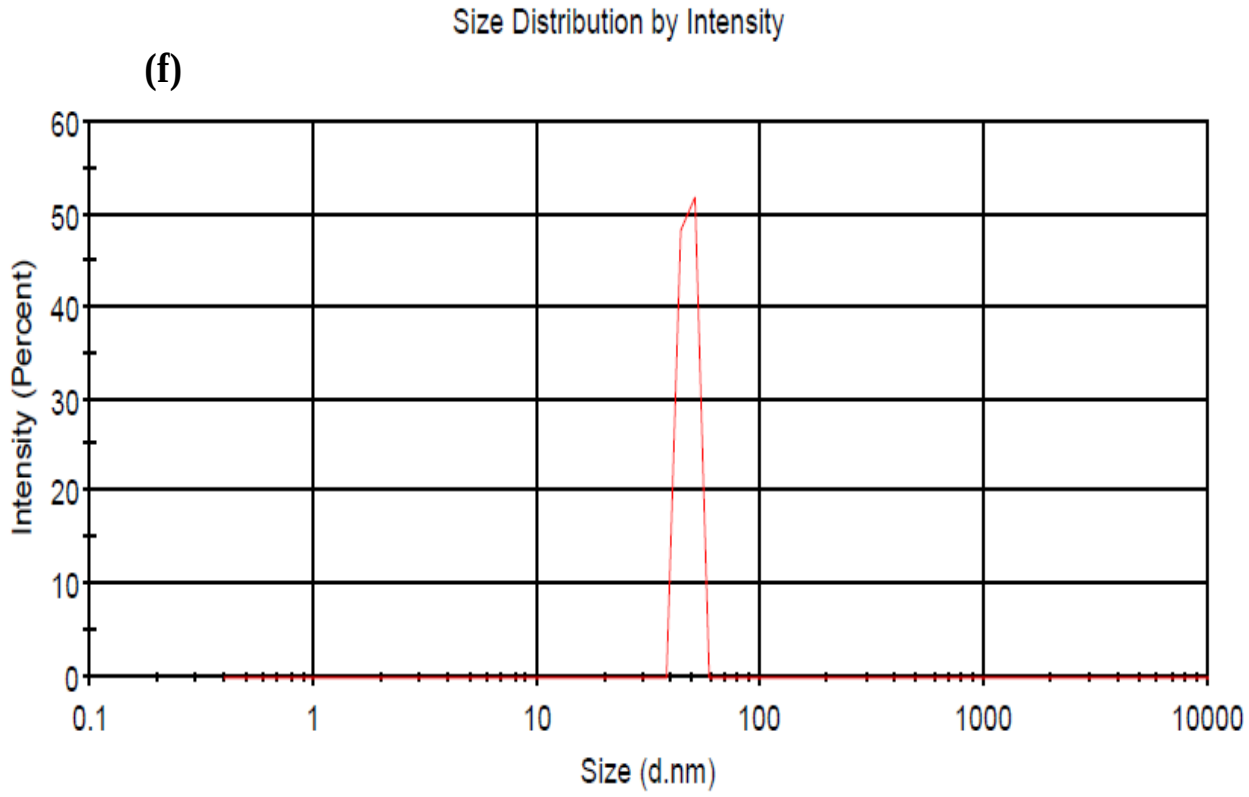
Size Distribution by Intensity
Intensity (Percent)
60
50
40
30
20
10
0
0.1
1
10
100
1000
10000
Size (d.nm)

Appendix-H Determination of Point of Zero Charge

Table H-1 Change in pH values to estimate surface charge of CNCs

Initial pH	2	4	6	8	10	12
Final pH	2.315	6.54	7.175	7.51	7.57	9.99
ΔpH	0.315	2.54	1.75	-0.49	-2.43	-2.01

Table H-2 Change in pH values to estimate surface charge of Ag@ZnO NPs

Initial pH	2	4	6	8	10	12
Final pH	2.27	6.42	7.32	7.15	7.84	10.44
ΔpH	0.27	2.42	1.32	- 0.85	- 2.61	- 1.56

Table H-3 Change in pH values to estimate surface charge of CNCs/Ag@ZnO (1:1) BNC

Initial pH	2	4	6	8	10	12
Final pH	2.35	6.84	7.02	7.21	7.37	10.99
ΔpH	0.35	2.84	1.02	- 0.79	- 2.63	- 1.01

Table H-4 Change in pH values to estimate surface charge of CNCs/Ag@ZnO (1:0.5) BNC

Initial pH	2	4	6	8	10	12
Final pH	2.08	6.56	7.82	7.56	7.83	10.66
ΔpH	0.08	2.56	1.82	- 0.44	- 2.17	- 0.34

Table H-5 Change in pH values to estimate surface charge of CNCs/Ag@ZnO (0.5:1) BNC

Initial pH	2	4	6	8	10	12
Final pH	2.17	6.42	7.22	7.45	7.69	9.44
ΔpH	0.17	2.42	1.22	- 0.55	- 2.31	- 0.56

Appendix-I Photocatalytic Degradation Study

Appendix-I-1 Pre-Photocatalytic Degradation Studies

Table - I-1.1 Photodegradation Efficiency of CNCs @ different initial pH value

Initial pH	Absorbance				MB dye degradation (%)
	Trial-1	Trail-2	Trail-3	Average	
2	0.1398	0.1545	0.1336	0.1425	40.60
4	0.1092	0.1227	0.1100	0.1140	52.50
6	0.0945	0.0968	0.0984	0.0967	59.70
8	0.0840	0.0844	0.0842	0.0842	64.90
10	0.0518	0.0510	0.0520	0.0516	78.50
12	0.0550	0.0570	0.0530	0.0505	78.95

Table - I-1.2 Photodegradation Efficiency of Ag@ZnO NPs @ different initial pH value

Initial pH	Absorbance				MB dye degradation (%)
	Trial-1	Trail-2	Trail-3	Average	
2	0.1290	0.1310	0.1300	0.1300	45.8
4	0.0752	0.0753	0.0755	0.0754	68.58
6	0.0690	0.0640	0.0650	0.0660	72.5
8	0.0325	0.0327	0.0327	0.0326	86.4
10	0.0190	0.0160	0.0200	0.0183	92.5
12	0.0175	0.0169	0.0168	0.0170	92.9

Table - I-1.3 Photodegradation Efficiency of CNCs/Ag@ZnO (1:1) @ different initial pH value

Initial pH	Absorbance				MB dye degradation (%)
	Trial-1	Trail-2	Trail-3	Average	
2	0.11853	0.11850	0.11858	0.11856	50.6
4	0.0639	0.0638	0.0630	0.0636	73.5
6	0.0493	0.0491	0.0494	0.0492	79.5
8	0.0225	0.0228	0.0224	0.0226	90.6
10	0.0086	0.0083	0.0082	0.0084	96.5
12	0.0071	0.0078	0.0076	0.0075	96.87

Appendix-I-2 Effects of Process Parameters studies

Appendix-I-2.1 Effects of pH of Dye Solution

Table - I-2.1.1 Effect of pH study using CNCs/ Ag@ZnO (1:1) BNC

Initial pH	Absorbance				MB dye degradation (%)
	Trial-1	Trail-2	Trail-3	Average	
2	0.0935	0.0936	0.0939	0.0937	60.95
4	0.0780	0.0777	0.0776	0.0778	67.6
6	0.0660	0.0659	0.0663	0.0661	72.45
8	0.0562	0.0543	0.0566	0.0564	76.5
10	0.0319	0.0318	0.0322	0.0320	86.65
12	0.0780	0.0777	0.0776	0.0778	67.56

Table - I-2.1.2 Effect of pH study using CNCs/ Ag@ZnO (1:0.5) BNC

Initial pH	Absorbance				MB dye degradation (%)
	Trial-1	Trail-2	Trail-3	Average	
2	0.0750	0.0747	0.0746	0.0748	68.85
4	0.0660	0.0663	0.0659	0.0661	72.45
6	0.0511	0.0512	0.0515	0.0513	78.62
8	0.0422	0.0418	0.0419	0.0420	82.5
10	0.0252	0.0251	0.0255	0.0253	89.45
12	0.0572	0.0569	0.0568	0.0570	76.23

Table - I-2.1.3 Effect of pH study using CNCs/ Ag@ZnO (0.5:1) BNC

Initial pH	Absorbance				MB dye degradation (%)
	Trial-1	Trail-2	Trail-3	Average	
2	0.0848	0.0844	0.0845	0.0846	64.75
4	0.0712	0.0716	0.0713	0.0714	70.23
6	0.0537	0.0540	0.0536	0.0538	77.56
8	0.0491	0.0492	0.0495	0.0493	79.45
10	0.0278	0.0274	0.0275	0.0276	88.5
12	0.0467	0.0466	0.0470	0.0468	80.5

Appendix-I-2.2 Effect of BNC dosage

Table - I-2.2.1 Effect of BNC dosage study using CNCs/ Ag@ZnO (1:1) BNC

BNC dosage (mg/L)	**Absorbance**				**MB dye degradation (%)**
	Trial-1	**Trail-2**	**Trail-3**	**Average**	
5	0.1108	0.1104	0.1105	0.1106	53.91
10	0.0292	0.0296	0.0293	0.0294	87.73
15	0.0115	0.0114	0.0118	0.0116	95.18
20	0.0086	0.0082	0.0083	0.0084	96.5
25	0.0080	0.0083	0.0079	0.0081	96.65
30	0.0078	0.0079	0.0082	0.0080	96.66
35	0.0078	0.0079	0.0082	0.0080	96.66

Table - I-2.2.2 Effect of BNC dosage study using CNCs/ Ag@ZnO (1:0.5) BNC

BNC dosage (mg/L)	Absorbance				MB dye degradation (%)
	Trial-1	Trail-2	Trail-3	Average	
5	0.0761	0.0758	0.0757	0.0759	68.37
10	0.0245	0.0248	0.0244	0.0246	89.74
15	0.0077	0.0073	0.0074	0.0075	96.87
20	0.0005	0.0008	0.0004	0.0006	99.75
25	0.0006	0.0002	0.0003	0.0004	99.8
30	0.0006	0.0002	0.0003	0.0004	99.8
35	0.0006	0.0002	0.0003	0.0004	99.8

Table - I-2.2.3 Effect of BNC dosage study using CNCs/ Ag@ZnO (0.5:1) BNC

BNC dosage (mg/L)	Absorbance				MB dye degradation (%)
	Trial-1	Trail-2	Trail-3	Average	
5	0.0890	0.0894	0.0891	0.0892	62.82
10	0.0248	0.0245	0.0244	0.0246	89.76
15	0.0076	0.0079	0.0075	0.0077	96.78
20	0.0033	0.0032	0.0036	0.0034	98.6
25	0.0035	0.0031	0.0032	0.0033	98.62
30	0.0035	0.0031	0.0032	0.0033	98.62
35	0.0035	0.0031	0.0032	0.0033	98.62

Appendix-I-2.3 Effect of MB Dye Concentration

Table - I-2.3.1 Effect of MB dye concentration study using CNCs/ Ag@ZnO (1:1) BNC

MB dye con. (mg/L)	Absorbance				MB dye degradation (%)
	Trial-1	Trail-2	Trail-3	Average	
5	0.0019	0.0018	0.0004	0.0002	99.98
10	0.0092	0.0096	0.0093	0.0094	96.5
15	0.0174	0.0170	0.0171	0.0172	95.25
20	0.1166	0.1169	0.1165	0.1167	75.89

Table - I-2.3.2 Effect of MB dye concentration study using CNCs/ Ag@ZnO (1:0.5) BNC

MB dye con. (mg/L)	Absorbance				MB dye degradation (%)
	Trial-1	Trail-2	Trail-3	Average	
5	0.0004	0.0018	0.0019	0.0002	99.98
10	0.0005	0.0004	0.0008	0.0006	99.75
15	0.0003	0.0006	0.0003	0.0004	98.99
20	0.0648	0.0647	0.0652	0.0650	86.57

Table - I-2.3.3 Effect of MB dye concentration study using CNCs/ Ag@ZnO (0.5:1) BNC

MB dye con. (mg/L)	Absorbance				MB dye degradation (%)
	Trial-1	Trail-2	Trail-3	Average	
5	0.0004	0.0018	0.0019	0.0002	99.98
10	0.0033	0.0032	0.0036	0.0034	98.6
15	0.0078	0.0075	0.0074	0.0076	97.9
20	0.0824	0.0827	0.0823	0.0825	82.95

Appendix-I-2.4 Effect of Irradiation Time

Table - I-2.4.1 Effect of irradiation time study using CNCs/ Ag@ZnO (1:1) BNC

Irradiation Time (min)	Absorbance				MB dye degradation (%)
	Trial-1	Trail-2	Trail-3	Average	
0	0.3630	0.3630	0.3630	0.3630	0
30	0.1366	0.1362	0.1363	0.1364	62.42
60	0.0708	0.0709	0.0712	0.0710	80.45
90	0.0486	0.0483	0.0482	0.0484	86.68
120	0.0333	0.0330	0.0329	0.0331	90.88
150	0.0151	0.0152	0.0155	0.0153	95.78
180	0.0151	0.0152	0.0155	0.0153	95.78
210	0.0151	0.0152	0.0155	0.0153	95.78
240	0.0151	0.0152	0.0155	0.0153	95.78

Table - I-2.4.2 Effect of irradiation time study using CNCs/ Ag@ZnO (1:0.5) BNC

Irradiation Time (min)	Final Absorbance				MB dye degradation (%)
	Trial-1	Trail-2	Trail-3	Average	
0	0.3630	0.3630	0.3630	0.3630	0
30	0.0893	0.0889	0.0890	0.0891	75.45
60	0.0331	0.0330	0.0334	0.0332	90.86
90	0.0110	0.0111	0.0114	0.0112	96.76
120	0.0034	0.0035	0.0038	0.0036	99
150	0.0034	0.0035	0.0038	0.0036	99.28
180	0.0034	0.0035	0.0038	0.0036	99.28
210	0.0034	0.0035	0.0038	0.0036	99.28
240	0.0034	0.0035	0.0038	0.0036	99.28

Table - I-2.4.3 Effect of irradiation time study using CNCs/ Ag@ZnO (0.5:1) BNC

Irradiation Time (min)	Absorbance				MB dye degradation (%)
	Trial-1	Trail-2	Trail-3	Average	
0	0.3630	0.3630	0.3630	0.3630	0
30	0.0900	0.0800	0.1200	0.1000	72.45
60	0.0410	0.0409	0.0413	0.0411	88.68
90	0.0199	0.0196	0.0195	0.0197	94.56
120	0.0053	0.0056	0.0052	0.0054	98.5
150	0.0053	0.0056	0.0052	0.0054	98.56
180	0.0053	0.0056	0.0052	0.0054	98.56
210	0.0053	0.0056	0.0052	0.0054	98.56
240	0.0053	0.0056	0.0052	0.0054	98.56

Appendix-J Kinetics Study of MB Dye Degradation

Table - J-1 The pseudo first order kinetics model of MB dye degradation @ C_o = 5mg/L

Irradiation time (min)	CNCs/ Ag@ZnO (1:1) BNC		CNCs/ Ag@ZnO (1:0.5) BNC		CNCs/ Ag@ZnO (0.5:1) BNC (%)	
	C_t (mg/L)	$ln(\frac{C_0}{C_t})$	C_t (mg/L)	$ln(\frac{C_0}{C_t})$	C_t (mg/L)	$ln(\frac{C_0}{C_t})$
0	5	0	5	0	5	0
30	2.914	0.54	0.810	1.82	1.440	1.24
60	1.072	1.54	0.081	4.13	0.398	2.53
90	0.364	2.62	0.020	5.52	0.059	4.43
120	0.039	4.84	0.003	7.51	0.005	6.12

Table - J-2 The pseudo first order kinetics model of MB dye degradation @ C_o =10mg/L

Irradiation time (min)	CNCs/ Ag@ZnO (1:1) BNC		CNCs/ Ag@ZnO (1:0.5) BNC		CNCs/ Ag@ZnO (0.5:1) BNC	
	C_t (mg/L)	$ln(\frac{C_0}{C_t})$	C_t (mg/L)	$ln(\frac{C_0}{C_t})$	C_t (mg/L)	$ln(\frac{C_0}{C_t})$
0	10	0	10	0	10	0
30	6.376	0.45	1.921	1.65	2.592	1.35
60	5.930	1.78	0.273	3.6	0.898	2.41
90	0.983	2.32	0.049	5.3	0.150	4.2
120	0.090	4.71	0.014	6.56	0.018	6.3

Table - J-3 The pseudo first order kinetics model of MB dye degradation @ C_o =15mg/L

Irradiation time (min)	CNCs/ Ag@ZnO (1:1) BNC		CNCs/ Ag@ZnO (1:0.5) BNC		CNCs/ Ag@ZnO (0.5:1) BNC	
	C_t (mg/L)	$ln(\frac{C_0}{C_t})$	C_t (mg/L)	$ln(\frac{C_0}{C_t})$	C_t (mg/L)	$ln(\frac{C_0}{C_t})$
0	15	0	15	0	15	0
30	5.978	0.920	2.479	1.80	3.414	1.48
60	2.156	1.940	0.769	2.97	1.597	2.24
90	1.534	2.280	0.336	3.80	0.676	3.1
120	0.336	3.800	0.111	4.91	0.220	4.23

Table - J-4 The pseudo first order kinetics model of MB dye degradation @ C_o =20mg/L

Irradiation time (min)	CNCs/ Ag@ZnO (1:1) BNC		CNCs/ Ag@ZnO (1:0.5) BNC		CNCs/ Ag@ZnO (0.5:1) BNC	
	C_t (mg/L)	$ln(\frac{C_0}{C_t})$	C_t (mg/L)	$ln(\frac{C_0}{C_t})$	C_t (mg/L)	$ln(\frac{C_0}{C_t})$
0	20	0	20	0	20	0
30	13.540	0.39	8.379	0.87	10.546	0.64
60	8.634	0.84	4.981	1.39	7.212	1.02
90	6.860	1.07	3.654	1.7	4.932	1.4
120	4.883	1.41	1.344	2.7	3.113	1.86

Appendix-K Photocatalysis Reaction under Dark Condition

The process of electron storage through the electron reduction mechanism under light irradiation were given in the following reaction:

$$A^+ + hv \longrightarrow h_{VB}^+ + e_{CB}^-$$

$$e_{CB}^- + Zn^{2+} \longrightarrow Zn^+$$

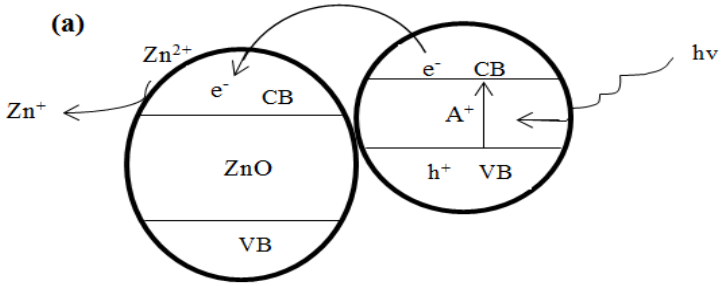

Figure K-1 Electron reduction mechanism

The further highlighted that the ability of nanomaterials to trap electrons from the reactant molecules determines its degradation efficiency in the dark were given in the following reaction:

$$C_{16}H_{18}ClN_3S \rightleftharpoons [C_{16}H_{17}ClN_3S]^- + H^+ \quad \text{(1)}$$

$$[C_{16}H_{17}ClN_3S]^- + \text{nanomaterials} \longrightarrow C_{16}H_{17}ClN_3S^- + \text{nanomaterials } (e^- \text{ trapped}) \quad \text{(2)}$$

$$\text{Nanomaterials } (e^- \text{ trapped}) + O_2 \longrightarrow \text{nanomaterials} + {}^{\bullet}O_2^- \quad \text{(3)}$$

$${}^{\bullet}O_2^- + H^+ \longrightarrow {}^{\bullet}OH \quad \text{(4)}$$

$${}^{\bullet}OH + C_{16}H_{17}ClN_3S^- \longrightarrow \ldots\ldots \longrightarrow Cl^- + H_2O + CO_2 \quad \text{(5)}$$

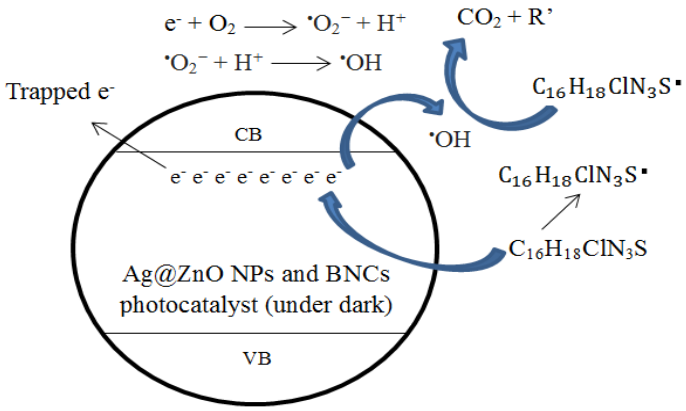

Figure K-2 The electron trapping process.

Appendix-L Optimization of Process Parameters using RSM-BBD

Appendix-L-1 The desirability ramp for optimization of process parameters

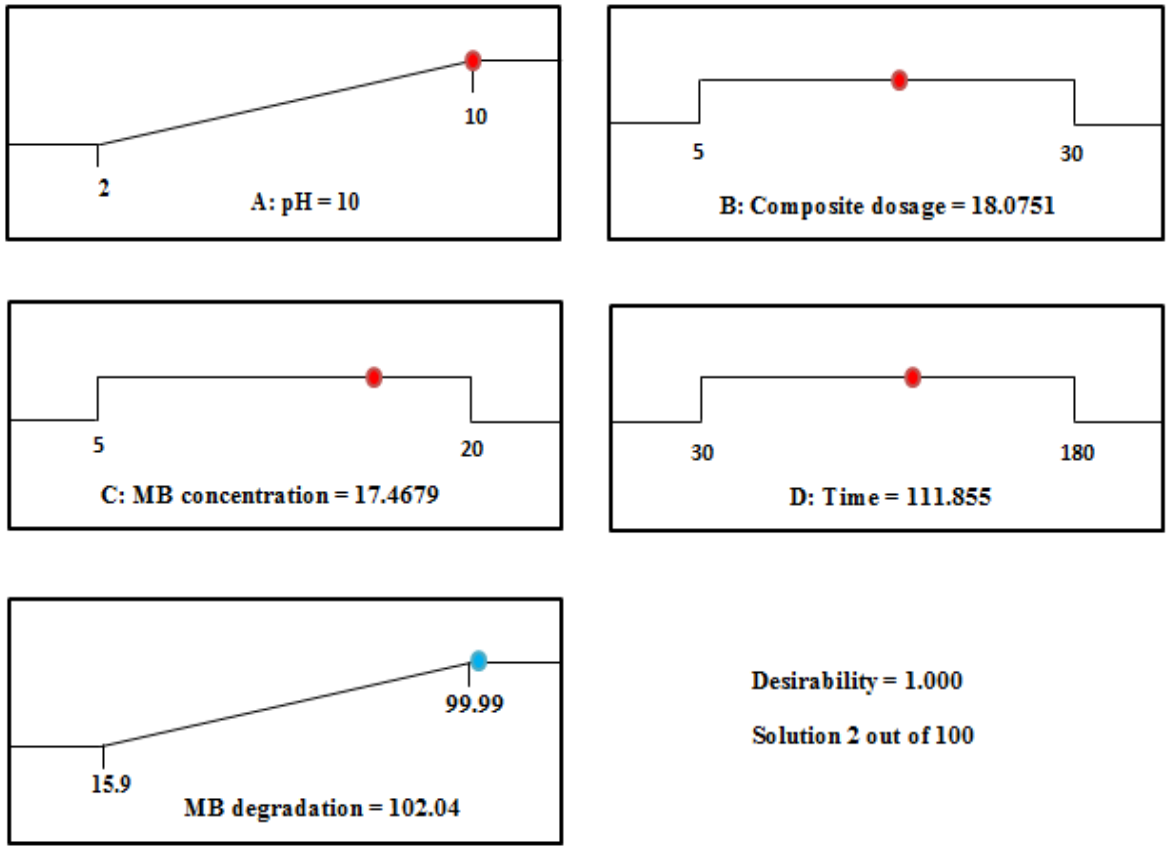

Table -L-1 Triplicate test by CNCs/Ag@ZnO (1:0.5) BNC using predicted process parameters of RSM-BBD

Experimental No.	Final absorbance				MB degradation (%)
	Trial-1	Trial-2	Trial-3	Average	
1	0.003	0.002	0.003	0.0026	98.82
2	0.002	0.003	0.001	0.002	99.3
3	0.003	0.004	0.005	0.004	98.43

Table -L-2 Triplicate test by CNCs/Ag@ZnO (1:1) and CNCs/Ag@ZnO (0.5:1) BNC using predicted process parameters of RSM-BBD

BNCs	Final absorbance				MB degradation (%)
	Trial-1	Trial-2	Trial-3	Average	
CNCs/Ag@ZnO (1:1)	0.043	0.048	0.047	0.046	83.8%
CNCs/Ag@ZnO (0.5:1)	0.013	0.008	0.006	0.009	96.8%

Appendix-M Photodegradation of Textile MB Dye Containing Wastewater

Appendix-M-1 Calibration Curve data

Table -M-1 Absorbance of standard solutions for calibration curve

Initial MB concentration	Absorbance			
	Trail-1	Trail-2	Trail-3	Average
5	0.1353	0.1340	0.1352	0.1348
15	0.358	0.361	0.370	0.363
25	0.596	0.583	0.588	0.589
35	0.823	0.834	0.801	0.8194
45	1.034	1.068	1.049	1.051

Appendix-M-2 Determination of Unknown Dye Concentration of Textile Wastewater

$A = \varepsilon bc$

Where: $\varepsilon = 2.289*10^{-2}$ L mol^{-1} cm^{-1}, b = 1cm and A = 0.264

$0.264 = 2.289*10^{-2}$ L mol^{-1} cm^{-1}* 1cm* C

$$C = \frac{0.264}{2.289*10^{-2}\ L\ mol^{-1}\ cm^{-1}*\ 1cm} = \underline{11.53mg/L}$$

Appendix-M-3 MB Dye Degradation from Textile Wastewater using BNCs

Table -M-3 Degradation of MB from textile wastewater

BNCs	Absorbance				MB dye Degradation (%)
	Trail-1	Trail-2	Trail-3	Average	
CNCs/Ag@ZnO (1:1)	0.008	0.005	0.007	0.006	97.73
CNCs/Ag@ZnO (1:0.5)	0.001	0.004	0.002	0.002	99.24
CNCs/Ag@ZnO (0.5:1)	0.004	0.003	0.002	0.003	98.86

Appendix-N Recyclability Study

Table –N-1 Recyclability Efficiency of CNCs/Ag@ZnO (1:1) BNC

No. of Cycle	Absorbance				MB dye Degradation (%)
	Trail-1	Trail-2	Trail-3	Average	
1	0.017	0.014	0.013	0.015	95.82
2	0.026	0.029	0.025	0.027	92.65
3	0.043	0.040	0.039	0.041	88.76
4	0.052	0.055	0.051	0.053	85.5
5	0.079	0.075	0.076	0.077	78.85
6	0.105	0.104	0.108	0.106	70.78
7	0.123	0.120	0.119	0.121	66.75

Table –N-2 Recyclability Efficiency of CNCs/Ag@ZnO (1:0.5) BNC

No. of Cycle	Absorbance				MB dye Degradation (%)
	Trail-1	Trail-2	Trail-3	Average	
1	0.0029	0.0025	0.0026	0.0027	99.25
2	0.001	0.005	0.002	0.003	99.18
3	0.0038	0.0035	0.0034	0.0036	99
4	0.0035	0.0036	0.0039	0.0037	98.98
5	0.0080	0.0076	0.0077	0.0078	97.85
6	0.0233	0.0237	0.0234	0.0235	93.5
7	0.0337	0.0336	0.0340	0.0338	90.67

Table –N-3 Recyclability Efficiency of CNCs/Ag@ZnO (0.5:1) BNC

No. of Cycle	Absorbance				MB dye Degradation (%)
	Trail-1	Trail-2	Trail-3	Average	
1	0.0044	0.0043	0.0047	0.0045	98.76
2	0.0056	0.0052	0.0053	0.0054	98.5
3	0.0084	0.0087	0.0083	0.0085	97.66
4	0.0341	0.0337	0.0338	0.0339	90.65
5	0.0412	0.0413	0.0416	0.0414	88.58
6	0.0861	0.0864	0.0860	0.0862	76.24
7	0.1056	0.1057	0.1060	0.1058	70.85

Appendix-O Photocatalysis Result Pictures

MB dye standard solution (5, 10, 15, 20 mg/L)

MB degradation process under sunlight irradiation with magnetic stirring

MB dye degradation using CNCs/Ag@ZnO (1:1) BNC

MB dye degradation using CNCs/Ag@ZnO (1:0.5) BNC

MB dye degradation using
CNCs/Ag@ZnO (0.5:1) BNC